

**UiO** : **Department of Geosciences**  
University of Oslo

# **Urban impact on water quality and the local water budget - Gaustad, Oslo**

Environmental Geoscience

**Frøya Vold Bjørvik**

Master's Thesis, Autumn 2021





©2021 Frøya Vold Bjørvik

Urban impact on water quality and the local water budget - Gaustad, Oslo

<https://www.duo.uio.no/>

Printed: Representralen, University of Oslo



---

# Abstract

---

This study aims to investigate the impact urbanization has on the water quality and the local water budget of Gaustad watershed in Oslo. The infiltration capacity of the area was studied, as well as the stratigraphy of the watershed. This resulted in a simplified stratigraphy and infiltration capacity map of the catchment. The water quality was investigated by analysis of the water properties, and testing for sewer influence. The water budget of the area was modeled by an up to date hydrological software, simulating scenarios of different degrees of urbanization as well as future climate scenarios. A hydrological station surveying the water level at Gaustadbekken weir was installed and operated through the study period.

Investigations into the infiltration capacity of the watershed revealed there to be very varying infiltration potential within a small area. The subsurface of Gaustad watershed was investigated through borehole data and logs, resulting in a simplified stratigraphy of the area, indicating presence of anthropogenic material in large areas. Infiltration capacity measurements conducted in the top soil might produce misleading high potential in the anthropogenic material than what is the reality with marine clay below.

To study the urban impact on the water quality, water samples were collected at several locations within Gaustad watershed for Gaustadbekken, as well as along the river Sognsvannbekken nearby. Samples were also taken at the point of merging for the two rivers to compare their properties. The analysis indicate there being a correlation between high chemical concentrations and urban degree of the drainage area.

The water quality of Sognsvannbekken is generally better than that of Gaustadbekken. All locations of Sognsvannbekken classifies as *good* related to the fresh water standards by the Norwegian Environmental Agency (NEA). The water of Gaustadbekken qualifies as *bad* after a rainfall event of 5.3 mm in 10 hours. No indication of sewer influence was found.

The hydrological situation of Gaustad watershed was modeled using Mike+. This was done to investigate the effects of urban development on the water budget. The results of the model shows there to be significant change in the parameters of the water budget related to urban development. Comparing a natural setting to the semi-developed situation of the watershed today, the evaporation has decreased 45.5 %, while the runoff has increased 53.4 %. The Life Science Building (LSB), presently under construction, was of special interest. The effect of changing the near natural site into a building complex was investigated, and the evaporation, surface runoff and interflow was estimated for the area before and after the completed construction. On the catchment scale the changes to the water budget was not significant. For the area representing the Life Science building, however, the evaporation decrease 65.5 %, the interflow decrease 80.0 %, while the surface runoff increases 286.5 %.

As the world is experiencing population growth and a changing climate, further urbanization in the years 2071-2100 was simulated together with possible climate changes as predicted by the IPCC (AR5). The simulations show that the climate scenario RCP4.5 might bring 7.8 % more runoff, while the evaporation decrease 6.8 %. The scenario RCP8.5 indicate a 3.0 % decrease of evaporation, while the runoff increase 12.6 % relative to today's situation.



---

# Acknowledgements

---

I want to start with thanking my supervisors Nils Roar Sælthun, Anja Sundal and Hong Li. I am especially grateful for Nils Roar being there through my finishing weeks where I really needed guidance and support. I also want to thank Jenny Ingelöv Eriksson for taking an interest in me, giving me advice and encouragement, and for following my progression with the thesis.

Thank you to Dansk Hydraulisk Institutt (DHI) for providing me with a student licence for the software Mike+, and introductory course in collection system modeling.

I want to thank Lasse Tilrem at the municipality of Oslo for being so helpful in giving access to relevant data and for answering my questions.

Mufak and Magnus at the lab of the Department of Geoscience, thank you for your instructions and help. Also, I want to thank Bård at the department of Biology for helping me with water analysis. Thank you Frode T. Kvernhaugen at the Norwegian Resource and Energy Directorate (NVE) for lending me equipment to survey the water level at Gaustadbekken weir.

My amazing friends in room 217, I am so happy to have shared this experience with you! I look forward to many more (less stressful) adventures together. A special thanks to Rannveig and Sofia for being there for me through all the frustrations, and for all the fun we have had together.

To my family, I love you and miss you! Thank you for always answering the phone when I call, and for supporting me no matter what.

The biggest thanks I could ever give goes to you, Trond, for your apparent endless patience and for loving me through everything. I am so lucky to have you. Love you forever.

August 2021, Frøya





---

# Contents

---

<b>Abstract</b>	<b>iii</b>
<b>Acknowledgements</b>	<b>v</b>
<b>Contents</b>	<b>vii</b>
<b>List of Figures</b>	<b>ix</b>
<b>List of Tables</b>	<b>xi</b>
<b>I Part one</b>	<b>1</b>
<b>1 Introduction</b>	<b>3</b>
1.1 Objectives of the study . . . . .	4
<b>2 Theoretical framework</b>	<b>5</b>
2.1 Water cycle . . . . .	5
2.2 Urbanization . . . . .	8
2.3 Urban hydrology . . . . .	9
2.4 Stormwater management . . . . .	12
2.5 Hydrologic model . . . . .	14
2.6 Mike+, Danish Hydraulic Institute (DHI) . . . . .	16
<b>3 Study area</b>	<b>21</b>
3.1 Geography and climate . . . . .	21
3.2 Geologic setting . . . . .	23
3.3 The area of the Life Science Building . . . . .	25
<b>4 Method</b>	<b>27</b>
4.1 Field methods . . . . .	27
4.2 Chemical analysis of the water samples . . . . .	38
4.3 Modelling . . . . .	40
4.4 Hydrologic model setup . . . . .	43
<b>5 Results</b>	<b>51</b>
5.1 Hydrological properties of the soil . . . . .	51
5.2 Study site investigations . . . . .	54
5.3 Discharge of Gaustadbekken during the study period . . . . .	58
5.4 Chemical properties of Gaustadbekken and Sognsvannbekken . . . . .	60
5.5 Escherichia coli . . . . .	69
5.6 Hydrologic Model calibration and validation . . . . .	70
	<b>vii</b>

5.7	Water budget, model results . . . . .	77
<b>6</b>	<b>Discussion</b>	<b>83</b>
6.1	Infiltration capacity of Gaustad watershed . . . . .	83
6.2	Subsurface of Gaustad watershed . . . . .	84
6.3	Groundwater - surface water interaction . . . . .	85
6.4	Filling material . . . . .	86
6.5	Discharge measurements . . . . .	86
6.6	Urban impact on water quality . . . . .	87
6.7	Hydrologic model in Mike+ . . . . .	91
6.8	Urban water budget . . . . .	95
6.9	Reflections on the drainage system network at Gaustad . . . . .	98
<b>7</b>	<b>Conclusions</b>	<b>101</b>
7.1	Further work . . . . .	102
	<b>Bibliography</b>	<b>103</b>
<b>II</b>	<b>Part two</b>	<b>109</b>
<b>A</b>	<b>Appendix</b>	<b>111</b>
A.1	Figures . . . . .	111
A.2	Fieldwork . . . . .	116

---

# List of Figures

---

2.1	Illustration of the hydrologic cycle. . . . .	5
2.2	Runoff concentration time as a function of the degree of impermeable surfaces and collection system network connectivity . . . . .	7
2.3	Historic photos of Gaustad, Oslo, illustrating the urban development. . . . .	9
2.4	Collection system network of Gaustad watershed. . . . .	11
2.5	Drainage lines and historical rivers of the Gaustad Watershed. . . . .	12
2.6	Three step strategy for stormwater management in Oslo . . . . .	13
2.7	RDI model schematics. . . . .	19
3.1	Overview of Oslo municipality and county and Gaustad watershed . . . . .	21
3.2	Open and closed river system of Gaustad watershed in Oslo. . . . .	22
3.3	Bedrock, quarternary deposits and infiltration potential at Gaustad (NGU). . . . .	23
3.4	Sites of anthropogenic material at Gaustad. . . . .	24
4.1	Location of field work in relation to infiltration capacity. . . . .	28
4.2	Illustration of the Mariotte cylinder. . . . .	29
4.3	Location of the Ott Orpheus mini logger device. . . . .	30
4.4	Ott Orpheus mini level logger device at Gaustadbekken weir. . . . .	32
4.5	Illustration of the Compound triangular-rectangular sharp crested weir (CTRSC). . . . .	33
4.6	Illustration of how the water level was measured in the Gaustadbekken weir. . . . .	34
4.7	Locations of field measurements and water sampling. . . . .	36
4.8	Area not included in the watershed due to inaccuracy of ArcGIS hydrological modeling tool. . . . .	41
4.9	Distribution of <i>urban</i> vs. <i>rural</i> sub-catchments in the model setup in Mike+. . . . .	46
5.1	Infiltration capacity map. . . . .	55
5.2	Surface cover types of Gaustad watershed. . . . .	56
5.3	Surface covers of the Gaustad watershed illustrated as a pie-chart. . . . .	57
5.4	Measured discharge of Gaustadbekken. . . . .	58
5.5	Rating curve comparing the discharge found by the method described in subsection 4.1 by the observed tracer dilution method results. . . . .	59
5.6	Gaustadbekken and Sognsvannbekken February 3rd, 2021. . . . .	63
5.7	Sewershed Gaustad. . . . .	70
5.8	Calibration plot for visual estimation of the simulated vs observed output for the calibration period of 8.10.20-28.2.21. . . . .	71
5.9	Correlation plot of the calibration period 8.10.20-28.2.21 for the discharge measurements at Gaustadbekken outlet. . . . .	72
5.10	Calibration plot for visual estimation of the simulated vs observed output for the validation period of 1.3-30.6.2021. . . . .	73
5.11	Correlation plot visualising the correlation of the simulated vs. observed discharge values for the validation period 1.3-30.6.2021. . . . .	74

## List of Figures

---

5.12	Snow storage in a representative sub-catchment during the calibration and validation period 8.10.20-30.6.21. The black line defines the divide between the calibration and validation period. The purple line marks the 20.2.20, the green line marks the 12.3.21. . . . .	75
5.13	Groundwater level in a representative sub-catchment during the calibration and validation period 8.10.20-30.6.21. The black line defines the divide between the calibration and validation period. . . . .	76
5.14	The location of the Life Science building presently under construction at Gaustad. Picture on the right from <i>Norgeskart.no</i> . . . . .	78
5.15	Precipitation together with runoff generated by the Kinematic Wave (KW) model and Rainfall Dependent Infiltration (RDI) model illustrating the different reactions to a rainfall event. The values are from the model with the Life Science Building as <i>rural</i> . . . . .	79
5.16	Precipitation together with runoff generated by the Kinematic Wave (KW) model and Rainfall Dependent Infiltration (RDI) model illustrating the different reactions to a rainfall event. The values are from the model with the Life Science Building as <i>urban</i> . . . . .	80
6.1	Sampling locations together with recorded anthropogenic material. . . . .	88
6.2	Accumulated precipitation [mm] for the input, the Kinematic Wave (KW) and RDI model, illustrating the deviation in the KW model. . . . .	93
6.3	Groundwater level through the hydrological year 2018-2019 for the sub-catchment representing the Life Science Building, before and after the construction of the building. The y-axis is groundwater level from surface elevation [m]. The start water level is -10m for both scenarios. The groundwater level is a result of the simulations by the hydrological model in Mike+. . . . .	96
6.4	Surface water problematic areas as registered by the owners and users of the parcel garden. Picture by L. J. Barkved/NIVA and Sogn Hagekoloni from Barkved et al. (2018). The map on the left illustrates the problem areas of the parcel garden, and the picture on the right exemplifies a situation of unwanted surface water. . . . .	98
6.5	Surface water accumulation at the bottom of Sogn Parcel garden after rainfall. Picture taken the 6.6.2020. . . . .	99
A.1	E. Coli investigation photos. . . . .	111
A.2	Simplified stratigraphy of Gaustad watershed illustrating presence of anthropogenic material at several areas of the catchment. Made as an illustration of the findings by ArcGIS Pro based on data by NGU and the subsurface archive as described in methods. Figure created in MODFLOW. . . . .	112
A.3	Root zone storage through the hydrological year 2018-2019 for the sub-catchment representing the Life Science Building, before the construction of the building. The y-axis is percentage [%]. Figure from Mike+. . . . .	113
A.4	Root zone storage through the hydrological year 2018-2019 for the sub-catchment representing the Life Science Building, after completion of the construction. The y-axis is percentage [%]. Figure from Mike+. . . . .	114
A.5	Gaustad watershed by NEVINA. . . . .	115
A.6	Field work with Mariotte cylinder together with fellow student Rannveig Brørvik Sæten. Location of Sognsvannveien. . . . .	116
A.7	Clearing the Gaustadbekken weir pond together with supervisors Nils Roar Sælthun and Hong Li. . . . .	117
A.8	Water sampling in front and measurement of pH in the background. Photo by Jorge Torres. . . . .	118
A.9	Filtering of the water samples. Photo by Jorge Torres. . . . .	119
A.10	Forskningsparken artificial stream as an open part Gaustadbekken. . . . .	120
A.11	Location Nils Bays vei (NBV), see map in figure 4.7. . . . .	121
A.12	Location Konvallveien (KV), see map in figure 4.7. . . . .	122
A.13	Location Gaustadbekken by Blindern station (GBBS), see map in figure 4.7. . . . .	123
A.14	Location Solvang Kolonihage (SK), see map in figure 4.7. . . . .	124

---

## List of Tables

---

4.1	Classification system of the water quality as set by the Norwegian Environment Agency.	38
4.2	Model specific parameters of the Kinematic Wave rainfall-surface runoff model, <i>Urban</i> areas.	47
4.3	Model specific parameters of the Kinematic Wave rainfall-surface runoff model, <i>Rural</i> areas.	47
4.4	Hydrologic parameters of the Kinematic wave rainfall-surface runoff model.	47
4.5	Rainfall dependent infiltration parameters for the <i>Urban</i> sub-catchments.	48
4.6	Rainfall dependent infiltration parameters for the <i>Rural</i> sub-catchments.	49
5.1	Results of fieldwork with Mariotte cylinder. The locations of the measurements are shown in figure 4.1.	52
5.2	Results of the Modified Philippe Dunne infiltrometer for the 3 tests surrounding Mariotte 1.	52
5.3	Grain size distribution of the soil samples collected in relation with the Mariotte cylinder infiltration measurements 1-5 (5.9.20 and 6.9.20). The locations of the measurements is shown in figure 4.1.	53
5.4	Hazen methods result together with the Mariotte hydraulic conductivity.	53
5.5	Surface cover percentages of the Gaustad watershed found by investigations into the catchment using ArcGIS Pro.	57
5.6	Electrical conductivity (EC) in microsiemens/cm, pH and temperature (°C) for Gaustadbekken measured the 25.8.20.	60
5.7	Electrical conductivity (EC) in microsiemens/cm, pH and temperature (°C) for Sognsvannbekken measured the 26.8.20 and 31.8.20.	61
5.8	Electrical conductivity (EC) in microsiemens/cm, pH and temperature (°C) for Sognsvannbekken and Gaustadbekken measured the 3.4.20 by Anja Sundal (see map in fig. 4.7).	61
5.9	Electrical conductivity (EC) in microsiemens/cm, pH and temperature (°C) for Gaustadbekken and Sognsvannbekken right before the two rivers merges into Frognerbekken.	62
5.10	Results of the heavy metals analysis of Gaustadbekken within Gaustad watershed at several points during 25.8.20.	63
5.11	Cations of water samples from Gaustadbekken within Gaustad watershed 25.8.20 (see map in fig. 4.7).	64
5.12	Anions of water samples from Gaustadbekken within Gaustad watershed 25.8.20 (see map in fig. 4.7).	64
5.13	Alkalinity and pH of Gaustadbekken 25.8.20 (see map in fig. 4.7).	65
5.14	Electrical balance of the samples gathered in Gaustadbekken 25.8.20.	65
5.15	Results of Heavy metals analysis of Sognsvannbekken at several points during 26.8.20 (see map in fig. 4.7).	65
5.16	Cations of water samples from Risbekken-Sognsvannbekken 26.8.20 (see map in fig. 4.7).	66
5.17	Anions of water samples from Risbekken-Sognsvannbekken 26.8.20 (see map in fig. 4.7).	66
5.18	Alkalinity and pH of Risbekken-Sognsvannbekken 26.8.20 (see map in fig. 4.7).	66

## List of Tables

---

5.19	Electrical balance of the samples gathered in Risbekken-Sognsvannbekken 26.8.20. . . .	67
5.20	Results of Heavy metals analysis for the samples from Gaustadbekken weir and Sognsvannbekken taken the dates of 17.12.20 and 2.1.21 (see map in fig. 4.3). . . . .	67
5.21	Cations of water samples from Gaustadbekken and Sognsvannbekken collected by the location of the joining rivers (see map in fig. 4.3). . . . .	68
5.22	Anions of water samples from Gaustadbekken and Sognsvannbekken collected from the joining point of the two rivers (see map in fig. 4.3). . . . .	68
5.23	Alkalinity and pH for Gaustadbekken and Sognsvannbekken water samples (see map in fig. 4.3). . . . .	69
5.24	Electrical balance of the samples gathered at the joining point of Gaustadbekken and Sognsvannbekken 17.12.20 and 2.1.21. . . . .	69
5.25	Water budget of the entire Gaustad catchment as a natural situation before urban development vs. today's situation as a semi-urbanized area. . . . .	77
5.26	Water budget of the total Gaustad catchment for the semi-urbanized scenario (2018-2019) before and after the construction of the Life Science Building (LSB) has been completed. . . . .	78
5.27	Water budget for the Life Science Building site before and after completion of the construction as a total of both KW and RDI. . . . .	80
5.28	Water budget of the entire Gaustad catchment representing today's situation and climate scenarios RCP4.5 and RCP8.5 simulated together with a 15 % increase of <i>urban</i> sub-catchments. . . . .	81
6.1	Locations of the rivers Gaustadbekken (KV, SK, NBV, GBBS) and Sognsvannbekken (R, RH, AMV) related to urban degree, environmental classification status and electrical conductivity. . . . .	87

PART I

---

**Part one**

---





# CHAPTER 1

---

## Introduction

---

The world's population growth and urbanization is changing the natural water cycle, consequently altering the water budget (e.g. Antrop, 2004; DeFries and Eshleman, 2004; Feng et al., 2016; Göbel et al., 2004; Haase, 2009; Nix, 1994; Schirmer et al., 2013; Semadeni-Davies et al., 2008). An evident consequence of urbanization is the loss of infiltration areas and thus storage of water, leading to increased surface runoff and decreased evapotranspiration (e.g. Baker, 2009; Feng et al., 2016; Fletcher, Andrieu et al., 2013; Göbel et al., 2004; Herricks, 1995; Healy et al., 2007; Nix, 1994; Schirmer et al., 2013; Trinh and Chui, 2013).

The population of Oslo is projected to increase (Syse, 2018), causing the need for further development. The densification of impermeable surfaces combined with intensifying rainfall events is strongly contributing to the increase of surface runoff due to stormwater (NOU15:16, 2015). The stormwater can cause damage to infrastructure and lead to costly events, reflected in the 4189 million kroner paid by Norwegian insurance companies for damages related to water intrusions 2008-2014 (NOU15:16, 2015). This leads to the need for understanding the urban water budget (DeFries and Eshleman, 2004; Feng et al., 2016) and assessing the urban water management.

In urban areas such as the city of Oslo, parts of the surface water is led into a drainage system designed to collect rainwater runoff, domestic sewage and wastewater in the same pipe (combined sewer system). The age and condition of the drainage system is varying, and the dimensions might not always be sufficient. The water is meant to be led to a sewage treatment plant before being discharged to a water body, but in cases of heavy rainfall or snow-melt the capacity of the sewer system or treatment facility can be exceeded. Untreated water might be discharged into nearby water bodies as a result. With both intensity and frequency of precipitation expected to increase (e.g. Hirabayashi et al., 2013) combined with the urbanization creating more wastewater (Oslo kommune, 2018; Lindholm et al., 2008), incidents of untreated water being discharged from combined sewer systems are likely to increase (Nie et al., 2009).

Urbanization is closely linked with sources of pollution. Surface runoff from impermeable surfaces might collect pollution from both point and non-point sources in an urban environment, and has been the cause of deterioration of surface waters quality in several locations (e.g. Müller et al., 2020).

Changes to the water budget is important, as urban environments are vulnerable to floods and contamination by untreated wastewater. The infiltration capacity of a watershed is of relevance as it influences the amount of overland flow generated. To limit the urban impact on the water, applying solutions for delaying and detaining water in permeable areas are advised. This reduce the stress on the collection system and allows for natural processes to clean the water, ultimately decreasing the urban effect on water bodies (Hood, 2006).

To implement sufficient water management in urban areas, a reliable water budget must be in place (Healy et al., 2007). There is thus a need for assessing the impact of climate changes on the water budget (Feng et al., 2016; Welty, 2009). The effects of the climate changes in Oslo combined with further urban development is therefore important to investigate. The changes might be especially evident in areas of rapid urbanization, and the Life Science Building (LSB) presently

under construction at Gaustad is an example of such an area. An evaluation of the effects urban development has on a local water budget in Oslo might be a contribution in the efforts of understanding the anthropogenic impact on the water cycle.

### 1.1 Objectives of the study

- Estimate the infiltration capacity of the Gaustad watershed.
- Investigate the correlation between urbanization and water quality of Gaustadbekken and Sognsvannbekken.
- Make a hydrological model of the Gaustad catchment using Mike+.
- Create a water budget for the Gaustad catchment, estimating the urban impact on the water budget.
- Investigate the impact the new Life Science Building might pose for the water budget, and estimate the local effects on the hydrologic situation at the site of construction.
- Evaluate the effect of increased urbanization in combination with projected climate changes.

## CHAPTER 2

---

# Theoretical framework

---

The theoretical background presents important and relevant terms and concepts, such as the water cycle, urbanization and urban water systems. The theoretical background also provides an introduction to the software that will be used to model the hydrological situation of the study site and investigate the effects of urbanization on the water budget.

### 2.1 Water cycle

The water cycle (fig. 2.1) describes the circulation of water in a system and is both applicable on a local and global scale. There are three main pathways; precipitation, evaporation and water vapour in a continuous process of water transported through different phases. The water near the Earth's surface evaporates to the atmosphere before being returned to the oceans by precipitation, surface runoff and groundwater flow (e.g. Appelo and Postma, 2005; Hiscock, 2009).

Within the water cycle evaporation must equal precipitation. In a global perspective this is true, average global precipitation rate = average global evaporation rate =  $496\,000\text{ km}^2\text{a}^{-1}$ . This is, however, not the case for most local water budgets. The imbalance is compensated for by oceanic water vapour transported to land masses, river runoff to the oceans and some direct groundwater discharge to the oceans (e.g. Hiscock, 2009).

The groundwater level is dynamic and dependent on the seasonal variations. It can provide input to rivers and lakes if they lie below the groundwater table (Dingman, 2015; Healy et al., 2007).

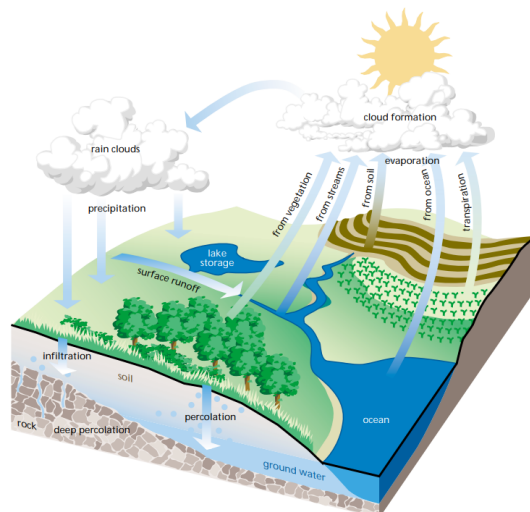


Figure 2.1: Illustration of the hydrologic cycle with the waters pathways. Figure from The Federal Interagency Stream Restoration Working Group US (2001).

### Water budget

To create a water budget for a watershed, it is necessary to consider the mechanisms that would potentially attenuate or delay the water flow above and below the ground surface, as well as the way the water moves with the topography (Freeze, 1974; Kirkby, 1988; Natural Resource Conservation Service, 2001).

The water budget describes the volumes of the components in the water cycle over a chosen time interval. Assuming the catchment is equal for both groundwater and surface water, the water budget can be calculated using the equation 2.1 (Hiscock, 2009; Welty, 2009). In a natural system, the water budget is found by defining lateral control volumes by the boundaries of the topography (precipitation catchment area) as well as vertically from the top of the vegetation to the bottom of the groundwater in the subsurface (Welty, 2009).

$$Precipitation = Runoff + Evapotranspiration + Net\ Groundwater\ outflow + \Delta Storage \quad (2.1)$$

### Precipitation and evaporation

Precipitation is the element of the water cycle of highest importance, and may fall as rain or snow depending on the air temperature (Ødegaard et al., 2014). Precipitation can be intercepted by vegetation, run off on the surface, or infiltrate through the soil and be stored in the subsurface.

Evaporation is water which, due to temperature and solar radiation, vaporizes to the atmosphere. Wind systems can then transport it to landmasses where it falls as precipitation (e.g. Hiscock, 2009; Klæboe, 1957). This is in natural settings the second largest component of the water budget (Feng et al., 2016; Trinh and Chui, 2013), but is difficult to parameterize. Potential evapotranspiration is the amount of water that could vaporize, while the actual evapotranspiration is the water that based on local parameters actually is removed to the atmosphere. It is an important and large contributor to the redistribution of water and energy at the soil-vegetation-atmosphere interface (Velpuri et al., 2013). Evaporation rates might also influence the water quality, as water evaporates in its clear state and thus leaves the chemical composition of the water more concentrated (Appelo and Postma, 2005).

It is acknowledged that urban areas has a significantly decreased evaporation due to the loss of vegetation and natural storage of water compared to natural areas. Dupont et al. (2006) found that with a storage capacity of 0.25-0.5 mm for urban surfaces such as roads and buildings, the evaporation decreased from 54.3 % on natural surfaces to 3.7 % for the urbanized areas.

### Infiltration and groundwater recharge

Infiltration is the process of water moving vertically from the surface through the soil profile. The infiltration of surface water through the soil depends on the permeability of the material and the saturation previous to the rainfall. At the point where the soil is saturated, the water will collect in small low-lying parts of the area before surface runoff removes the water (Ødegaard et al., 2014). Infiltration of surface water down to the groundwater usually begins in the fall, and ends in the spring (Appelo and Postma, 2005). During warm summer months there might be no infiltration as the actual evapotranspiration is at its highest, while frozen ground can prohibit infiltration in the wintertime. Infiltration is a complicated component of the water budget both in natural and urban areas, mainly due to heterogeneity of the soil.

The groundwater aquifers serve as storage potential of the water, prolonging the cycle. The recharge happens through surface water reaching the permanent water table, either by direct contact or downward percolation through the unsaturated zone (Hiscock, 2009). In urban areas the infiltration may differ greatly from natural situations due to impermeable surfaces (Baker, 2009; Feng et al., 2016; Fletcher, Andrieu et al., 2013; Göbel et al., 2004 Healy et al., 2007; Schirmer et al., 2013; Trinh and Chui, 2013). Urbanization of a natural area can also cause the water percolating through the soil to collect contaminants and exaggerated amounts of minerals, consequently polluting the aquifer.

The link between the surface hydrology and hydro-geology illustrates the need for knowledge in both disciplines in how to build a realistic water balance (Hiscock, 2009).

### Surface runoff

Surface runoff is the water running off on the surface due to higher precipitation rate than evapotranspiration and infiltration. The amount of surface runoff generated is also strongly dependent on the surface cover and inclination (Ødegaard et al., 2014). In urban areas where developed areas are dominating, the surface runoff increase by lack of infiltration sites (Healy et al., 2007), and the water is usually dealt with by redirecting it to either a separate or a combined sewer system (Ødegaard et al., 2014). The impervious area hydraulically connected to a drainage system is called "the effective impervious area", while impermeable surfaces where surface runoff is being directed towards an area that allows for infiltration is considered "ineffective" or "disconnected". The residence time of surface runoff will depend on the degree of impermeable surfaces as well as the contributing areas connectivity to an urban drainage system (Shuster et al., 2005). As figure 2.2 illustrates, the residence time is thus a function of the degree of impermeable surfaces combined with the connectivity to a collection system or a permeable field. If surface runoff generated from impermeable surfaces is directed to an area allowing infiltration, the concentration time is prolonged and infiltration might be ensured. If the surface runoff is drained to a collection system, the residence time is reduced (Shuster et al., 2005).

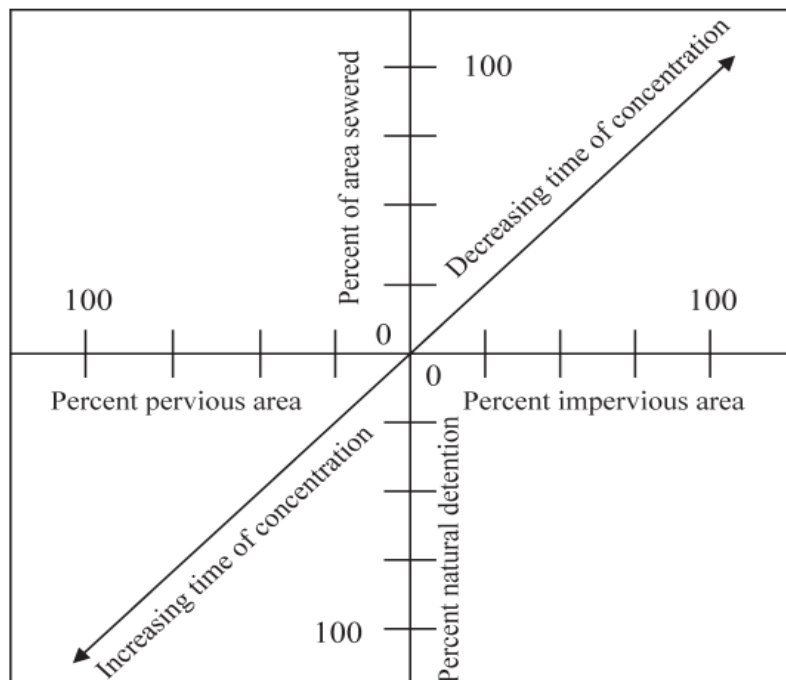


Figure 2.2: Runoff concentration time as a function of the degree of impermeable surfaces and collection system network connectivity. Figure from Shuster et al., 2005.

### Interaction between surface water and groundwater

Hydrology can be defined as the study of water and its movements on the surface of the earth. Hydrogeology is defined as all occurrence, distribution, movement and geological interaction of water in the Earth's crust (Hiscock, 2009). Hydrology and hydro-geology is closely connected through the water cycle and interact depending on local properties. In areas of shallow groundwater table, surface streams might be fed by the groundwater, keeping a steady flow even in dry periods.

To look at hydrology and hydro-geology as two separate cases is inapplicable when trying to find the anthropogenic impact on the aquatic environment. A holistic view of the Earth's water is important when looking at the effects of human activities such as pollution, over-exploitation and climate changes (Hiscock, 2009; Younger, 2009). To do this, the water cycle is an important base (Hiscock, 2009). The importance of collaboration between the hydrologists and hydrogeologists are evident in the fact that it is almost impossible not to affect the groundwater when changing surface water components (Younger, 2009).

### **2.2 Urbanization**

Urbanization is the process of humans developing natural spaces into urban areas, with people moving permanently from rural areas to relatively small areas (e.g. Chaolin, 2020). This involves changing natural vegetation into impermeable surfaces such as roads and houses, and building infrastructure to support an urban human lifestyle. The development of rural areas into urban cities has an enormous impact on the natural habitat and ecosystems, as well as altering the local water budget.

The removal of infiltration areas by introduction of impermeable surfaces results in increased runoff, less infiltration and evapotranspiration and a lowered water quality (e.g. Healy et al., 2007; Trinh and Chui, 2013). To adapt for construction, streams and rivers has to a large extent been placed in underground pipe-systems, collecting surface water and removing it from the city streets. The urbanization thus effectively alters the natural water balance, as the water ways are altered compared to the natural situation.

#### **Urbanization of Oslo**

Norway's most intensive period of urbanization was the years after 1850, where Oslo (then Kristiania) increased from 65 000 inhabitants in 1860 to 330 000 in 1920 (Myhre, 2015). The area of Gaustad has had substantial development in the years 1937-1971 as illustrated in figure 2.3. The site of the Life Science Building presently under construction is marked by an orange oval circle. The city of Oslo has kept increasing, and by the year 2020 housed 676 813 inhabitants.

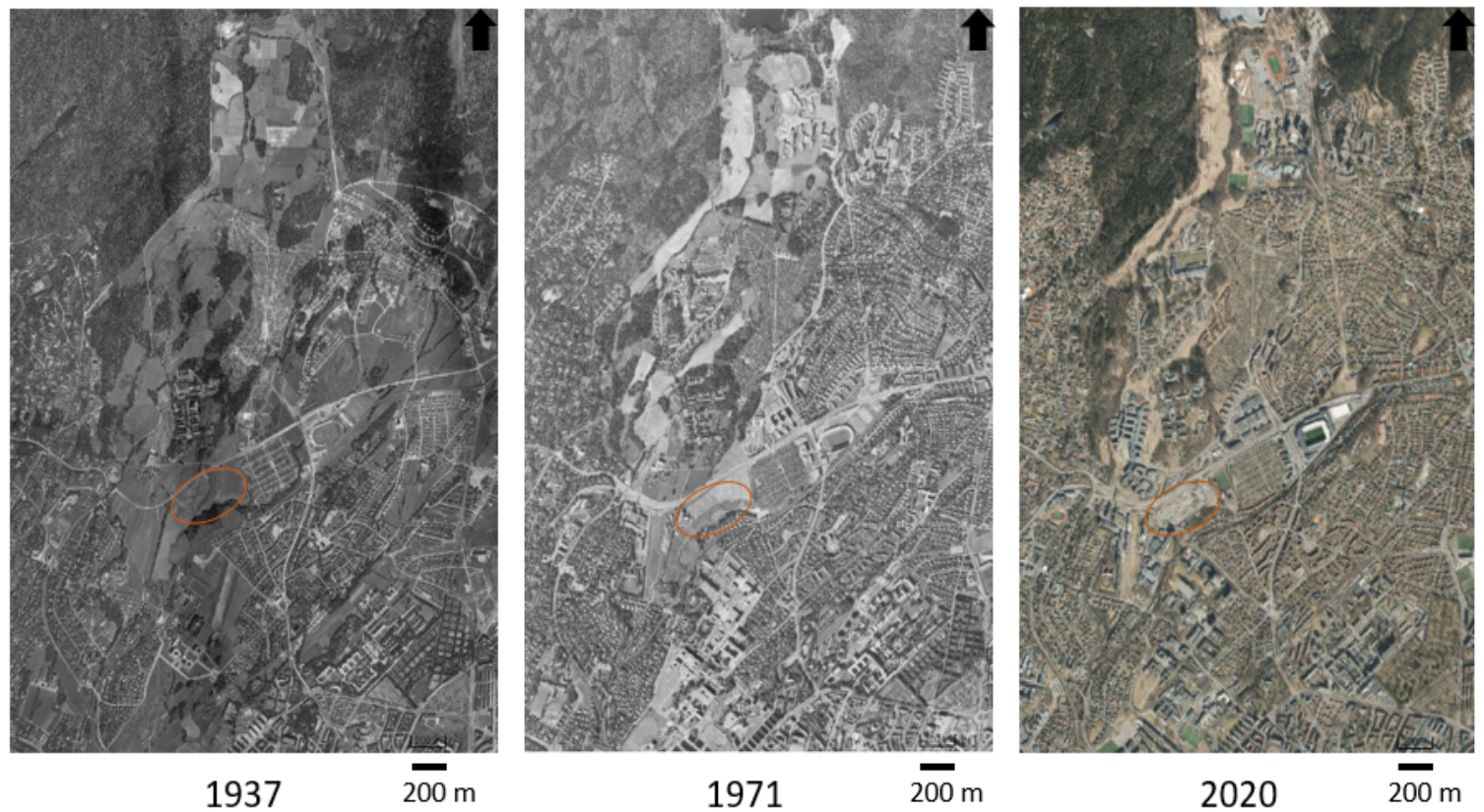


Figure 2.3: Historic photos of Gaustad, Oslo, illustrating the urban development. The site of the Life Science building is marked by an orange circle. Historic photos from Finn.no.

## 2.3 Urban hydrology

### Urban water cycle

Booth et al. (2002) found that the hydrology, morphology and aquatic biota of streams are seriously affected when 10-20 % of the watershed is covered by impervious surfaces. Urbanization of an area changes the characteristics of a watershed, resulting in numerous changes to the natural water paths. The water flow paths might be either shortened or lengthened related to the surface cover and degree of connection to the urban drainage system (Herricks, 1995), or they could be changed altogether (Welty, 2009).

### Urban water budget

The urban water budget is more complicated than the natural situation, as city infrastructure can move water across natural flow boundaries (Welty, 2009). The urban wastewater system can transport great amounts of surface water out of the system, and snow might be removed during wintertime. The urban water budget can be expressed as equation 2.2 (Welty, 2009).

$$\begin{aligned}
 & \textit{Precipitation} + \textit{Net Potable Water Imported} \\
 & + \textit{Net Wastewater Imported} + \textit{Net Stormwater Imported} = \textit{Runoff} \\
 & + \textit{Net Groundwater Outflow} + \textit{Evapotranspiration} + \Delta \textit{Storage}
 \end{aligned}
 \tag{2.2}$$

## 2. Theoretical framework

---

where Net Water Imported is water imported minus exported by pipe-systems. In an urban catchment there can be several combinations of systems importing or exporting water across natural boundaries (e.g. groundwater withdrawal, drainage systems), which can cause a net loss or gain compared to a system without urban impact (Welty, 2009).

The urban water budget is, however, difficult to quantify due to the complexity of the urban system (Feng et al., 2016). In cases of extreme urbanization and extensive subsurface pipe-systems crossing natural catchment boundaries, it might even be appropriate to define sewersheds for water management practices (Welty, 2009).

### **Urban collection system and sewage network**

Oslo city has an intricate network of rivers and waterways both on the surface and in the subsurface. The urbanization of the city has resulted in the closure of rivers into pipelines under the city's surface. The pipelines that were built to stand the amount of sewage and stormwater in the 1950s might now experience too much pressure, with the resulting floods and leakage. During heavy rainfall, the sewer-system can be overloaded and cause contamination of the rivers and the fjord (Oslo kommune, 2013).

The sewer in Oslo city is transported through both separate and combined sewer systems. Separate sewer systems (also called sanitary sewer systems) is a system of two separate pipelines, one carrying the stormwater from drains to nearby streams, and one that carries the sewage to a wastewater treatment facility. The combined sewer system, however, has one pipeline transporting both the sewer and stormwater. The water is collected by stormwater drains and households into the same pipe which is brought to, and cleaned at, a wastewater treatment plant before the release into a suitable water body. This solution is sensitive to heavy rainfall and can experience overflow, which cause untreated waters to be released into streams or other water bodies (combined sewer overflow, CSO). The overflow of combined sewer systems poses a threat to the health of the communities as well as the ecological state of the waters. It is therefore of concern in several cities as the amount of precipitation is increasing, while the natural infiltration of surface water is decreasing due to the development of impermeable surfaces.

The collection system of Gaustad watershed is shown in figure 2.4, revealing there to be a substantial amount of combined system. Some of the surface water drainage system is not functioning as a separate system, as it is in contact with the combined system (see fig. 2.4). There are several points of discharge from the combined sewer system into Gaustadbekken, posing a risk of CSO incidents in cases of heavy rainfall.

In 2014, a report from the Norwegian Food Safety Authority (NFSA, Mattilsynet, 2014) on the sewage system in Norway was issued. The status of the collection system of Norway was assessed, stating that leakage from the sewer system could cause contamination of receiving water bodies and even the drinking water network. This report was an important step in aiming for a better water supply and sewer system network, but there is still work to be done.



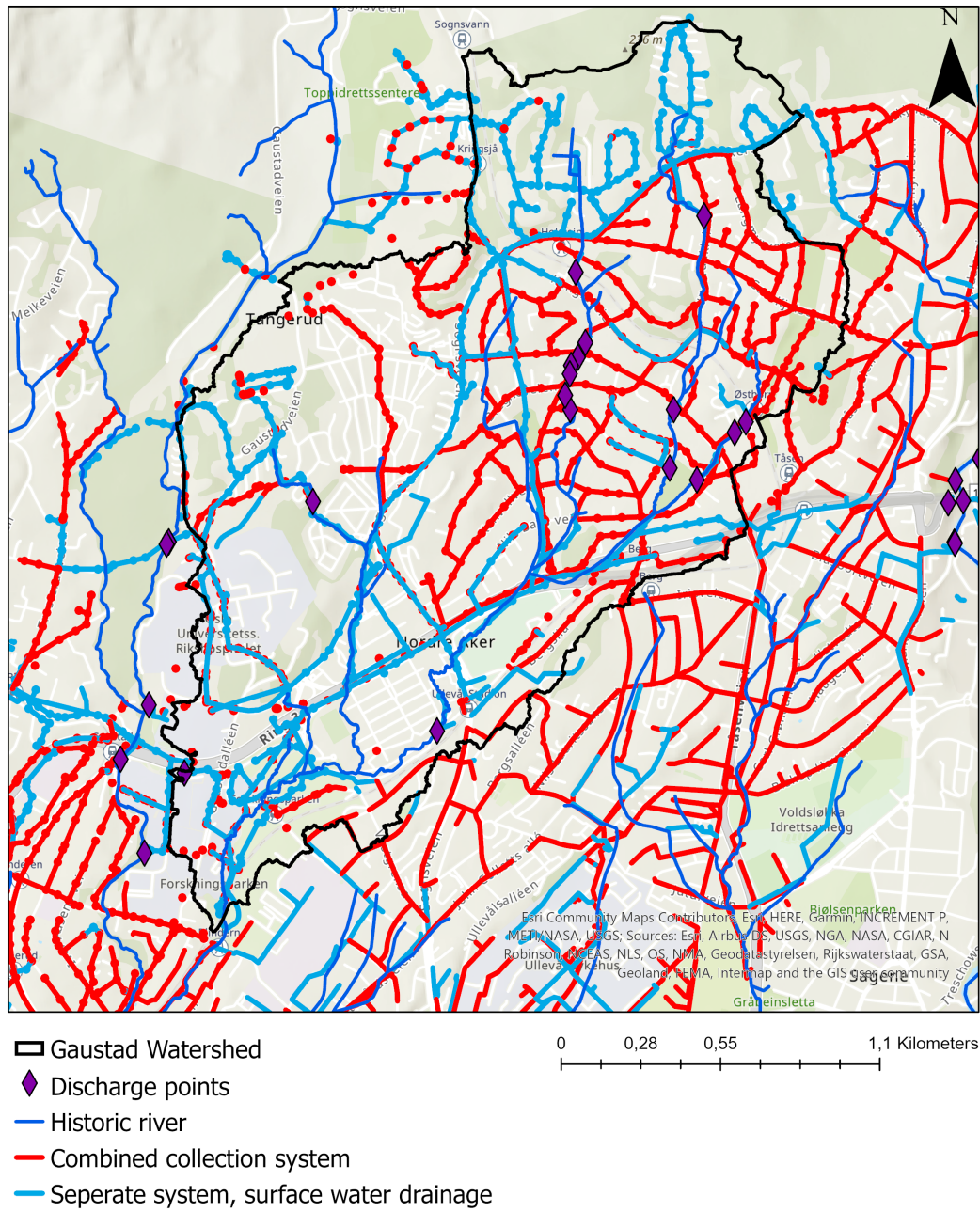


Figure 2.4: Combined and separate drainage system of Gaustad watershed, showing points of discharge within the watershed. Data supplied by Oslo municipality (VAV).

## 2.4 Stormwater management

Norway is a country with varied topography and large amounts of surface water. With this comes challenges. It is therefore established ways of stormwater management in urban areas, an important step in adapting to the future climate.

Events of heavy precipitation is expected to increase in intensity and frequency, causing a heavier load on the existing stormwater management solutions in Oslo. The climate changes demand stormwater management using a different approach than the traditional collection system, as the increased amount of water causes the velocity to increase and thus erosion of the river beds. To deal with the future stormwater, Oslo's "Klimaprofil" (Norsk KlimaServiceSenter, 2021) suggest adding a climate factor for dimensioning of measures. In an effort to manage the stormwater challenges in the future, a guide for climate-adapted stormwater management has been developed (Lindholm et al., 2008).

The stormwater flood-ways (drainage lines) in Oslo city shows a clear tendency to follow historical streams in the terrain (Oslo kommune, 2013, fig. 2.5). To a large extent, the historic waterways are today covered with impermeable surfaces, creating a need for handling of the surplus water to avoid it causing problems in regards to the infrastructure of the city, and leakage of contaminants.

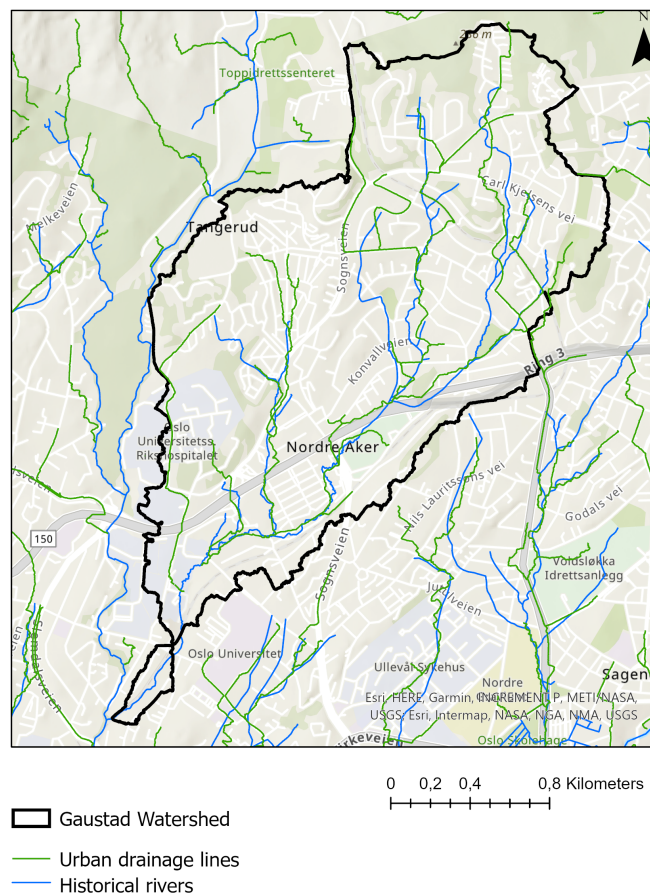


Figure 2.5: Drainage lines and historical rivers of the Gaustad Watershed. Data provided by the municipality of Oslo (VAV), map created in ArcGIS Pro.

Oslo has a green-blue vision for further development and aims to re-open closed rivers and brooks. Stormwater is to be dealt with in a three step strategy: infiltrate, delay and retain, and ensure

safe flood-paths (see fig. 2.6) (Lindholm et al., 2008; Oslo kommune, 2013;). Green areas, rainbeds and permeable surfaces will serve as areas of infiltration to which runoff can be directed to from impervious surfaces. When the rain is too intense for the soil to infiltrate sufficiently, the water is to be collected in suitable areas and detained. These solutions provide green and blue inputs in the city and are considered to increase the recreational value of the city. An example is the artificial stream by Forskningsparken, shown in figure A.10. The last measure for dealing with stormwater in cases where the two first steps are not enough, are safe flood paths for the water into the fjord. The flood ways for the water is to be secured so as to not damage infrastructure or be a source of unnecessary contamination (Oslo kommune, 2013).

Lindholm et al. (2008) suggests rainfall limits for the three steps of stormwater management (step 1:  $< 20$  mm, step 2:  $>20$  mm and  $< 40$  mm, step 3:  $>40$  mm). These intervals of precipitation are, however, not easy to use as it does not account for the duration of the rainfall. 20 mm over the course of a day is not dramatic, while 20 mm in 15 minutes might pose a significant risk of flooding and cause large amounts of surface runoff. In practice, step 2 and 3 of the strategy is typically applied for rainfall events of frequency 20 and 200 years. Step 1, however, is meant as a measure to deal with daily rain and to ensure that the water balance is not altered more than necessary (Paus, 2018). When planning for these measures it is important to account for the probable climate changes through the climate factor (Paus, 2018) as described in (Norsk KlimaServiceSenter, 2021).

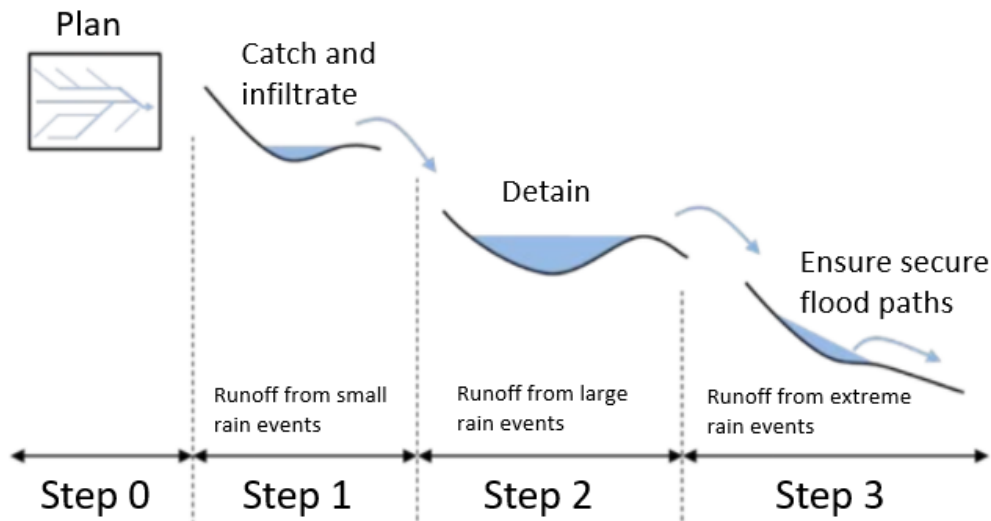


Figure 2.6: Strategy of surface water handling in Oslo as proposed by Paus (2018) on the base of Lindholm et al. (2008). Figure adapted from Paus, 2018

### Low Impact Development (LID)

Low Impact Development (LID) is a term used to describe the strategy of dealing with surface runoff from impermeable surfaces by infiltrating or delaying the water as close to its origin as possible (Endresen, 1998). The LID practices aims to preserve, restore, and create green and blue areas in cities as a measure for infiltrating and detaining water, as well as creating recreational spaces for inhabitants.

There are several terms describing the strategy of sustainable urban water management. The low impact development (LID) term appeared in 1977, sustainable urban drainage systems (SUDS) was introduced in 1997, water sensitive urban design was discussed in 1994 and 2007, best management practices (BMPs) in 1949, alternative techniques in 1980s and green infrastructure (GI) in the 1990s. In northern countries like Sweden and Norway, the term "Local handling of stormwater" (Lokal overvannshåndtering, LOD) is frequently used (Fletcher et al., 2015). These terms are slightly

## 2. Theoretical framework

---

different and might incorporate local needs and knowledge. They are, however, all based on the principles of limiting the urban effects of the water regime and improving the water quality (Fletcher et al., 2015). For simplicity the term LID will be used in this study.

LID solutions can ensure less erosion along the waterways and less stress on the collection system. The water being infiltrated and/or delayed will also let natural processes clean the water (Hood, 2006), and can thus improve the biodiversity (Endresen, 1998). The hydrograph in areas where LID measures have been implemented resembles a natural situation as opposed to an urban area without any measures taken (Hood, 2006).

### Climate changes

The International Panel on Climate Change (IPCC) states in their fifth report (AR5) there has been a 0.85 global increase in temperature ( $^{\circ}\text{C}$ ) on land and in the ocean from the year 1880 to 2012. The climate changes is causing alterations to natural systems such as hydrologic properties and terrestrial and aquatic eco-systems. Changes in extreme weather events has been observed since the 1950s, including an increase of heavy precipitation events. IPCC has worked out different scenarios of climate change to be used by decision makers, and for dimensioning of infrastructure and other measures. There are four scenarios of climate impact depending on emissions scenarios. These are explained in detail in the fifth report from the IPCC (Pachauri and L. Meyer, 2014) by the names RCP2.6, RCP4.5, RCP6 and RCP8.5 (RCP = Representative Concentration Pathway). The scenarios depend on the political will to cut anthropogenic emissions and assumes that no major volcanic eruptions adds to the effect of the human impact of the climate. The climate change scenarios show the expected outcome of different emission scenarios, and for all RCP4.5, RCP6.0 and RCP8.5, the aim of not exceeding a temperature increase of  $1.5^{\circ}\text{C}$  is not likely to be achieved. In Scenario RCP2.6, however, it is likely that the temperature will not increase with more than  $1.7^{\circ}\text{C}$  (Pachauri and L. Meyer, 2014).

## 2.5 Hydrologic model

### Hydrologic modelling

To simulate components of the hydrological cycle, hydrological models can be applied. As heterogeneity and uncertainties characterize the hydrologic properties in nature, a hydrologic model aims to represent the natural setting and systems as well as possible (Ogden, 2021). A hydrological model can be either lumped, distributed, or a combination of the two (semi-distributed). By applying a lumped model, the spatial variability is not considered and thus the heterogeneity of the model will be reduced. A distributed model uses geospatial data which will represent the characteristics of the site in its computation of hydrological processes and water budgets. Spatial variation such as terrain, soil, surface cover, precipitation and other important parameters are therefore considered in a distributed model, while a lumped model will use a spatially averaged data-set for the entire region in question. A semi-distributed model divides the catchment into sub-catchments to comprehend more of the complexity of the system. Each of the sub-catchments are lumped, but the spatial variability will be better accounted for through the diverse sub-catchments.

### Calibration and validation

The calibration of a model is important to ensure the models quality. When calibrating, observed values are compared to simulated values produced by the model. The parameters of the model are changed to obtain the best possible correlation between the simulated and the observed data (Dingman, 2015). Most programs offer an automatic optimization of the parameters, which uses an objective function as a measure of quality and aims to fit the parameters of the model for best possible correlation between the observed and simulated values. The automatic optimization method is quick, requires little of the programmer and is purely objective. The method is not without its disadvantages though, as the algorithms assume the model parameters are mutually independent

which very often is not the case in reality. The method does not abide by laws of physics and in an effort to compensate for errors it might produce unrealistic parameter values (Lohani, 2018). Trial and error is another form of calibrating a model, which enables the modeller full control over the change of parameters. This method can be time consuming and allow for interpretation that might be wrongful. However, information about the catchment not loaded into the model, as well as personal knowledge, might enhance the quality of the model parameters. This is the most used and recommended method for complicated models, and will likely produce the most realistic parameter values and thus simulations (Lohani, 2018).

The calibration can be tested by the Nash-Sutcliffe Efficiency ( $NSE$ ) of the model, which describes how well the computed values correlate with the observed values. It can be calculated by equation 2.3, and is a value from  $-\infty$  to 1 (Nash and Sutcliffe, 1970).

$$NSE = 1 - \frac{\sum(Q_{obs} - Q_{sim})^2}{\sum(Q_{obs} - \overline{Q_{obs}})^2} \quad (2.3)$$

where  $Q_{obs}$  is the observed discharge,  $Q_{sim}$  is the simulated discharge,  $\overline{Q_{obs}}$  is the mean of the observed discharge.

The NSE reveals the difference between observed and simulated values at corresponding time steps (Nash and Sutcliffe, 1970), and according to Moriasi et al. (2007) the model simulation can be considered satisfactory if the NSE is above 0.5.

A statistical measure of estimating the simulation outputs efficiency is the coefficient of determination  $R^2$ , calculated by equation 2.4. An  $R^2$  value of 0 indicates no correlation at all, while an  $R^2$  value of 1 indicates the dispersion of the prediction is equal to that of the observations (Krause et al., 2005).

$$R^2 = 1 - \frac{\sum_{j=1}^m (P - \hat{P})^2}{\sum_{j=1}^m (P - \overline{P})^2} \quad (2.4)$$

where  $P$  is the observed values,  $\hat{P}$  is the estimated values,  $\overline{P}$  is the observed mean and  $m$  is the number of discharge peaks.

Another way of evaluating the calibration of the model is through the Root Mean Square Error (RMSE). The RSME is the standard deviation of the residuals, indicating how concentrated the data is around the line of best fit. The overall RMSE of the simulation is given by equation 2.5 (DHI, 2021b). A low ( $<1$ ) RMSE is considered to indicate a good correlation.

$$RMSE = \left[ \frac{1}{N} \sum_{j=1}^N [Q_{obs,i} - Q_{sim,i}(\theta)]^2 \right]^{\frac{1}{2}} \quad (2.5)$$

where  $Q_{obs,i}$  is the observed discharge at time  $i$ ,  $Q_{sim,i}$  is the simulated discharge at time  $i$ ,  $\theta$  is the set of model parameters to be calibrated and  $N$  is the number of time steps in the calibration period.

When the model is calibrated sufficiently, the model is validated. This is a process of analysing the performance of the simulation to find if it is satisfactory for the desired use. To validate the model, different data from what was used during the calibration, should be tested against simulated output (Stephenson and Freeze, 1974). To find if the model is truly satisfactory, a scenario close to what the model is intended to be used for should be simulated and compared to observed values different from the ones used in the calibration (Klemeš, 1986).

## 2.6 Mike+, Danish Hydraulic Institute (DHI)

Mike+ uses an holistic approach to urban water management (DHI, 2021d) and was therefore chosen for this study. It is an urban water management tool powered by DHI (Danish Hydraulic Institute) and is suitable for modeling water distribution systems, storm water drainage systems and sewer collection in both separate and combined systems in urban areas (DHI, 2021a). Mike+ is a relevant tool for dealing with the ongoing urbanisation in relation to water management. The software can also address climate change scenarios and lets the programmer focus on planning, designing and operating urban infrastructure with the aim of better understanding and management of urban water (DHI, 2021f).

### Model engine, MIKE 1D

Mike+ represents a discretized form (in time and space) of the continuous real-world system. The flows and water levels are calculated in discrete (grid) points (DHI Course material, 2021).

Mike+ uses the model engine MIKE 1D, which offers 4 different rainfall-runoff computation concepts; Time/area, Kinematic Wave, Linear Reservoir and the Unit Hydrograph Module. Each of the models uses different input data and model parameters, as well as applying different computation concepts. Each of the models can be run in combination with the Rainfall Dependent Infiltration model (RDI) to account for groundwater in the system. This study will apply the Kinematic Wave (KW) model together with the RDI model to simulate the hydrologic situation of Gaustad.

A properly calibrated and validated model in Mike+ can help create an urban water budget. Mike+ can also assess the water quality as well as sediment transport, but this was not the main focus of this study, and will therefore not be addressed in the modelling.

### Sewer water system

The collection system in Mike+ is a combination of nodes and structures, connected by links. The node types used were manholes and outlets. The network can be classified as combined, sanitary or stormwater systems, which will affect the inflow of water through the nodes. The flow in the network is computed with following assumptions; water is in-compressible and homogeneous, the cosine of the angle the bottom slope makes with the horizontal is 1, the direction of the water is parallel to the bottom i.e. vertical accelerations is neglected and a hydrostatic pressure variation along the vertical can be assumed. There is no acceleration of water perpendicular to the flow direction of a reach (DHI, 2021b p.49).

By these assumptions, the Saint-Venant equations can be derived from the Navier-Stokes equations as shown in 2.6 and 2.7. The *mass equation* or *continuity equation*, 2.6, is an expression for the conservation of mass. A volume of water  $\delta q$  is added in reach section of length  $\delta x$  and is balanced by increase in cross section area  $\delta A_{fl}$ . The *momentum equation* is an expression of the conversion of momentum as illustrated in 2.7 (DHI, 2021b p.50).

$$\frac{\delta q}{\delta x} + \frac{\delta A_{fl}}{\delta t} = q_{in} \quad (2.6)$$

$$\frac{\delta q}{\delta t} + \frac{\delta \left( \alpha \frac{q^2}{A_{fl}} \right)}{\delta x} + g A_{fl} \frac{\delta h}{\delta x} + g A_{fl} I_f = \frac{f}{\rho_w} \quad (2.7)$$

where  $q$  is discharge,  $A_{fl}$  is the flow area i.e. cross section area,  $q_{in}$  is the lateral inflow per length unit,  $h$  is the water level,  $\alpha$  is the momentum distribution coefficient,  $I_f$  is the flow resistance term in the form of a friction slope,  $f$  is the momentum forcing per length unit and  $\rho_w$  is the density of water.

The derivation of the Saint-Venant equations can be viewed in detail in DHI reference manual for Mike+ Water Resources, appendix A.1 (DHI, 2021b).

The Saint-Venant equations are solved in a finite difference scheme. This solution scheme is only applicable for sub critical flows with a Froude number less than 1. If the Froude number is above 1 it is considered a supercritical flow and a simpler approximation where non-linear terms are suppressed provides an accurate flow description (DHI, 2021b p.50).

The Saint-Venant equations are, however, only applicable for flows with free surface. This means that when the water in the pipes fill up, the computation for free surface is no longer valid. If the closed pipes are full of water, a fictitious slot in the top of the reach is introduced into the computation (DHI, 2021b p.50-51).

### Surface runoff routing

The surface runoff is a consequence of the effective precipitation, meaning the precipitation that is left after losses such as infiltration and evaporation has been accounted for. The Kinematic Wave rainfall-surface runoff model computes the surface runoff based on the kinematic wave computation, and depends on hydrological losses and the contributing area. The runoff is computed as in an open channel which accounts for gravitation and friction forces (DHI, 2021b p.209).

The catchment of the study site was divided into several (915) sub-catchments that each flow into a suitable manhole nearby. This allows for spatial variability such as surface cover, topology and soil properties. In the Kinematic Wave model (KW), the sub-catchments can be divided into five categories based on the surface cover properties, and only the relevant processes will be computed for the different categories. The total runoff for the sub-catchments is the sum of the surface water generated on the different types of surface covers (DHI, 2021b p.210). The five surface categories are *impermeable steep* or *flat*, and *permeable small*, *medium* or *large*. On the impermeable surfaces there is 100% contribution to surface runoff, while the permeable surfaces allow for infiltration computed through Horton's equation. The hydrologic parameters for each contributing area type can be edited, and sets the basis for the runoff computation. The *impermeable steep* fraction has no storage, while *impermeable flat* has some. The pervious surfaces are categorized after the infiltration potential, assigned as Horton's infiltration capacity, with Low, Medium and High infiltration capacity.

The shape of the surface runoff hydrograph will depend on the roughness, slope, and length of the catchments surface. Manning's number can be edited if necessary, or Mike+ uses suitable Manning's number for the specific surface type.

### Rainfall Dependent Infiltration (RDI)

The RDI module is a level of computing the rainfall-runoff which involves a continuous hydrological model Rainfall Dependent Infiltration. The input of the model (precipitation) is routed by four storage ways (snow, surface, unsaturated zone (root-zone) and groundwater) (see figure 2.7), and is therefore useful when longer time-series through both wet and dry seasons are modelled. The RDI can be combined with any rainfall-runoff model and will provide a platform for accurate and reliable computation of urban runoff (DHI, 2021c p.108). The RDI model, also known as NAM, can be characterized as a deterministic, lumped, conceptual model and is based on a set of linked mathematical equations (DHI p.167).

The concept of the RDI is two hydrological behaviours; FRC and SRC. FRC is the Fast Response Component, which comprise the rain induced inflow and fast infiltration. SRC is the Slow Response Component that comprises the slow infiltration. The FRC is not dependent on previous rainfall in terms of soil moisture, but acts as a direct consequence of a rainfall event. It will provide inflow to the sewer system as well as fast flow component of the infiltration (DHI, 2021c p.108). The SRC, however, is strongly dependent on hydrologic conditions previous to the rainfall event, and will have a slow reaction to the rainfall. It will ensure the remaining precipitation induced infiltration as well as infiltration between rainfall events.

## 2. Theoretical framework

---

When the surface storage ( $U$ ) is bigger than maximum capacity  $U_{max}$ , the surplus water  $P_N$  becomes either overland flow, or infiltrates dependent on the overland flow coefficient ( $CQof$ ). Some of the water available for infiltration ( $P_N - CQof$ ) goes to the soil moisture (lower zone storage), while the rest is assumed to percolate and recharge the groundwater storage (DHI, 2021b p.173).

### **Snow storage and melting**

The Kinematic Wave model accumulates snow when the temperature is below 0 °C, and melts at a rate given by the snow melt coefficient when a time series of temperature is provided (DHI, 2021b p.213).

The RDI model estimates the snow accumulation and melting depending on the air temperature (provided by the modeler as a time series dfs0 file). When the temperature is below 0 °C, precipitation will be considered snow and accumulated until the temperature is above 0 °C. At plus degrees the snow-melt begins, controlled by the snow-melt coefficient decided by the modeler (DHI, 2021c p. 121).

### **Model parameters and data requirements**

The Kinematic Wave model (KW) can be run together with the Rainfall Dependent Infiltration model (RDI) to account for both the surface runoff, as well as the fast and slow response after a rainfall event including interflow and recharge of groundwater. Mike+ generally works with SI units both for input and output data, with the exception of the time constants for the flow components in the RDI model.

### **Model specific data**

The length [m] of the catchment is the characteristic length of the sub-catchments. The model will assume a prismatic flow channel with a rectangular cross section and a channel bottom width resulting from the catchments area and length (DHI, 2021b p.210). The slope of the catchment represents the average slope of the catchment, and is used as a component in the Manning's equation for computation of the runoff (DHI, 2021b p.210).

### **Kinematic Wave model (KW) Parameters**

Wetting loss [m] represents the wetting of the surface of the catchments and is a one-off loss for each rainfall event. The Storage loss [m] represents the depressions of the catchment that is to fill up before surface runoff occurs, and is thus a one-off loss of precipitation as specified by the user. The storage is linked to the surface cover type, and Mike+ offers a range of default values for each of the cover categories. Start infiltration rate [m/s] and End infiltration rate [m/s] is the maximum and minimum rate of infiltration (Horton) for a specific surface type. The Wet Horton Exponent [ $s^{-1}$ ] is a time factor characteristic soil parameter. It is dependent on the surface cover type and determines the dynamics of the infiltration capacity rate reduction over time during rainfall events. The actual infiltration capacity is time dependent only from the beginning of the rainfall event. The Dry Horton Exponent [ $s^{-1}$ ] is, like the Wet Horton Exponent, also dependent on the surface cover type. The parameter is, however, used in the inverse Horton's equation, which determines the recovery rate of the infiltration capacity after a rainfall event. The Manning's number [ $m^{\frac{1}{3}}s^{-1}$ ] is a measure of the roughness of the surface in the catchments and is used in Manning's formula for the hydraulic runoff routing (DHI, 2021b p.211).

### **Rainfall Dependent Infiltration (RDI) parameters**

The RDI model accounts for surface storage capacity ( $U_{max}$ ), as well as the capacity of the lower root zone storage ( $L_{max}$ ). The  $U_{max}$  is important for evapotranspiration, and a reduction reduces the actual evapotranspiration.  $L_{max}$  controls several of the different water transports of the RDI



model, and a reduction of the  $L_{max}$  might increase the discharge. The overland flow coefficient ( $C_{Qof}$ ) represents the fraction of runoff going to overland flow, while the groundwater coefficient ( $C_{area}$ ) describes the relative size of the groundwater reservoir. The overland flow coefficient can be adjusted to fit the distribution of volume between peak flows and the baseflow of the model. A reduction in  $C_{Qof}$  will result in a reduction of overland flow while increasing the infiltration and consequently the baseflow. The  $C_{area}$  is a measure of the ratio between the groundwater catchment and surface catchment. When changing the ratio it affects the ratio of the baseflow and other runoff components as well.

Time constants are given for the overland flow component ( $CK$ ) [h], interflow ( $CK_{if}$ ) [h] and baseflow ( $BF$ ) [h] for the runoff component. The  $CK$  influence the shape of the peak flows, the  $CK_{if}$  decides the response of the interflow while the  $BF$  affects the response of the baseflow (build-up and regression).

Specific yield of the groundwater reservoir ( $GWSy$ ) corresponding to the porosity of the groundwater aquifer, the minimum groundwater depth ( $GWL_{min}$ ) measured from the surface, maximum groundwater depth causing baseflow ( $GWL_{bf0}$ ) estimating the bottom of the groundwater storage from the surface and the groundwater depth for unit capillary flux ( $GWL_{f1}$ ) are all controlling the groundwater aspect of the simulation DHI, 2021c.

Threshold parameters indicate at which relative water content of the root zone the overland flow, interflow and baseflow is caused. They will have no effect when the root zone storage is full. If appropriate, a snow-melt computation might be activated and given a snow-melt coefficient at which temperature snow-melt might occur.

The schematics of the RDI model is illustrated in figure 2.7.

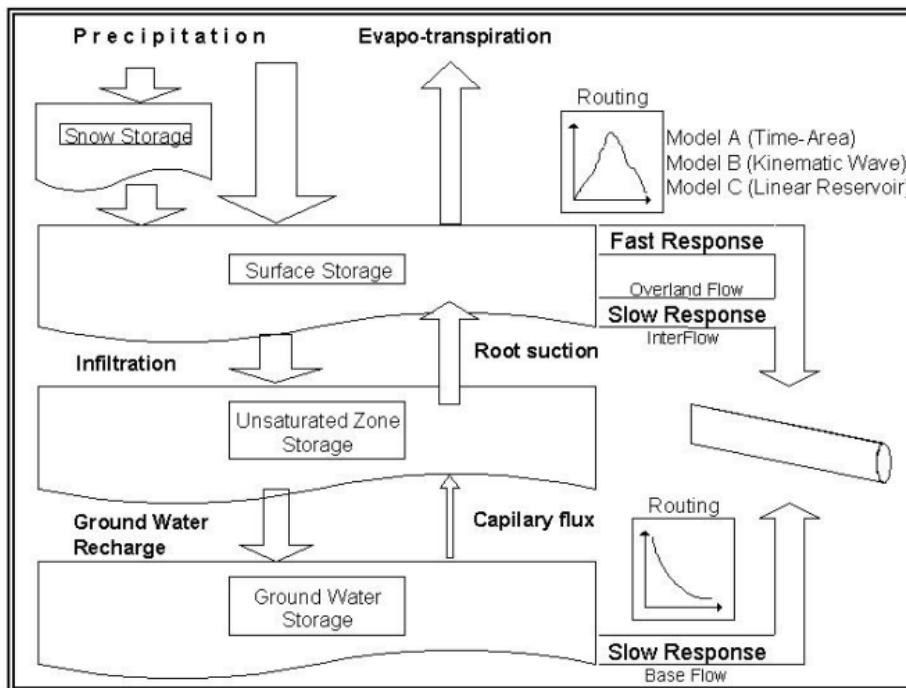


Figure 2.7: Schematics of the RDI module in Mike+. Figure from DHI (2021), p.109.



# CHAPTER 3

## Study area

Gaustad watershed was chosen because of its relevance in regards to urbanization of Oslo, both historically and ongoing. A new large building (Life Science Building), presently under construction, is a pilot case for evaluating the impact such development has on the local water budget. The study site is an area at Gaustad, Oslo, marked in figure 3.1.

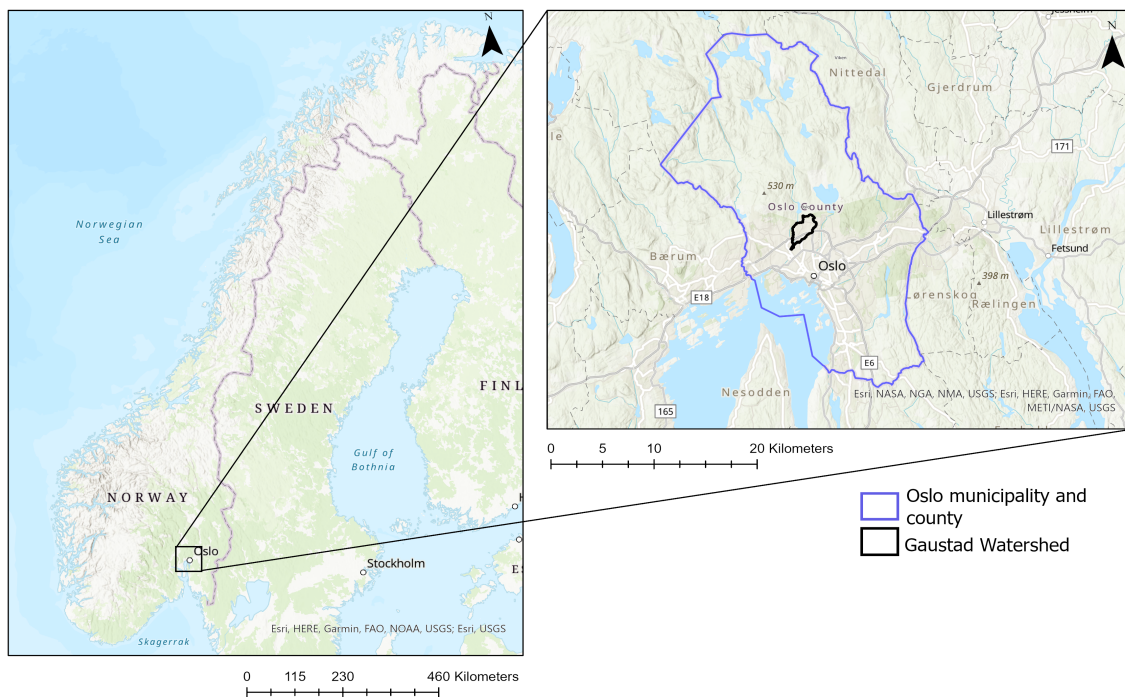


Figure 3.1: Overview of Oslo municipality and county and the Gaustad watershed. Map produced in ArcGIS Pro with managing units data from Geodata, and modeling of the watershed based on DEM data from Oslo Municipality.

### 3.1 Geography and climate

The area is characterized by villa buildings, parcel gardens as well as a football stadium and science institutions such as Forskningsparken and parts of Blindern Campus. Oslo's climate is classified as humid continental climate with warm summers and cold winters (Dfb by Köppen's classification

### 3. Study area

system (Peel et al., 2007)). The average temperature from 1971-2000 was 6.2 °C with annual precipitation of 755 mm (Norsk KlimaServiceSenter, 2021).

Through the catchment of Gaustad, the river Gaustadbekken is running both as surface streams and in closed pipes (see fig. 3.2). Gaustadbekken drains from Korsvoll, Gaustad, Sogn and Ullevål and formes the watershed illustrated in figure 3.1 and 3.2. The river was investigated in terms of discharge through a measurement series obtained by an Ott Orpheus mini water level logger device, and used to calibrate a hydrological model of the watershed. It was also of interest to have a look at the quality of the water in regards to pollution by urban development. The quality of Gaustadbekken water can be seen in comparison with the water of Sognsvannbekken as it is a river of similar properties, running through a less urbanized area. An overview of the rivers Gaustadbekken and Sognsvannbekken is provided in figure 3.2.

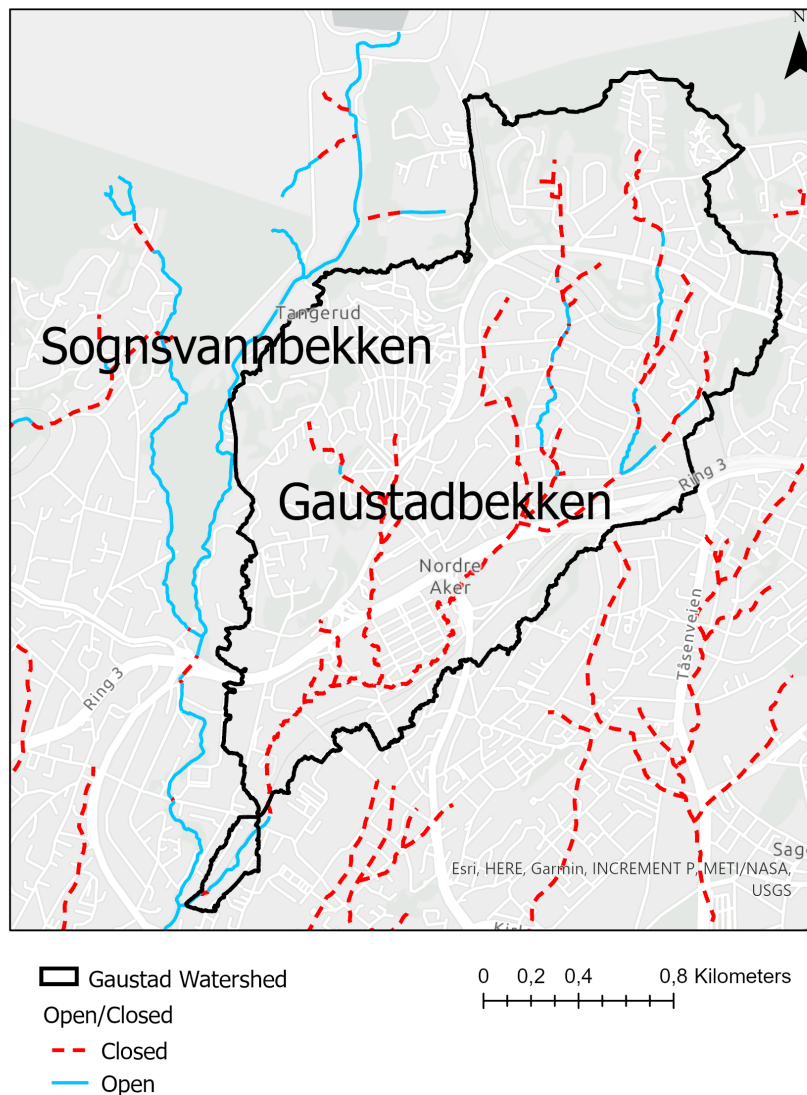


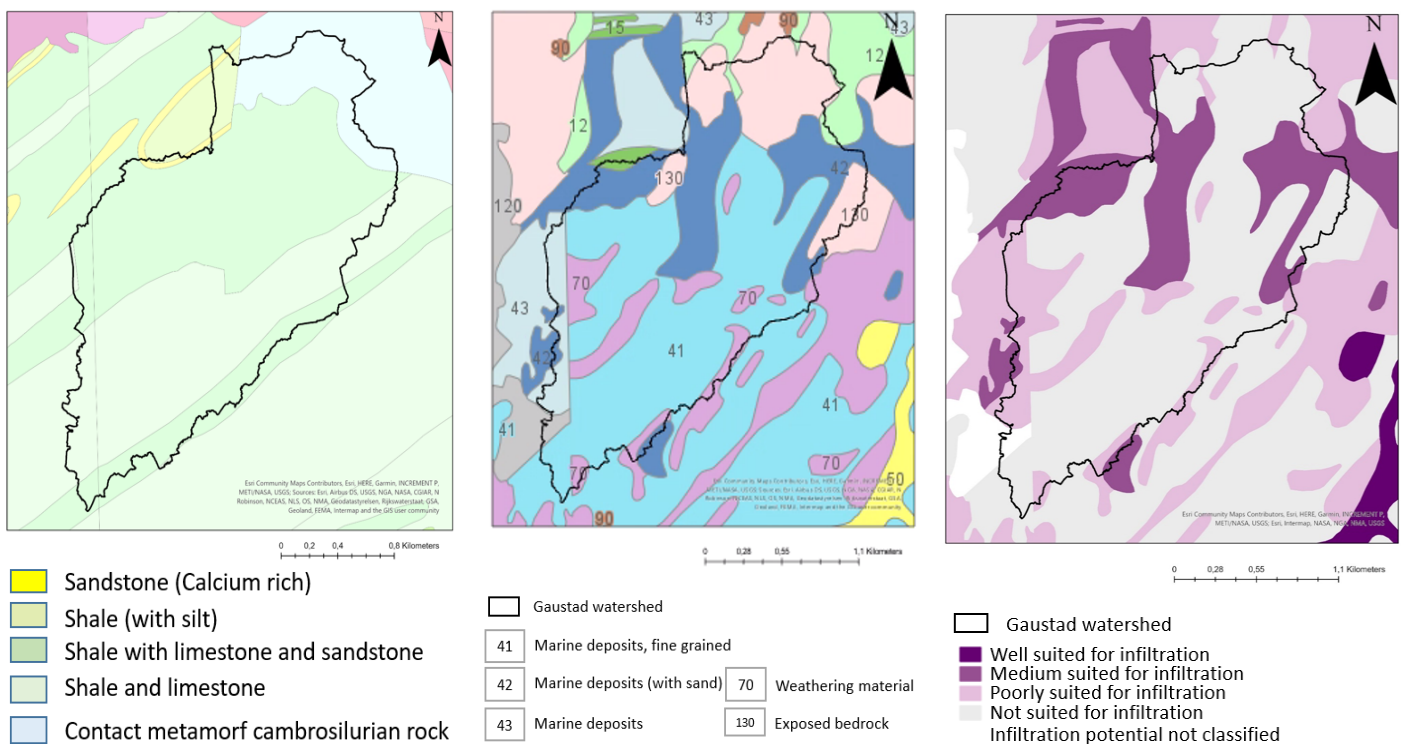
Figure 3.2: Open and closed systems of streams in Gaustad watershed. Figure produced in ArcGIS Pro, data from Oslo municipality.

Oslo's climate is as the rest of Norway experiencing an increase of temperature, and the prognoses for the future suggests a need for adaptation. January 2021, the *climateprofile* of Oslo and Akershus was updated (Norsk KlimaServiceSenter, 2021), providing a summary of the current climate situation and the challenges to come as presented by the fifth report from IPCC (AR5). It is created to be used as a tool when making decisions in relation to climate adaptation. It is intended to be used as guidance when dimensioning infrastructure and in risk analysis. An increased discharge of streams and rivers is expected in Oslo, as well as an increased risk of avalanches due to the increased precipitation (Norsk KlimaServiceSenter, 2021).

The annual precipitation in Oslo is expected to increase by 15 %, and a as general rule in project planning a climate surcharge of 40 % is advised when dimensioning for precipitation events of less than 3 hours (Norsk KlimaServiceSenter, 2021). More detailed description and climate factors can be found in the report by "Klimaprofilen", including modified specific Intensity-Duration-Frequency-curves (IDF-curves). The climate factors is a reflection of the expected changes from the baseline 1971-2000 to 2071-2100. The mean annual temperature is expected to rise with approximately 4 °C, with the highest change during winter causing the growth season in Oslo to be extended with about two months (Norsk KlimaServiceSenter, 2021).

### 3.2 Geologic setting

The Gaustad catchment has a bedrock of alternating shale and limestone from Cambro-Silurian time, with an overlying layer of marine deposits (Geological Survey of Norway B, 2020; Geological Survey of Norway C, 2020, fig. 3.3a and 3.3b).



(a) Bedrock at Gaustad watershed, data from NGU. (b) Quaternary deposits of Gaustad watershed, data from NGU. (c) Infiltration potential of Gaustad watershed, data from NGU.

Figure 3.3: Bedrock, quaternary deposits and infiltration capacity at Gaustad. Data from the Norwegian geological survey, figures created in ArcGIS Pro.

### 3. Study area

There are areas with filling material, and some till deposits on top of the bedrock (GrunnTeknikk AS, 2019). Igneous intrusions within the watershed also influence the catchments properties. The infiltration potential of the area is classified by NGU as shown in figure 3.3c, and can be viewed at their official website under the map of superficial deposits.

The urban progression of the area was conducted mainly in the years 1937-1971 (see fig. 2.3), a time where there were no real restrictions as to what could be used as material or how to dispose of it. There are therefore several areas within the watershed that have anthropogenic material on top of the quaternary deposits (ref. fig. 3.4), posing a risk of contamination.

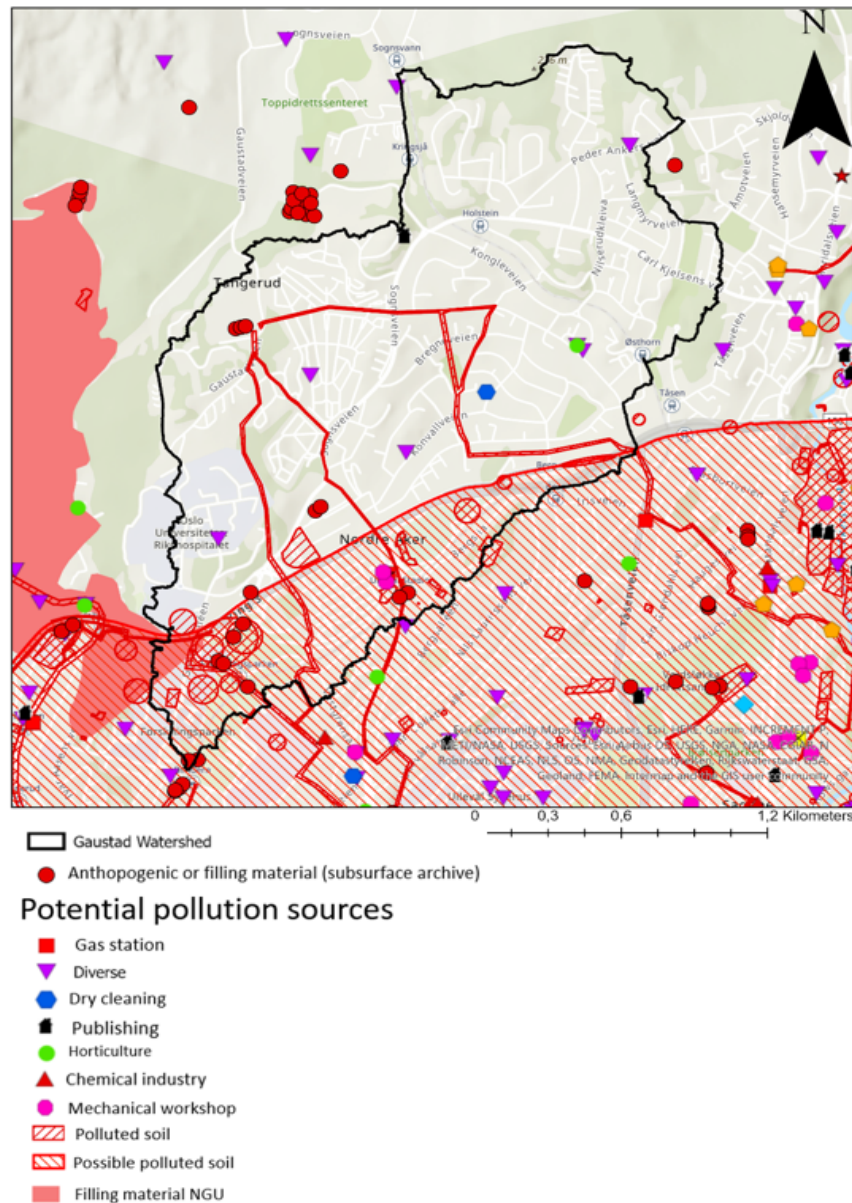


Figure 3.4: Documented contaminated or suspected polluted sites within the Gaustad Watershed (as recorded by NGU, the subsurface archive and the municipality of Oslo). The red lines are polluted soil as presented in the legend, but due to the areas being narrow it might be hard to see.

### 3.3 The area of the Life Science Building

The area of interest for this thesis (ref. fig. 3.1) includes a construction site for the new Life Science building at the University of Oslo. This kind of development affects the infiltration of surface water to the groundwater, and can change the water budget dramatically (Vázquez-Suñé et al., 2005). To prevent this, the project aims to adapt to the local water-situation by creating an open artificial branch of Gaustadbekken, hopefully reducing some of the impact this building will cause to the waterways of the area.

The LSB field was historically a ravine landscape used for agriculture. The site has since undergone severe alterations, and today consists of up to 8 meters of anthropogenic material containing waste products together with other unidentified material. Beneath the fill masses, there is quick clay and some till deposits on top of the bedrock (GrunnTeknikk AS, 2019). The building was planned to cover  $66\,700\text{m}^2$ , but might be expanded in relation to the University Hospital of Oslo (University of Oslo, 2021). The impermeable surfaces constructed for the building and relating development creates more surface runoff, water that might carry surface pollutants into the closest outlet. The infiltration to the groundwater could decrease, with the water level potentially lowered to a point where the pore pressure reduction will cause severe damage to the infrastructure.

Like large parts of the historical rivers in Oslo the water running on the site was redirected in a subsurface pipeline, with a capacity of about  $8\text{--}9\text{ m}^3/\text{s}$  (Erichsen Horgen AS, 2016). However, in line with Oslo's blue-green vision, the Life Science Building project will use water as a resource and include a small surface stream to enhance the exterior of the architecture. The stream will incorporate water flow up to  $1.4\text{ m}^3/\text{s}$  from a culvert at the north end of the site, and flow towards the south end of the area to a small pond. From the pond,  $0.2\text{ m}^3/\text{s}$  will be led through a system of stairs, fit for fish migration, towards an existing open creek. Any water flow above the  $0.2\text{ m}^3/\text{s}$  threshold will be redirected into the closed Gaustadbekken stream (Erichsen Horgen AS, 2016). The closed river pipe system in the subsurface is projected to have a capacity of  $10\text{ m}^3/\text{s}$ , sufficient for dimensioned 100 year floods. In cases of 1000 year floods ( $13\text{ m}^3/\text{s}$ ), however, the closed pipe system capacity is exceeded (Erichsen Horgen AS, 2016). The stairs system should be therefore be facilitated to endure a water flow of  $3\text{ m}^3/\text{s}$  when necessary to avoid damage and flooding of nearby roads.

The partial re-opening of the river together with the culvert constructed in relation to the LSB is an improvement, both visually and ecological. It also represents the vision of Oslo as it is opening for some of the water to flow on the surface, creating recreational space as well as letting natural processes such as UV radiation and microbiological cleaning of the water (Erichsen Horgen AS, 2016).





# CHAPTER 4

---

## Method

---

The infiltration capacity of the top-soil in the watershed was investigated to get an insight into the amount of water that could potentially infiltrate. Soil samples were taken to validate the findings by the infiltration investigation methods. Water samples of Gaustadbekken and Sognsvannbekken were gathered for comparison of the water quality between two rivers of similar properties, running through different degrees of urbanized area. A hydrological model was created to investigate the effects of urbanization in combination with climate changes. The water level at the Gaustadbekken weir was monitored in order to obtain a discharge series that could be used to calibrate the hydrological model.

### 4.1 Field methods

Locations of the infiltration measurements sites Solvang Kolonihage and Sognsvannveien is shown in figure 4.1. By investigating the infiltration capacity of these sites, the infiltration potential of the soil could be estimated. The locations were chosen to investigate the properties of the weathering material recorded by NGU (see fig. 3.3b).

#### Mariotte cylinder

To estimate the infiltration capacity of the top layer of the soil, both the Mariotte cylinder and Modified Philipe Dunne infiltrometer was applied at two locations within Gaustad watershed (fig. 4.1). The Mariotte cylinder was applied in September and November, 2020, to investigate seasonable variations. The Mariottes in November was applied at approximately the same locations as the ones in September.

The Mariotte cylinder simulates a steady state situation by the Guelph permeameter method. The Mariotte consists of an inner and an outer cylinder with plastic tubes connected to each outlet (fig. 4.2, A.6). The inner tube provides the air supply to the permeameter and the outer tube provides the water into the system (Reynolds and Elrick, 1986).

A hole of 25x25 cm was dug into the soil at the chosen locations before inserting a sponge to stabilize the walls of the hole. The Mariotte cylinder is supported by a tripod situated on top of the hole, with the two plastic tubes leading from the cylinders into the hole (fig. 4.2). Before starting the experiment the hole is saturated with water to a satisfying level.

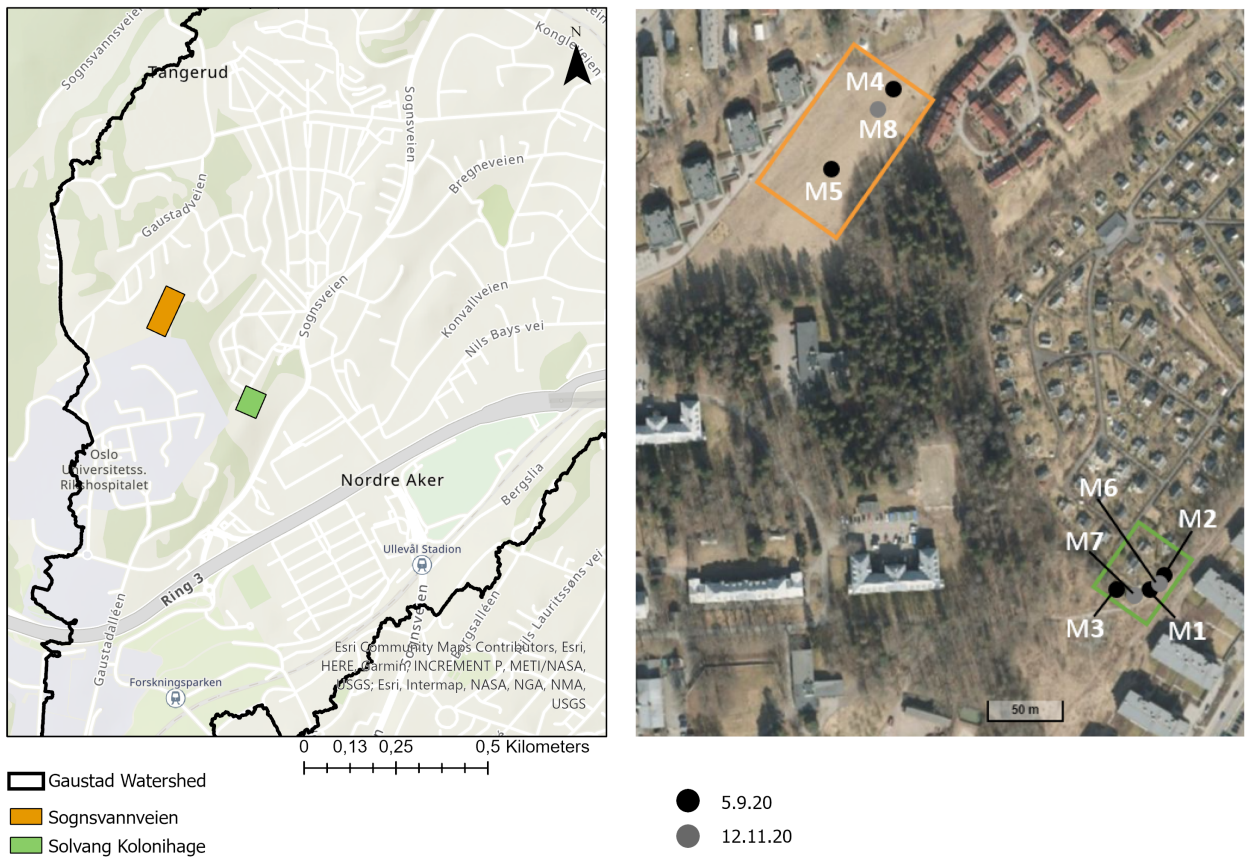


Figure 4.1: Locations of the fieldwork done to obtain information of the infiltration capacity and collection of soil samples. The locations are marked by the abbreviations M1-M8, corresponding to Mariotte 1 to Mariotte 8. Map on the left created in ArcGIS Pro, picture on the right from *Norgeskart.no*

When the cylinder is opened from the bottom, the experiment begins, and the outflow of water from the column (which equals the inflow of water into the system by the steady state principle) is marked as a function of the time spent. The saturated hydraulic conductivity ( $K$ ) can then found by the equation 4.1.

$$K = \frac{Q}{a^2 + 4ab} \tag{4.1}$$

where  $K$  is the saturated hydraulic conductivity ( $\text{cm/s}$ ),  $a$  is the length of the sides of the quadratic hole (25 cm),  $b$  is the constant water level in the hole, and  $Q$  is the measured water discharge out of the cylinder by the time interval (found by  $(\pi r^2 h)/\text{time}$ ) ( $\text{cm}^3/\text{s}$ ).

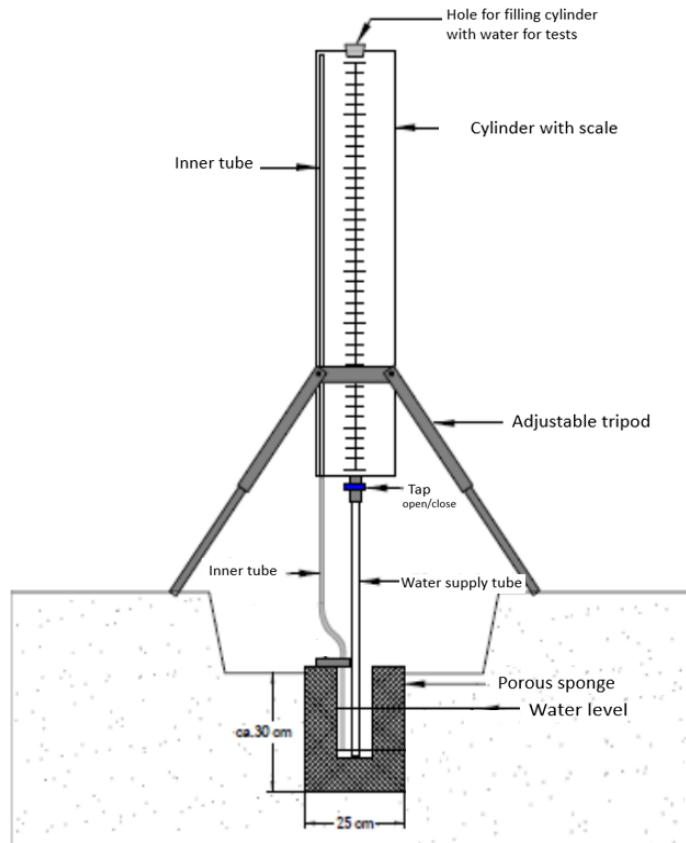


Figure 4.2: Illustration of the Mariotte cylinder, figure adapted from Mæhlum T and G.R. (2010).

### Modified Philippe Dunne falling head infiltrometer

To measure the infiltration capacity of the soil, the Modified Philippe Dunne falling head infiltrometer (MPD) can be used. According to Solheim et al. (2017) and Nestingen (2007), the Modified Philip Dunne infiltrometer is both a cost-effective and an efficient way of measuring the infiltration capacity in the top soil. The MPD was applied in three locations surrounding Mariotte 1 infiltration measuring point, to verify the findings of the Mariotte device.

The measuring begins when water is poured into the cylinder, and the change in the water volume is then recorded manually as a function of the time. This is used to estimate the saturated hydraulic conductivity ( $K$  [cm/s]) in the top soil by the equation 4.2 (Solheim et al., 2017).

$$K = \frac{\Delta h}{\Delta t} \quad (4.2)$$

where  $\Delta h$  is the change of water level in the cylinder between two measurements (cm) and  $\Delta t$  is the change in time (s) corresponding to the measurements.

## 4. Method

The structure of the MPD makes it very mobile and simple to use in field work. To operate the MPD, the only thing needed in addition to the device itself, is a timer and water. The MPD consists of a hollow PVC cylinder with a height of 50 cm and a diameter of 10 cm. Inside the cylinder is an attached measure tape so that one can easily read the change in water volume. The edge of the cylinder is rounded to ease the insertion into the top soil, in this case 5 cm. The depth of which the MPD is inserted will strongly affect the infiltration rate (Nesting, 2007), and thus it is important for the accuracy of the data to insert it exactly 5 cm into the soil.

### Ott Orpheus Mini water level logger Device

For reliable results from a hydrological model, it is important to conduct proper calibrations before running simulations. To do calibrations, there is a need for observed data that can be compared with simulated to find the best fit of the model parameters. The discharge of Gaustadbekken was viewed as the best data-set for calibration of the model in Mike+, and therefore a measurement series of water discharge at the outlet of the watershed was necessary. To obtain a continuous measurement series of the water level in Gaustadbekken, an Ott Orpheus mini water level logger device was installed the 8th of October, 2020 (location shown in figure 4.3).

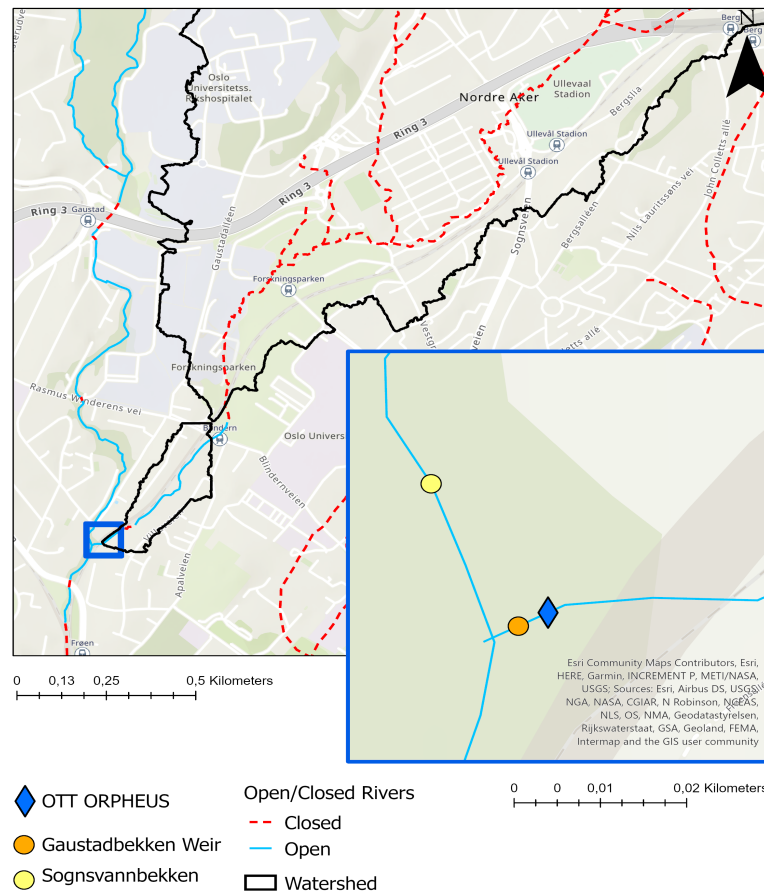


Figure 4.3: Location of the Ott Orpheus mini water level logger device.

This is a robust device perfect for long time series due to its undemanding setup, accuracy, and

simple maintenance. The total weight of the device is 0.71 kg, with dimensions of the communication unit being 40x2.2 cm and the pressure probe 19.5x2.2 cm which are connected through a cable wire. This also makes it very flexible, and it can easily be installed in most locations (Ott, 2020). The setup is illustrated in figure 4.4.

The built in data logger stores and manages the data, easily accessed and manipulated through a software downloaded from [ott.com/resources/](http://ott.com/resources/). When communicating with the logger for setup of the device and collecting data, a cable connecting from the logger to the computer was used. The device in Gaustadbekken was programmed to log water level and temperature every 15 minutes.

Before installment of the Ott Orpheus mini water level logger, the river was cleared (in collaboration with supervisors Hong Li and Nils Roar Sælthun, see fig. A.7) of large rocks with significant disturbance of the water flow. There was considerable sedimentation in the river, which was not possible to remove prior to the installing of the logger device. There is thus less than optimal conditions for discharge measurements as there is still presence of rocks and sediments that might disturb the water flow.

While clearing the river, old equipment for surveying the river was found. This was identified as property of the Norwegian Water Resource and Energy Directorate (NVE), but was no longer in use. It can be seen in the figure 4.4 (b) as a blue box next to the logger used in this study. NVE has been informed.



Figure 4.4: a) Picture of the Gaustadbekken weir after large disturbances were removed. The location of the logger is marked in a yellow rectangular and the location of the sensor is marked with an orange rectangular. The sensor is connected to the logger through a cable. b) Installed logger. Old equipment is visible under the logger as a blue box connected to a wire. c) Sensor installed in the river, marked by an orange rectangular. The sensor itself is not visible as it is under water.

## Discharge calculations

In the river, there is a sub-critical water flow with a Froude's number of  $<1$ . At the weir crest, the flow has a transition to critical flow ( $F_r = 1$ ). This situation equals the water level decreasing to a level where there is maximal transportation of water by the given energy the stream inhabits. Any disturbance of the water flow beneath this point will not propagate up-streams of the cross section. Due to this, water level measurements of the river can be done to obtain the discharge of the river at the point of the weir (Ødegaard et al., 2014 p.78-79). The discharge can then be found by a suitable equation for the weir type.

The weir at Gaustadbekken outlet is a compound triangular-rectangular sharp crested weir (CTRSC) (see figure 4.4). This complicates the discharge measurements as it has to incorporate both the triangular part as well as the rectangular.

The dimensions of the weir was measured by a levelling instrument and is illustrated in figure 4.5.

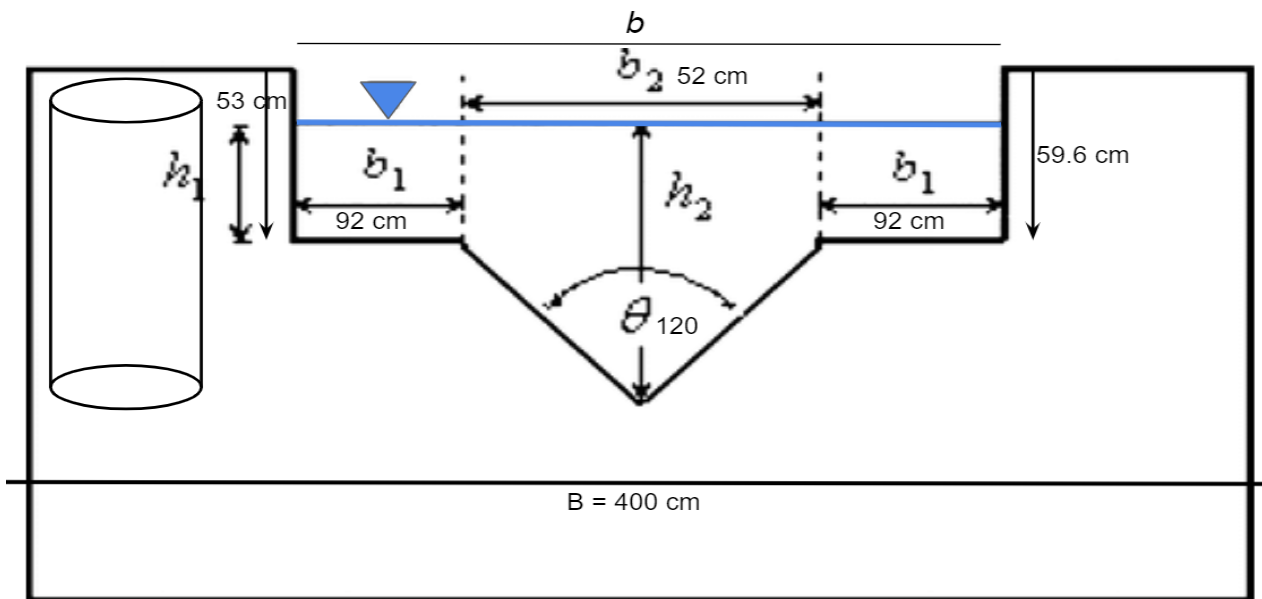


Figure 4.5: Illustration of the Compound triangular-rectangular sharp crested weir (CTRSC). Figure modified from Jan et al., 2006

The discharge of the river ( $Q$ ) [ $m^3/s$ ] can be found by the equation presented in Jan et al. (2006) (adapted from Martinez et al. (2005)) as shown in equation 4.3.

$$Q_t = \frac{8}{15} C_{td} \sqrt{2g} \tan\left(\frac{\theta}{2}\right) (h_{2e}^{\frac{5}{2}} - h_{1e}^{\frac{5}{2}}) + \frac{2}{3} C_{rd} \sqrt{2g} (2b_1) h_1^{\frac{3}{2}} \quad (4.3)$$

where  $\theta$  is the notch angle in radians and  $g$  is the gravitational force [ $m/s^2$ ],  $b_1$  is the side of the rectangular weir [m] (see fig. 4.5) and  $h_1$  is the water level of the crest [m],

$C_{td}$  [-] is the discharge coefficient for triangular sharp-crested weirs and calculated by the equation 4.4 when the notch angle  $\theta$  is in radians,

$$C_{td} = 0.6085 - 0.0525\theta + 0.02135\theta^2 \quad (4.4)$$

the  $C_{rd}$  [-] is the discharge coefficient of the rectangular sharp crested weir and can be found by the equation 4.5 when  $b$  [m] is the length of the weir [m] ( $2b_1 + b_2$ ),  $B$  is the channel width [m],  $h_1$  is the

#### 4. Method

head on the crest [m] and  $h_2$  is the weir height [m] (see figure 4.8),

$$C_{rd} = \frac{0.611 + 2.23\left(\frac{B}{b} - 1\right)^{0.7}}{1 + 3.8\left(\frac{B}{b} - 1\right)^{0.7}} + \frac{0.075 - 0.011\left(\frac{B}{b} - 1\right)^{1.46}}{1 + 4.8\left(\frac{B}{b} - 1\right)^{1.46}} \frac{h_1}{h_2} \quad (4.5)$$

and the  $h_e = h + K_h$  = effective head [m]. The  $k_h$  [m] is the correction head accounting for viscous and surface tension effects.

$$K_h = \frac{3.9058 - 3.8558\theta + 1.1940\theta^2}{100} \quad (4.6)$$

The equations 4.4 and 4.6 have been developed by the authors of Jan et al. (2006) as empirical relations.

To calculate the discharge of Gaustadbekken weir, the bottom of the V-notch was used as the point of 0 discharge. The water level obtained by the Ott Orpheus therefore had to be adjusted for the level of the V-notch. The water level was manually measured at several occasions and used to correct the water level obtained by the Ott Orpheus. The manually measured water level from the bottom of the V notch was compared to the recorded water level by the sensor (see figure 4.6). This method estimated that the water level measured by the Ott had to be deducted 0.15-0.17 m (varying through the measurement period) before applying the discharge calculation in equation 4.3.

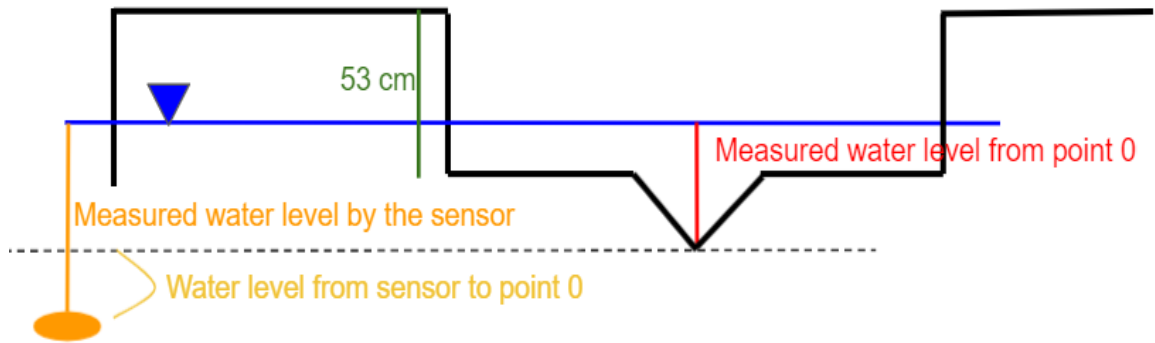


Figure 4.6: Illustration of how the water level was measured in the Gaustadbekken weir.



### Validation of the discharge series

The saltwater dilution method was applied as a verification of the data obtained from the Ott Orpheus mini water level logger device (Ott) and calculations. As the Ott device is not placed upstream of the river weir in the middle of the water stream, it was necessary to do other measurements to verify the discharge series obtained by the Ott and calculations.

For this field work the main purpose was to verify the results obtained from the Ott Orpheus mini water level logger device (location illustrated in 4.3). The measuring location was therefore chosen to be as representative for this point as possible, as the dilution of a tracer can be used for calibration of discharge measurements (Gilman, 1994; Herschy, 1995). NaCl is one of the most common chemical tracers used in dilution methods (Herschy, 1995), and was chosen for this field work due to its ability to dilute in water without being adsorbed by the river bed. The method takes advantage of the natural turbulence of the stream creating a mixture of the tracer with the water (Gilman, 1994).

Measurement of the electrical conductivity (EC) was conducted before the tracer was added to the water, providing background conditions for the stream. The discharge of the river was considered constant through the gauging site, with sufficient turbulence to create mixing of the water and tracer. A known volume of the tracer (NaCl) was then added to the stream approximately 30 m upstream of the Gaustadbekken weir, as a sudden injection. The EC measuring device (Hanna electrical conductivity meter) can then detect the change of concentration of ions in the water, creating the curve used for the calculation of the discharge (eq. 4.8). The EC was measured approximately 50 cm upstream of the weir, in the middle of the water flow.

The discharge ( $Q$ ) was calculated based on the standards ISO 9555-1 (1994) and ISO 9555-3 (1992) by the equation 4.7.

$$Q = \frac{m}{k} \left( \int_0^{\infty} (K - K_b) dt \right) \quad (4.7)$$

where  $Q$  is the discharge of the river  $m^3/s$ ,  $k$  is a conversion factor between the tracer (NaCl) and the conductivity - a linear relationship that is dependent on the temperature,  $m$  is the mass of the tracer (g), and the integral is the areal under the curve created by the field measurements after the background measured electrical conductivity  $K_b$  is removed. This gives the equation 4.8.

$$Q = \frac{m}{k} A \quad (4.8)$$

where  $A$  is the area under the curve,  $k$  is a conversion factor between the tracer (NaCl) and the conductivity and  $m$  is the mass of the tracer (g).

The simplicity of the method is one of its greatest advantages, providing an extremely inexpensive technique that in suitable rivers produces accurate results (Herschy, 1995).

### Sample collection and measurement of field parameters

Water samples of Gaustadbekken and Sognsvannbekken was collected for an insight to the water quality of urban rivers as well as comparison between two rivers of similar properties running through different degrees of urbanization. At the locations of the water samples, there was also conducted measurements of the field parameters pH, electrical conductivity (EC) and temperature (°C). Locations of the water sampling and field parameter measurements are shown in figure 4.7.

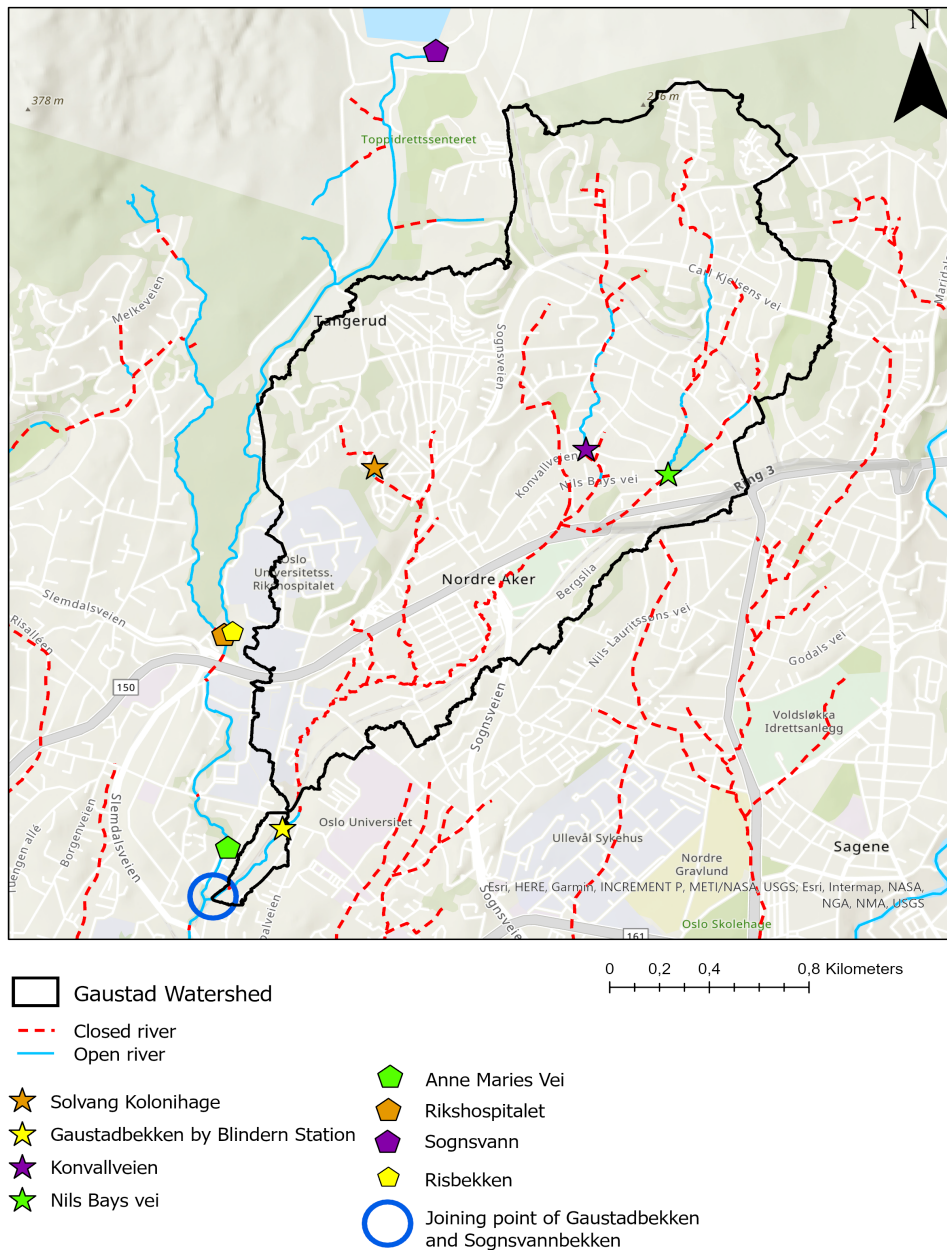


Figure 4.7: Locations of field measurements and water sampling.

### Water samples

Water samples from different locations within the Gaustad watershed (fig. 4.7) was collected in collaboration with fellow students during the course "Field Methods in Hydrogeology (GEO4360)" at the University of Oslo (25.8.20). The river is mostly in pipes, so the points were chosen based on the availability of the water as well as getting a representative picture of the river water as it progresses to Gaustadbekken weir. Pictures of the locations within Gaustad watershed is shown in the appendix, figures A.11, A.12 A.13 and A.14. Water samples from Sognsvannbekken, as well as measurements of field parameters was obtained the 26.8.20, also in collaboration with students from the course GEO4360.

Water samples from the joining point of the rivers Gaustadbekken and Sognsvannbekken (fig. 4.7) were collected after relatively heavy rainfall in December 2020 and January 2021. In December the samples were taken when the water discharge was still high, while the samples in January were taken after the rain had ended and the discharge of the river had returned to relatively normal flow. The samples were taken to investigate the water quality of Gaustadbekken. Samples taken at the same time in Sognsvannbekken served as results for comparison of two surface streams with similar properties, where one (Gaustadbekken) is running through heavier developed areas.

The water was collected by a syringe that was rinsed with the river water prior to the sampling (picture of water sampling provided in fig. A.8). The water was filtered through a  $45\mu\text{m}$  filter (see fig. A.9) into suitable plastic 50 ml containers and labeled with the appropriate name and date for each specimen. For cation analysis, three drops of acid  $\text{HNO}_3^-$  was added to avoid oxidation.

### Field parameters

The electrical conductivity, pH and temperature was measured in the field by Hanna devices inserted into the water for approximately five minutes, obtaining stable and reliable values.

### Soil Samples

The soil samples were collected to compare the findings of the Mariotte cylinder 1-5 with known hydraulic conductivities for different soil by Freeze and Cherry, 1979. Locations of the soil sampling is equal to the infiltration measurements of Mariotte 1 to Mariotte 5, shown in figure 4.1. The samples were taken approximately 25 cm deep in the hole with the exception of two sites (M4 and M5) where the soil showed a high degree of layering, and samples was taken from both layers to get a representative result for the site. The soil was sampled in suitable plastic containers and brought to the laboratory at the Department of Geosciences.

### Grain size analysis

To verify the hydraulic conductivity found by the Mariotte cylinder, a grain size distribution analysis was conducted on the soil samples collected. Approximately 100 g of the sample, previously sieved for particles larger than 8 mm and dried at  $60^\circ\text{C}$ , was measured correctly and noted as the total weight of the sample. The sample was then placed in a sieving stack with 7 different particle-size intervals with decreasing mesh size downwards. The mesh grids used in the analysis of these samples were  $>2$  mm, 2-1 mm, 1-0,5 mm, 0,5-0-25 mm, 0,25-0.125 mm, 0,125-0.063 mm and  $<0.063$  mm.

The different sized grains were held back by the mesh grid of the sieves, leaving the sample to be fractioned in the individual intervals. The grains in each sieve was then weighed exactly and compared to the total weight of the sample to determine the percentage of the different grain sizes. This was plotted cumulatively to find the d10 value, the value at which 10 % of the sample has a lower grain size. This diagram also reveals the d60, the value at which 60 % of the sample has a lower grain size. To use the Hazen method for estimation of the saturated hydraulic conductivity, the ratio  $d60/d10$  should ideally be below 5 (Mæhlum T and G.R., 2010).

## 4. Method

---

Hazen's method for estimating the hydraulic conductivity (cm/s) for loose sand is proposed as the equations  $K_{min}$  and  $K_{max}$  in 4.9 and 4.10.

$$K_{min} = 1.0d10^2 \quad (4.9)$$

$$K_{max} = 1.5d10^2 \quad (4.10)$$


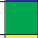

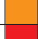

### 4.2 Chemical analysis of the water samples

#### Heavy metals (ICPMS - Inductively Coupled Plasma Mass Spectrometry)

To analyse for heavy metals in the water samples, the Q-ICPMS was applied - an Aurora Elite equipped with a Cetac ASX-250 autosampler and an ESI oneFAST sample introduction system. This is an analytical technique that can detect heavy metals due to the way it generates ions. The instrument achieves ionisation by using argon gas to produce plasma, with the ability of ionising almost all of the elements in the periodic table. The plasma ionizes the sample before it is transported through the instrument to the mass separator and further to the detector. The separator filters out unwanted elements, while the detector reveals the heavy metals of the medium (University of Oslo, 2019).

The concentration of heavy metals in the sample can then be compared to the standards for freshwater as set by Miljødirektoratet (Norwegian Environment Agency (NEA)) in "Veileder M608" and classified from *background* to *very bad* (table 4.1) (Miljødirektoratet, 2020). *Background* indicates the background level of concentration, while *very bad* means there could be severe toxic effects when drinking the water.

Table 4.1: Classification system of the water quality as set by the Norwegian Environment Agency.

Classification		Consequence
Background		Background level
Good		No toxic effects
Moderate		Chronic effects by long term exposure
Bad		Acute toxic effects by short term exposure
Very bad		Comprehensive toxic effects

#### Anions and cations (Ion Chromatography)

Ions were detected by the Ion Chromatography method (ICS-2000) with suppression of an Eluent (Potassium Hydroxide (KOH) for anions, and Methanesulphonic Acid (MSA) for cations) (Borba and Rohrer, 2003; Thomas and Rohrer, 2013). The water samples were added into the eluent and transported through two ion exchange columns. The inside of the analyst column has a positive or negative charge depending on the elements investigated, and the ions are thus separated by their affinities for the exchange sites in the column. The eluent will keep flowing, and by time, exchange for the ions in the water solution. The ions can then be identified by known retention times. To find the quantity of the different ions the peak height or the area of the curve (from the travel time) is measured.

#### Alkalinity

The alkalinity refers to the acid-neutralizing capacity of a medium. It can be defined by the amount of an acid it will take to give the medium a pH of 4.5 (Appelo and Postma, 2005). It is therefore an expression of the medium's ability to buffer for a change in the pH.

The alkalinity of the water samples was found in the chemistry lab at the institute of Geo Science. This is determined by titration with an acid until the sample reached a pH of about 4.5 (Appelo and Postma, 2005). A titrator of the brand Metrohm type 702 SM Titrino was used for titrating the sample, while a 728 Metrohm Stirrer homogenized the sample. The acid used was a 0.01 mol solution of Hydrogen Chloride (HCl) to acidify the sample until it became acidic. The device tracks the change of pH and creates a graph representing the pH in the sample. The alkalinity was calculated by the equation 4.11.

$$Alk(\text{meq/L}) = 1000 \left( \frac{V_{ep} N \text{HCl}}{V_{sample}} \right) \quad (4.11)$$

where  $V_{ep}$  is the volume of acid needed to reach the equivalence point,  $N$  is the molar strength and  $V_{sample}$  is the volume of the sample (ml).

The alkalinity can also be expressed as the concentration (meq/L) of  $\text{HCO}_3^-$  when the range of pH is between 6.3 and 8.3 (Appelo and Postma, 2005 p.180-184).

### Electrical balance

The electrical balance can be calculate to evaluate the accuracy of the sample analysis. An electrical balance of below 5% is considered sufficient as most laboratories are not able to produce analysis results with less than 2% (Appelo and Postma, 2005). The electrical balance (EB) can be found by equation 4.12 as discussed in Appelo and Postma (2005).

$$EB (\%) = \frac{(\text{Sum Cations} + \text{Sum Anions})}{(\text{Sum Cations} - \text{Sum Anions})} \times 100 \quad (4.12)$$

when cations and anions are expressed as meq/L and inserted with their charge sign.

### Escherichia coli

A test for the presence of Escherichia coli (E. coli) bacteria was performed at the Department of Biology at the University of Oslo. This was done as it is a so called “indicator bacterium” for sewer contamination, and its presence in the water would indicate a sewer leakage in the area.

The bacteriological analysis of the water consists of several steps, where each step has to produce adequate results to continue the chain of tests until the bacteria can be identified. The first step is a presumptive test, where 1 ml of the water sample was added to a 10 ml test tube of lactose broth (prepared by Bård Mathiesen). Inside the test tube, there was placed a small glass with the bottom up. The samples were then incubated for 48 hours at 37 °C while slightly shaken. This tests the ability to grow on lactose in the presence of bile salt with the production of gas. If there was any E. coli bacteria in the water sample, there would be produced gas as the bacteria was allowed to grow in the good conditions provided (BIOS 3910, 2021). The samples were watched at 24 as well as 48 hours.

### 4.3 Modelling

#### ArcGIS Pro

To model in GIS (Geographic Information System) offers many advantages. It is a complete computer system for capturing, checking, storing and displaying data and information related to positions on the Earth. It can combine layers of different information and data, and enables the modeller to visualize the input in a simple and useful way. It provides the tools to combine data in a beneficial way and lets the programmer relate seemingly unrelated data to understand spatial patterns and relationships.

As one of the aims for the thesis was to create a hydrologic model of the study area using Mike+, ArcGIS Pro was an important tool to view and moderate the attributes of the data before importing it into the hydrologic model. This was necessary to match the target source of the Mike software.

#### Watershed

In hydrology a watershed is important, and serves as the lateral boundary conditions in natural settings. In urban areas, however, infrastructure might alter the waterways by pipes and gutters, but the watershed is still an important base. The Gaustad watershed was created in ArcGIS Pro by using the hydrological toolbox, based on a digital elevation model (DEM) available from the municipality of Oslo.

The catchment area used in the representation of the Gaustad watershed does not extend all the way down to the weir. This is inaccurate, and could be caused by limitations in the resolution of the DEM. The accumulated flow-lines indicating the water paths (derived from the DEM) shows there to be water flow from the watershed illustrated in the figures and down to Gaustadbekken weir. When using the watershed tool in ArcGIS Pro from the point of the weir, however, the result equals only a small area that begins just below where the catchment used in the illustrations end (see figure 4.8). The watershed generated by Nevina (see appx. fig. A.5) also illustrates how the Gaustadbekken weir is a part of the Gaustad watershed. The issue could not be resolved by the time this study was completed. The figures are only illustrative, and the water budget in this study has been made on the basis of the watershed created in Mike+.

#### Surface cover

When creating a water budget for urban areas, the degree of surface sealing is important. It can be obtained either through predicting (modeling) or by using maps and remote sensing (Bogena et al., 2004). The surface cover was therefore mapped in ArcGIS Pro by the use of municipal data of construction and parks, orthophoto as well as local knowledge of the area. As the recharge to groundwater is strongly dependent on the vegetation cover on the surface (Nachabe et al., 2005) polygons depending on the surface cover were made, dividing the catchment into 4 different categories. Buildings, roads and other construction as well as recreational spaces were derived from the FKB (Felles kartdatabase) database of maps for Oslo city. Forest in the catchment was included by manually creating polygons based on observations and orthophoto (NGU). The area left in the catchment was then classified as lawns and/or areas of sparse vegetation.

#### Subsurface

For this study, the infiltration of surface water is of special interest in relation to development of urban areas. To assess a realistic infiltration of the surface water through the soil, the geology of the catchment had to be mapped. This was done by thorough investigation into available data resources such as the NGU database and online maps of Norway. The regional geology can be found by these methods, but for a closer and more detailed view of the geology, further studies needed to be done. The municipality of Oslo gave access to geotechnical borelogges from the catchment area (Undergrunnsarkivet (Subsurface archive)), which gave further insight as to what is located in the

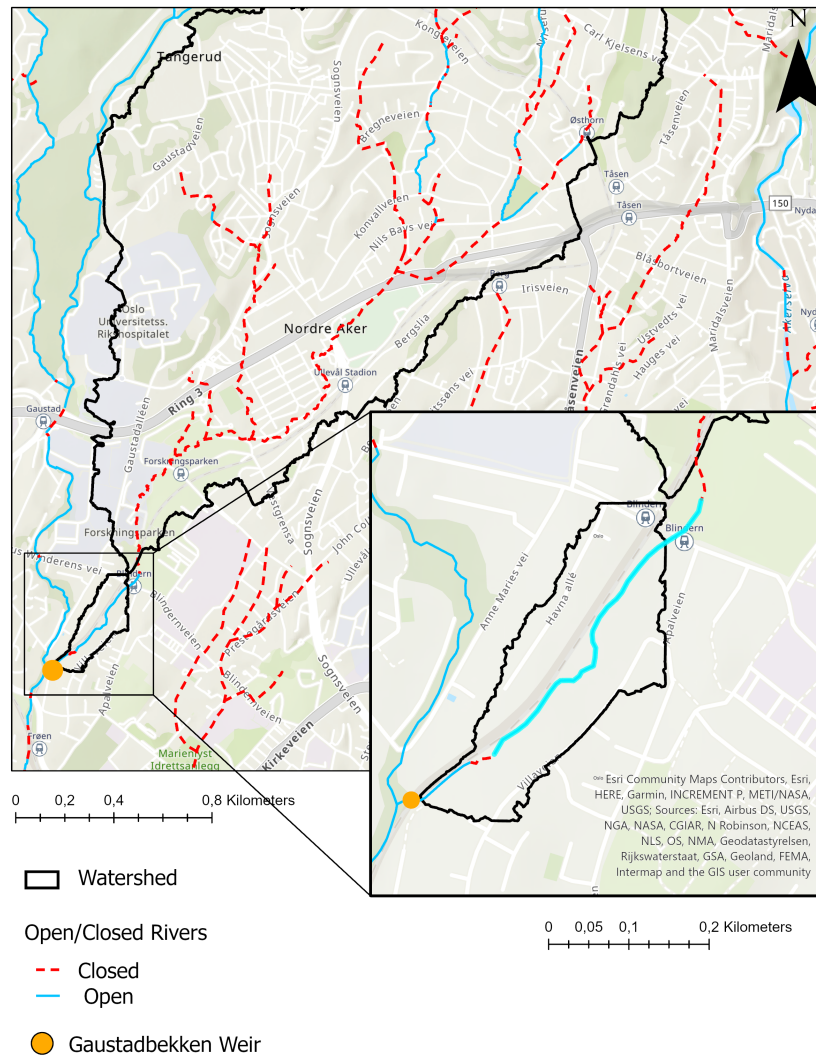


Figure 4.8: Area not included in the watershed due to inaccuracy of ArcGIS hydrological modeling tool.

subsurface of the Gaustad catchment. By these data, the thickness of the marine clay layer could be estimated by interpolation (Empirical Bayesian Kriging) in ArcGIS Pro, as well as create an assumed depth to the bedrock.

### Subsurface archive

Data from the subsurface archive (Undergrunnsarkivet) was provided for a chosen area covering the Gaustad watershed by the Oslo municipality. The information was given as shapefiles with points for boreholes and bedrock observations in coordinate system UTM32, as well as corresponding reports for some of the points.

The first step in creating the geological layers was merging the shapefiles into one in ArcGIS Pro.

The points were assigned coordinates before being exported as an excel sheet. Some of the points had no information about the subsurface and was correlated with available reports to insert the terrain, bedrock and clay elevation as well as presence of fill masses and anthropogenic material. A few of the reports provided only reference to an unspecified ground elevation, and the terrain was therefore interpolated with Empirical Bayesian Kriging, EBK (ArcGIS Pro) to fill in the gaps. In cases of duplicate points, the maximum value was chosen. The interpolated layer was exported as points in the same locations as was imported to easily correlate the missing values from the initial data-set. The attribute table was then exported as an excel sheet and the results of the interpolation were inserted into the data-set and used as reference value to calculate the elevation of the geological layers. The same interpolation technique (EBK) was applied for the bedrock, but in cases of duplicate points, a mean was used. The clay layer elevation was then estimated by interpreting the recorded quaternary deposits as clay, together with information from the available reports. These points were then applied in ArcGIS Pro for interpolation, and the missing values were inserted on the basis of the result. The thickness of the clay layer was then calculated by the layer's elevation value minus the bedrock height. The depth to bedrock was calculated by the ground elevation minus the bedrock elevation.

### Numerical Modeling

To get a better understanding of the water budget in urban areas, a hydrologic modelling tool can be applied. A hydrologic model is useful when the aim is to simulate and make predictions in a complex system. Mike+ is a sophisticated software with many tools for urban hydrology modeling and was therefore chosen for this modeling assignment. Mike+ uses the MIKE 1D engine, which computes the hydrodynamic simulation of the networks by solving the complete St. Venant (dynamic flow) equations throughout the network (DHI, 2021e).

### Data selection and adaptation

When modeling in Mike+, the import of data is the first challenge. The attributes has to match the target source in Mike and thus had to be identified in advance and in some cases reformatted. The reformatting of the attributes was done in feature management engine (FME) and ArcGIS Pro by field calculations based on the specifications of the data requirements of the Mike software. Identifying which data that match the attributes in Mike+ was a time consuming process, as not all data from VAV was marked with appropriate names and the lack of units of the data (e.g. the dimension of the manholes).

Mike requires a minimum of certain data to be able to simulate a collection system network; diameter, ground level and bottom level for nodes and ID, diameter, from node ID, to node ID, up level and down level for the links. The data-set from Oslo municipality was lacking bottom levels for all nodes and most of their diameter. The links had no up and down level (corresponding to the elevation where it starts and ends). FME provided the up and down level for the links by the operation "coordinate extractor", which could then be manually inserted as the bottom level of the nodes in Mike+. This was done for all nodes in the data-set. The diameter of the nodes were set to 1.5 m for all but a few manholes where the links diameter required the manholes to be of a bigger size.

The wastewater pipeline in the separate network was removed as well as outlets with less than 10 pipes connected to the outlet. This led to several nodes being *orphaned* and therefore removed from the model by the network simplification method. The removal of the wastewater network should have no impact on the results of the model as it is not of interest, nor does it affect the runoff parameter. The removal of outlets with less than 10 connected pipes could potentially alter the runoff in small areas of the model, but was deemed not significant. The runoff that would potentially be collected by the removed pipes would be released back into the model in such close proximity that the only actual effect is the possible altered route of the runoff, but the end result would be the same. The advantage of reducing the amount of data in the model outweighed the consideration for the exact runoff path in every small sub-catchment of the model. The purpose of the model was to investigate



the water balance of the area, and the exact flow paths of the surface runoff was of less importance for the holistic approach of this study.

The data-set also had several pipe-systems that led nowhere, without any outlet or joint reach to explain the disconnection. These were either removed or connected to a suitable system downstream as assessed by the modeller. This is cause for potential errors, and might contribute to inaccurate results in the model output. It was, however, made clear in a phone conversation with an employee at the VAV that there might exist errors like these in the data-set and that there would be a need for modifying the collection system by logic reasoning. Another source of error by this method is the catchment connection to the collection system network. The strategy in the hydrologic model applied in this study was to connect the sub-catchments to the closest manhole, which by removing certain manholes might cause sub-catchments to connect to another pipeline than in reality. This would, however, not influence the results much, as most of the pipes in the model lead to the same outlet.

## 4.4 Hydrologic model setup

The model was set up using the collection system data retrieved by VAV Oslo municipality after some modifications to fit the purpose. For this study, the rainfall-surface runoff model Kinematic Wave (KW) was computed together with the Rainfall Dependent Infiltration (RDI) model to incorporate both surface runoff as well as the groundwater aspect of the hydrological situation at Gaustad.

### Boundary conditions

#### Watershed

The watershed created in ArcGIS Pro was inserted into the Mike+ project and used as the initial boundary conditions for the precipitation. The watershed did, however, not cover the area of pipelines contributing to the outlet in Gaustadbekken, and the lateral boundary condition for the model in Mike+ had to be adapted (see fig. 5.7) to include all areas of surface water inflow to the collection system carrying water into the Gaustadbekken measurement point. This illustrates the need for the "sewersheds" as discussed by Welty (2009). The watershed was then divided into several (915) sub-catchments and connected to a suitable manhole for simulation of the surface water inlet into the collection system.

#### Precipitation and temperature

A time series of rainfall in the format of a dfs0 file was inserted into the model, and serves as the time limitation as well as the precipitation input for the hydrological model. The rainfall data was collected from *seklima.met.no* from the Blindern gauging station (SN18700), together with the recorded temperature for the period. Seklima.met.no is a service provided by the Norwegian Climate service-center (KSS) in collaboration with the meteorological institute of Norway, the Norwegian water resources and energy directorate (NVE), the Norwegian research centre (NORCE) and Bjerknnes Centre for Climate Research (Bjerknessenteret).

The precipitation used as input for the hydrologic model was considered to fall evenly distributed across the entire watershed. A suggestion for improving the model is to include spatial variation in precipitation input, as it can vary also within a relatively small watershed. Mejia and Moglen (2010) found that interaction between the spatio-temporal variability of rainfall and degree of impervious surfaces result in hydrologic response, for example higher flow peaks for less urbanized areas. There are several meteorological stations in Oslo and it would be interesting to apply spatial variation in rainfall input to examine potential effects.

#### Evaporation and infiltration

Potential evaporation was calculated by Thornthwaite's equation (4.13 and 4.14) (Thornthwaite, 1948) and inserted as a mm/day potential of evapotranspiration into the hydrological model in the

#### 4. Method

---

format of a dfs0 file.

$$PET_{noncorrected} = 16 \left( \frac{10t}{I} \right)^\alpha \quad (4.13)$$

where  $t$  is the mean monthly temperature in  $^{\circ}C$  and  $I$  [-] is the annual heat index as a sum of the monthly Thornthwaite heat indexes calculated by  $(t/5)^{1.514}$ .

$\alpha$  equals  $6.75 \times 10^{-7}I^3 - 7.7110^{-5}I^2 + 1.792 \times 10^2I + 0.49239$ .

$$PET = PET_{noncorrected} \left( \frac{N}{12} \right) \left( \frac{d}{30} \right) \quad (4.14)$$

where  $N$  are theoretical sunshine hours for each month and  $d$  is number of days in each month. The theoretical hours of sunlight was found by averaging the length of day (2018-2019) in Oslo (Time and date Oslo, 2020) and rounded to the closest half hour.

Mike+ then calculates the evaporation based on the potential evaporation ( $E_p$ ) provided, following the equation 4.15 in the Kinematic Wave model, and equation 4.16 in the RDI model.

$$E(t) = \begin{cases} E_p(t) \text{ for } (P(t) \geq E_p(t)) & OR(y(t) > 0) \\ P(t) \text{ for } (P(t) < E_p(t)) & AND(y(t) = 0) \end{cases} \quad (4.15)$$

where  $P(t)$  is the actual precipitation at time  $t$ ,  $E(t)$  is the evaporation loss at time  $t$ ,  $E_p(t)$  is the potential evaporation at time  $t$  and  $y(t)$  is the accumulated depth at time  $t$ . The Kinematic Wave model thus treats the evaporation as an immediate loss from the precipitation (DHI, 2021b p.214).

The Rainfall Dependent Infiltration model estimates the actual evaporation  $E_a$  proportional to the potential evaporation ( $E_p$ ), varying linearly with the relative soil moisture content. The evapotranspiration is estimated by the assumption that in cases where the potential evaporation ( $E_p$ ) is bigger than the surface storage ( $U$ ), there is withdrawal from the lower root zone storage ( $L$ ) at an actual rate  $E_a$  (DHI, 2021b p.173).

$$E_a = (E_p - U) \left( \frac{L}{L_{max}} \right) \quad (4.16)$$

where  $E_p$  is the potential evaporation,  $U$  is the moisture content in the surface storage,  $L$  is the root zone storage and  $L_{max}$  is the maximum water content in the root zone storage (DHI, 2021b p.173).

The infiltration is estimated by the Kinematic Wave model through Horton's equation 4.17 or 4.18.

$$I_H(t) = I_{Imin} + (I_{Imax} - I_{Imin})e^{-k_a t} \quad (4.17)$$

where  $I_H(t)$  is infiltration loss calculated according to Horton,  $I_{Imax}$  is maximum infiltration capacity (after a long dry period),  $t$  is time since the start of the storm,  $k_a$  is the time factor (characteristic soil parameter) for wetting conditions.

The original Horton's equation (4.17) is only valid for events where the rainfall intensity exceeds the infiltration capacity of the soil. This is, however, not always the case and is solved by implementing the integrated form of the equation (4.18).

$$I_{ICUM}(t_P) = \int_0^{t_P} I_H dt = I_{Imin}t_P + \frac{I_{Imax} - I_{Imin}}{k_a}(1 - e^{-k_a t_P}) \quad (4.18)$$

where  $I_{ICUM}(t_P)$  is a cumulative infiltration (mm) at time  $t_P$  i.e. the area under the Horton's curve.

The infiltration is estimated by the RDI model as a proportion of the excess water  $P_N$ . The interflow (Qif) is assumed proportional to surface storage ( $U$ ) and varies linearly with the relative lower zone storage moisture content ( $L$ ) by equation 4.19 (DHI, 2021b p.173).

$$Q_{if} = \begin{cases} (CK_{if})^{-1} \frac{L/L_{max} - T_{if}}{1 - T_{if}} U & \text{for } L/L_{max} > T_{if} \\ 0 & \text{for } L/L_{max} \leq T_{if} \end{cases} \quad (4.19)$$

where  $CK_{if}$  is the time constant for interflow and  $T_{if}$  is the root zone threshold values for interflow ( $\geq T_{if} \geq 1$ ).

### Calibration

To calibrate the hydrologic model in Mike+, physical properties as well as hydrological parameters were changed to find the optimal combination. The period of 8.10.20-28.2.21 was applied as calibration period to ensure a time-span including wet and dry periods.

In a rainfall-runoff model, it might be reasonable to focus attentions on parameters determining surface runoff, such as surface sealing factor and soil properties (Lohani, 2018). The parameters of special interest during the calibration process was therefore the surface cover properties, overland flow time as well as the interflow and baseflow time aspect.

The Kinematic Wave (KW) model was applied in combination with the Rainfall Dependent Infiltration model (RDI), where several parameters had to be adjusted. The time of overland flow and interflow were important parameters for the simulation of the peak flows and the regression time, and the overland coefficient determining the fraction of runoff going to overland flow or baseflow had to be fitted for the situation and degree of urbanization. The Manning's number for contributing areas was based on suggestions by Mike+ (DHI, 2021c table 4.25) for different surface types. Threshold values for recharge of the groundwater and baseflow was found by trial and error.

As often practiced in manual calibration, the simulated and observed values of discharge was compared in a plot and visually evaluated (e.g. Hafezparast et al., 2013; Madsen, 2000). The  $R^2$ ,  $NSE$  and  $RMSE$  (described in subsec. 2.5) was also assessed to check the efficiency of the model.

When manually calibrating a model, there are several challenges as many different combinations of the model parameters might produce the equally good efficiency criteria. The advantage of this method is that it allows for personal knowledge about the parameters, and reasoning in relation to their influence on each other. This is, however, most effective when the modeller has years of experience with hydrological modeling and extensive knowledge about the study area and its properties.

### Model parameters

The sub-catchments were classified as *urban* or *rural* depending on the degree of urban development. The distribution of *urban* vs *rural* sub-catchments was based on the surface covers found by investigation into the watersheds properties (ref. 5.5, 5.2) and adjusted to obtain a reasonable correlation between the observed and simulated discharge of Gaustadbekken. Illustration of the distribution is presented in figure 4.9.

The *urban* sub-catchments were assigned 20 % RDI with the parameter set *urban*, and 80 % Kinematic Wave model parameters as shown in table 4.2 and 4.4.

The *rural* sub-catchments were assigned 80 % RDI with the parameter set *rural*, and 20 % Kinematic Wave model parameters as shown in table 4.3 and 4.4.

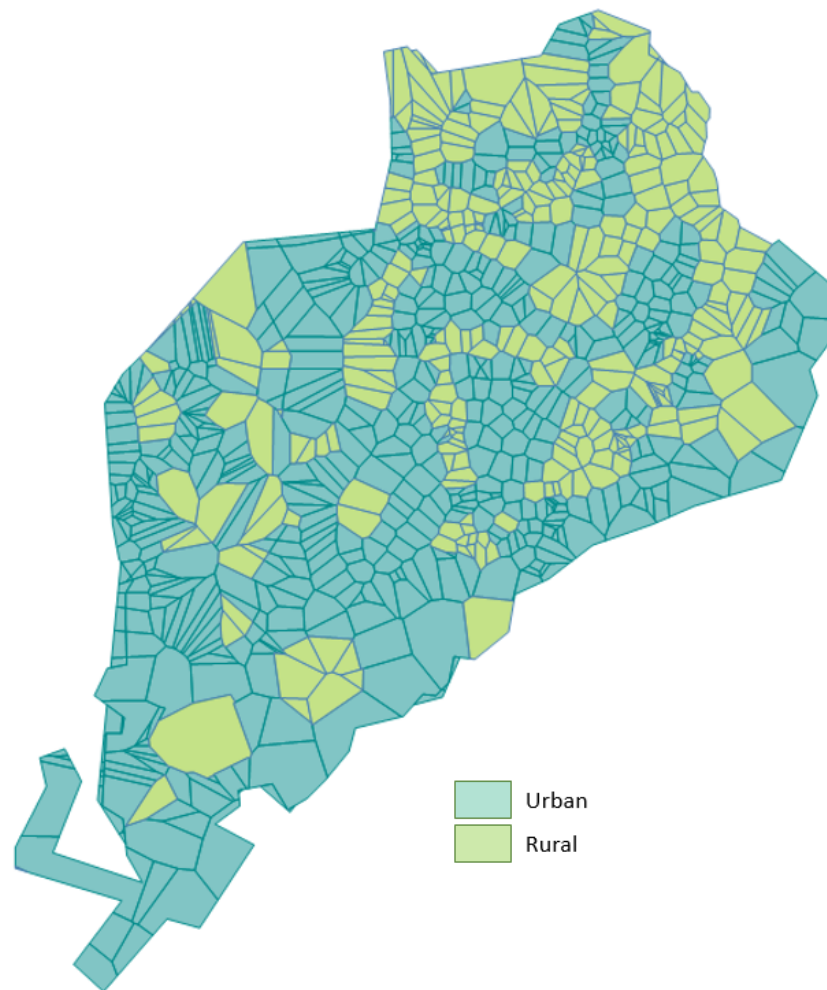


Figure 4.9: Distribution of *urban* vs. *rural* sub-catchments in the model setup in Mike+.

### Calibrated Kinematic Wave (KW) parameters

The calibrated model specific data for the Kinematic Wave (KW) simulation are shown in table 4.2 for the *urban* sub-catchments and table 4.3 for the *rural* sub-catchments. The hydrologic parameters of the Kinematic Wave (KW) model is shown in table 4.4.

Table 4.2: Model specific parameters of the Kinematic Wave rainfall-surface runoff model, *Urban* areas.

Parameter			Unit
Length		13	[m]
Slope		4.4	[%]
Contributing area	Impervious Steep	20	[%]
	Impervious Flat	50	[%]
	Pervious Low	10	[%]
	Pervious Medium	0	[%]
	Pervious High	0	[%]

Table 4.3: Model specific parameters of the Kinematic Wave rainfall-surface runoff model, *Rural* areas.

Parameter			Unit
Length		50	[m]
Slope		8.7	[%]
Contributing area	Impervious Steep	0	[%]
	Impervious Flat	2	[%]
	Pervious Low	10	[%]
	Pervious Medium	8	[%]
	Pervious High	0	[%]

Table 4.4: Hydrologic parameters of the Kinematic wave rainfall-surface runoff model.

	Impervious		Pervious		
	Steep	Flat	Low	Medium	High
Initial Loss					
Wetting [mm]	0.05	0.05	0.05	0.05	0.05
Storage [mm]	-	0.4	0.7	1	2
Horton's infiltration capacity					
Maximum [mm/h]	-	-	$3.6 * 10^{-6}$	36	450
Minimum [mm/h]	-	-	0	3.6	25
Horton's infiltration exponent					
Wet condition [/s]	-	-	0.0015	0.0015	0.0015
Dry conditions [/s]	-	-	$5 * 10^{-5}$	$1 * 10^{-5}$	$5 * 10^{-5}$
Manning [ $m^{(1/3)}/s$ ]	80	70	30	30	12

The infiltration capacity of the *Pervious : Low, Medium and High* was decided based on the findings of the soil infiltration investigations done at Gaustad watershed and adjusted in the calibration process.

### Calibrated Rainfall Dependent Infiltration (RDI) parameters

The surface storage ( $U_{max}$ ) was decided by relating to the vegetation associated with the surface cover type. The overland coefficients (CQof) were based on Mays (2001) for the different types of identified surface covers at the Gaustad watershed, as described in subsection 4.3 and presented in the results, figures 5.2 and 5.3. The *urban* and *rural* sub-catchments in Mike+ were then assigned fitting values for the root zone storage ( $L_{max}$ ), time of concentration for the overland flow (CK), interflow (CKif) and baseflow (BF) after manual calibration by trial and error. The remaining parameters are equal for all sub-catchments in the model after careful calibration of the model output. The snow-melt module was activated for all sub-catchments, with a melting coefficient of 3. The rainfall dependent infiltration model parameters are presented in table 4.5 for the *urban* sub-catchments and table 4.6 for the *rural* sub-catchments.

Table 4.5: Rainfall dependent infiltration parameters for the *Urban* sub-catchments.

<b>Main parameters</b>		Unit
Surface storage (Umax)	2	[mm]
Root zone storage (Lmax)	50	[mm]
Overland coefficients (CQof)	0.75	[-]
Groundwater coefficient (Carea)	0.1	[-]
TC overland flow (CK)	0.7	[h]
TC interflow (CKif)	4	[h]
TC baseflow (BF)	100	[h]
<b>Threshold parameters</b>		
Overland (Tof)	0	[-]
TC interflow (Tif)	0.7	[-]
Groundwater (Tg)	0.7	[-]
<b>Groundwater parameters</b>		
Specific yield (GwSy)	0.03	[-]
Min. GW depth (GWLbf0)	9	[m]
Max. GW depth causing baseflow (GWLbf0)	9	[m]
GW Depth for Unit Capillary Flux (GWLf1)	9	[m]
<b>Initial conditions</b>		
Surface storage (U)	2	[mm]
Root zone moisture (L)	50	[mm]
Overland flow	0	[mm/h]
Interflow	0	[mm/h]
Min. GW depth (GWLbf0)	10	[m]

Table 4.6: Rainfall dependent infiltration parameters for the *Rural* sub-catchments.

<b>Main parameters</b>		Unit
Surface storage (Umax)	3	[mm]
Root zone storage (Lmax)	65	[mm]
Overland coefficients (CQof)	0.3	[-]
Groundwater coefficient (Carea)	0.1	[-]
TC overland flow (CK)	1.1	[h]
TC interflow (CKif)	4	[h]
TC baseflow (BF)	100	[h]
<b>Threshold parameters</b>		
Overland (Tof)	0	[-]
TC interflow (Tif)	0.7	[-]
Groundwater (Tg)	0.7	[-]
<b>Groundwater parameters</b>		
Specific yield (GwSy)	0.03	[-]
Min. GW depth (GWLbf0)	9	[m]
Max. GW depth causing baseflow (GWLbf0)	9	[m]
GW Depth for Unit Capillary Flux (GWLf1)	9	[m]
<b>Initial conditions</b>		
Surface storage (U)	3	[mm]
Root zone moisture (L)	65	[mm]
Overland flow	0	[mm/h]
Interflow	0	[mm/h]
Min. GW depth (GWLbf0)	10	[m]

The calibrations efficiency was mainly tested by visual comparison of observed discharge measurements from the Ott Orpheus mini logger device (Ott) together with the simulated output of the model for the pipe leading to the location of the Ott. The calibration conducted focused mainly on getting the peak flows to simulate correctly, while also obtaining reasonable  $R^2$ ,  $RMSE$  and  $NSE$  of the model.

### Validation

To validate the hydrological model in Mike+, the calibrated parameter values was tested by precipitation input for a different time interval than the calibration period. The results of the validation was evaluated by comparing the observed and simulated hydrographs along with the Nash-Sutcliffe efficiency  $NSE$ ,  $R^2$  and  $RMSE$  the same way as for the calibration of the model.

The calibrated and validated model was then applied for the scenarios, contributing to parameterizing the water budgets for the different urbanization scenarios of Gaustad watershed.

### Model scenarios

The following scenarios was modeled in Mike+, and water budgets estimated for each scenario. The urban impact was especially investigated in the area of the Life Science Building (LSB) construction, comparing the water water budgets of the sub-catchment before and after the development.

The entire Gaustad catchment was modeled as a natural setting by applying 80 % RDI and 20 % Kinematic Wave on all sub-catchments. The fractions assigned to the KW was 10 % *Pervious Low* and 10 % *Pervious Medium* (see subsec. 2.6). The RDI parameter set used was equal to the *rural* parameter set (ref. 4.6), with  $CQof = 0.1$ .

Today's situation of the watershed was modeled by dividing the catchment in *rural* and *urban* sub-catchments, each with their own set of parameters. These were found through calibration of the model and can be seen in tables 4.2-4.6. The distribution of the rural and urban sub-catchments is illustrated in figure 4.9.

The Life Science building (LSB), presently under construction, was characterized as natural area in the catchment properties investigations (see fig. 5.2). This will be transformed to more than  $70\,000m^2$  of building area, removing potential for infiltration and consequently causing surface runoff from the impermeable surfaces. The effect of this change was investigated by running two simulations, with the LSB area classified first as *rural*, then as *urban* with an overland coefficient (CQof) of 0.9, length of 10m and a slope of 2.5 %.

The climate scenarios RCP4.5 and RCP8.5 was modeled to study a possible future scenario in Oslo. The amount of *urban* sub-catchments was increased by 15 % (from 66 % to 76 %), reflecting the ongoing urbanization of the city.

1/3 of the climate changes was considered to already have happened, as the projection is set in relation to 1971-2000, and the rainfall previously used in this modeling was from year 2018-2019. The scenarios were built on the basis of RCP4.5 and RCP8.5 data for Oslo as presented by Norsk KlimaServiceSenter (2021), using the average projection. The scenario RCP4.5 was therefore ran with a precipitation increase of 4.6 % together with a temperature increase of 1.65 °C, and the scenario RCP8.5 with precipitation increase of 9.2% and temperature increase of 2.84 °C relative to the hydrological year 2018-2019.



# CHAPTER 5

---

## Results

---

Chapter 5 presents the results obtained during the study. This includes results from field measurements such as infiltration capacity by Mariotte cylinder and Modified Philipe Dunne falling head infiltrometer, and grain size distribution from the soil samples (locations shown in figure 4.1). Measured chemical properties of the rivers Gaustadbekken and Sognsvannbekken at the locations shown in 4.7, as well as the analysis of the water samples collected at the same locations. The surveying results of the Gaustadbekken weir is presented, together with model calibration and validation results. The results produced by the hydrological model in Mike+ are shown as water budgets for the different scenarios, and graphs of relevant parameters.

### 5.1 Hydrological properties of the soil

To investigate the infiltration capacity of Gaustad watershed, the Mariotte cylinder and Modified Philipe Dunne infiltrometer was applied at locations shown in figure 4.1. Soil samples were taken at the locations of the Mariotte 1-5 to look at the grain size distribution for comparison of measured infiltration capacity with known hydraulic conductivities for different sediments as presented in Freeze and Cherry (1979).

#### Hydraulic conductivity results from Mariotte cylinder

The soil removed to dig the holes at Solvang Kolonihage revealed there to be substantial pollution, for example by metal and plastic. Sognsvannveien had a more homogeneous soil, with some rocks of approximately 5-8 cm size. The soil appeared layered as the compactness of the soil seemed to differ about 30 cm down. Soil samples were taken from both "layers" to investigate any difference in the stratigraphy. There was not found any anthropogenic material at this site. The experience while digging the holes at Sognsvannveien was, however, that the soil was more compact than the one of Solvang Kolonihage.

The results of the fieldwork with the Mariotte cylinder device shows great variation within a small area as illustrated by the results from Solvang Kolonihage (5.9.20 and 12.11.20). In September, Solvang Kolonihage has values ranging from 0.02634 cm/s to 0.00894 cm/s while Sognsvannveien has significantly lower hydraulic conductivity within the range of 0.00045-0.00056 cm/s. In November, Solvang Kolonihage resulted in a hydraulic conductivity of 0.01141 cm/s and 0.00797 cm/s, while Sognsvannveien no longer was able to infiltrate any water.

#### Modified Philipe Dunne falling head infiltrometer

The Modified Philipe Dunne falling head infiltrometer (MPD) brought in the field was destroyed by rocks in the soil while trying to insert the device 5 cm into the soil. The backup MPD was a version of half the height, otherwise identical. This was also wrecked by a rock in the soil after 3 tests had been conducted in a triangle around Mariotte 1 (approximately 40 cm from the Mariotte point). It was therefore decided that the MPD was not applicable for the sites investigated in this study. The results of the 3 MPD tests that was able to be conducted is shown in table 5.2.

## 5. Results

Table 5.1: Results of fieldwork with Mariotte cylinder. The locations of the measurements are shown in figure 4.1.

Location and date		Hydraulic conductivity (K)
5.9.20 Solvang Kolonihage	Mariotte 1	0.02634 cm/s
	Mariotte 2	0.00291 cm/s
	Mariotte 3	0.00894 cm/s
6.9.20 Sognsvannveien	Mariotte 4	0.00045 cm/s
	Mariotte 5	0.00059 cm/s
12.11.20 Solvang Kolonihage	Mariotte 6	0.01141 cm/s
	Mariotte 7	0.00797 cm/s
12.11.20 Sognsvannveien	Mariotte 8	No water was able to infiltrate

Table 5.2: Results of the Modified Philipe Dunne infiltrometer for the 3 tests surrounding Mariotte 1.

MPD	Saturated hydraulic conductivity (K)
M1, 1	0.00830 cm/s
M1, 2	0.02130 cm/s
M1, 3	0.00394 cm/s
Average	0.01108 cm/s

The saturated hydraulic conductivity of the MPD measured around Mariotte 1, was in average (0.01108 cm/s, table 5.2) quite close to the K obtained by the Mariotte cylinder (0.02634 cm/s, table 5.1).

### Grain size distribution

Table 5.3 shows the results of the grain size analysis done for the soil samples gathered at the locations of Mariotte 1-5. For simplicity, the locations are named M1-M5 in the table illustrating the grain size fractions. The grain size was classified based on the Wentworth scale as presented in Bjørlykke (2001). The percentages indicate how much of the sample that classifies as the corresponding size fraction or smaller.

Table 5.3 finds that the soil samples gathered at the locations of Mariotte 3 (M3) and Mariotte 4 (M4 0-34 cm and M4 34-35 cm) classifies as very fine sand. The samples from the locations of Mariotte 1 (M1), Mariotte 2 (M2) and Mariotte 5 (M5 0-31 cm and 31-38 cm) are classified as coarse sand.

Table 5.3: Grain size distribution of the soil samples collected in relation with the Mariotte cylinder infiltration measurements 1-5 (5.9.20 and 6.9.20). The locations of the measurements is shown in figure 4.1.

Wentworth classification	<mm	M1	M2	M3	M4 0-34cm	M4 34-35cm	M5 0-31cm	M5 31-38cm
Clay	0.002	7.4	11.5	16.2	19.5	26.1	8.82	114.1
Very fine silt	0.004	14.4	22.4	31.4	31.9	42.7	18.0	24.6
Fine silt	0.008	25.3	37.9	53.2	53.9	61.0	32.1	37.6
Silt	0.010	29.3	42.9	60.3	59.6	66.1	37.0	41.5
Medium silt	0.016	37.7	52.2	73.5	69.9	75.3	46.5	48.7
	0.020	41.7	56.1	78.8	74.4	79.5	50.6	52
	0.032	50.7	63.1	87.0	82.8	87.4	57.5	57.9
Coarse silt	0.050	59.3	68.2	91.6	88.9	93.5	61.8	62.2
	0.063	63.0	70.4	93.2	90.9	95.3	63.2	63.8
Very fine sand	0.090	68.3	73.7	95.4	93.5	97.4	65.1	65.8
	0.100	69.6	74.6	95.9	94	97.8	65.6	66.4
	0.125	71.5	76.1	96.8	94.8	98.4	66.6	67.4
	0.250	78.5	82.6	99.9	99.9	99.9	73.8	76.1
Medium sand	0.500	86.5	89.4	100	100	100	88.3	89.5
Course sand	1.000	99.3	99.9	100	100	100	99.9	99.9
Very course sand	2.000	100	100	100	100	100	100	100

### Hazen method

The grain size distribution of 5/7 of the soil samples taken from the locations of Mariotte 1-5 (locations shown in fig. 4.1) were too poorly sorted for the Hazen method to be applied. The soil sample from the upper part of the location for Mariotte 3 and the lower part of the Mariotte 4, had adequate  $d_{60}/d_{10}$  values for applying the Hazen method.

Table 5.4: Hazen methods result together with the Mariotte hydraulic conductivity.

	Hydraulic conductivity	Hazen K range
Mariotte 1	0.02634 cm/s	-
Mariotte 2	0.00291 cm/s	-
Mariotte 3	0.00894 cm/s	0.0012-0.0018 cm/s
Mariotte 4	0.00045 cm/s	0.0009-0.09 cm/s
Mariotte 5	0.00059 cm/s	-

The Hazen method results shown in table 5.4 are within range for Mariotte 3, while the range for Mariotte 4 somewhat differs from the findings of the Mariotte device. This further illustrates the uncertainty of the data.

### 5.2 Study site investigations

Investigation into the study site was done to obtain relevant information about the surface covers of the area, as well as looking into the infiltration capacity of the watershed.

#### Soil infiltration map

The infiltration capacity map was derived from NGUs official map of superficial deposits. Hydraulic conductivities were assigned based on Freeze and Cherry (1979), GrunnTeknikk AS (2020) and fieldwork results.

The map in figure 5.1 was made in an effort to parameterize the original infiltration potential map from NGU (ref. fig. 3.3c). The K values determined in this study was therefore inserted into the original infiltration potential map from NGU.

The infiltration capacity estimated in this study generally follows the same trend as the infiltration potential mapped by NGU, as seen in figure 5.1. The areas classified as "Well suited for infiltration" by NGU was assigned a hydraulic conductivity of  $10^{-6}cm/s$ , while the "Poorly suited for infiltration" classification of the NGU map was assigned a K value of  $8.3 \times 10^{-3}cm/s$  (see fig. 5.1) as a the average of the results produced by the infiltration measurements obtained by fieldwork. The area of no classification in the original map from NGU was not assigned an infiltration capacity as the superficial deposits are filling material. There are no records of what this consists of, and it was therefore impossible to assign any properties to the material.

A simplified stratigraphy of Gaustad watershed is illustrated in appendix A, figure A.2.

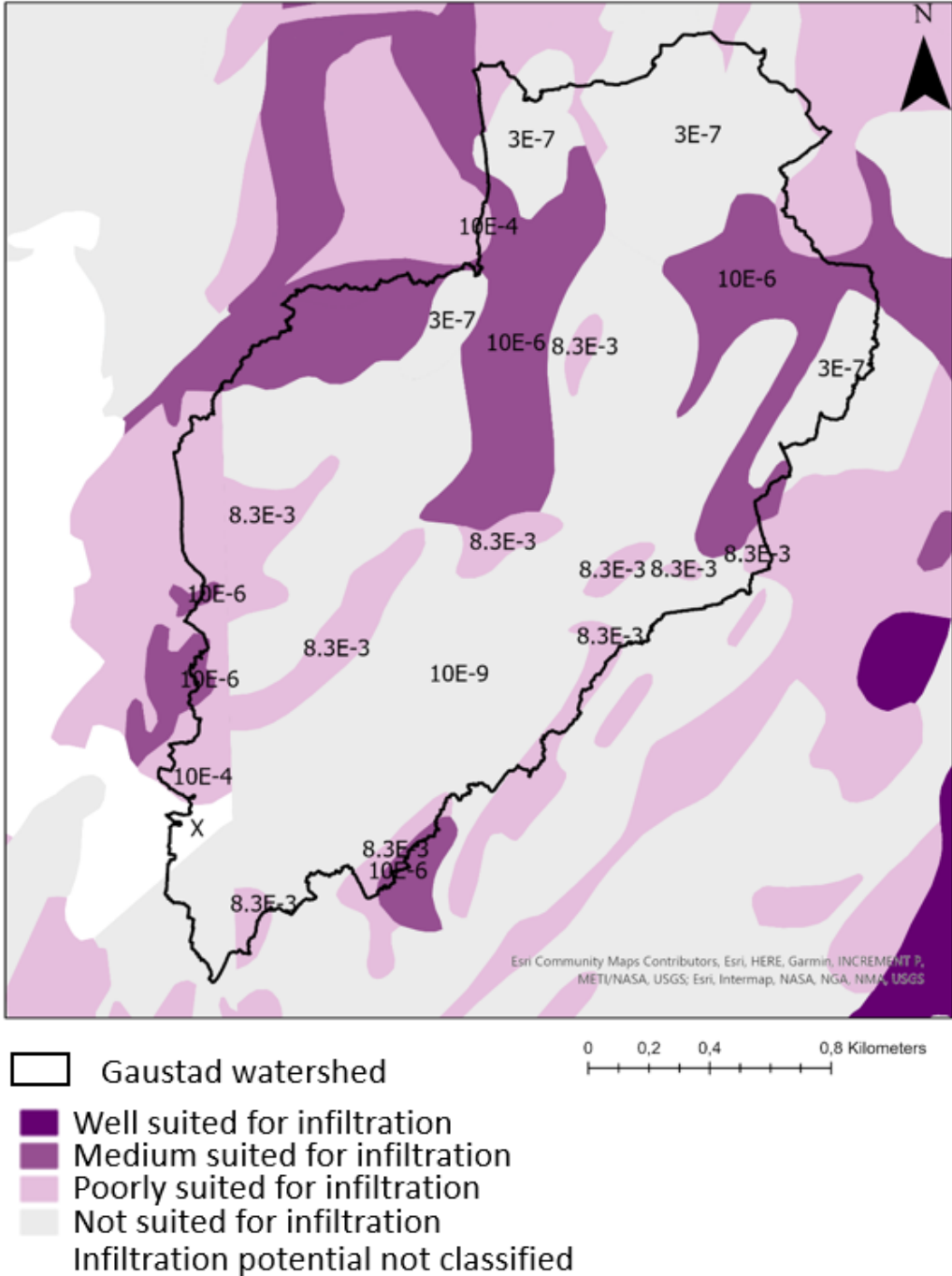
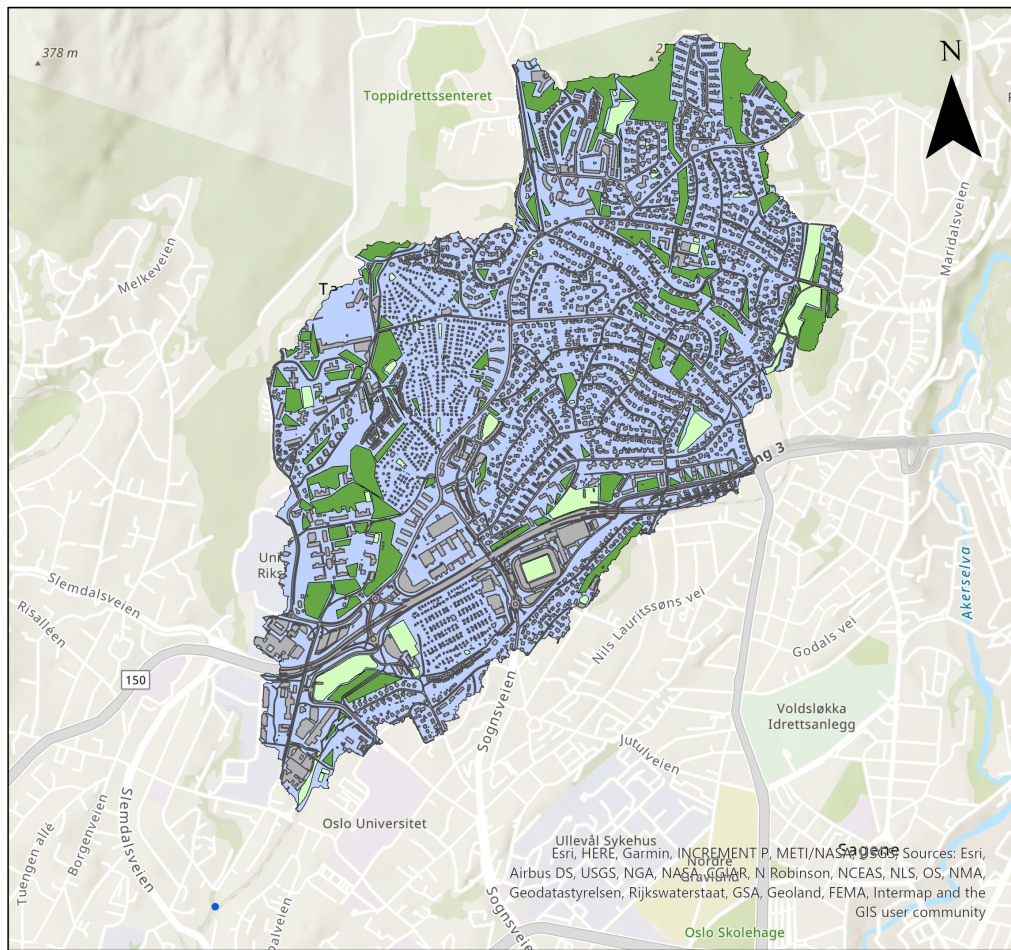


Figure 5.1: Soil Infiltration map created from NGUs quaternary geology description in relation to hydraulic conductivities (cm/s) by Freeze and Cherry (1979), fieldwork results and GrunnTeknikk AS (2020). Map created in ArcGIS Pro, with K values determined in this study on top of the infiltration potential map from NGU.

Surface cover



- Gaustadbekken Weir
- Roads and Buildings
- Parks and Artificial grass
- Lawns and Pebblestreets
- Forest

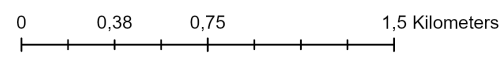


Figure 5.2: Surface covers of Gaustad watershed, produced in ArcGIS Pro. Data from FKB.

Table 5.5: Surface cover percentages of the Gaustad watershed found by investigations into the catchment using ArcGIS Pro.

Surface cover type	Sum areal [ $m^2$ ]	Percentage [%]
Roads and buildings	959850	24.1
Lawn and gravel roads	2445842	61.4
Parks and artificial grass-fields	134842	3.4
Forest	441065	11.1

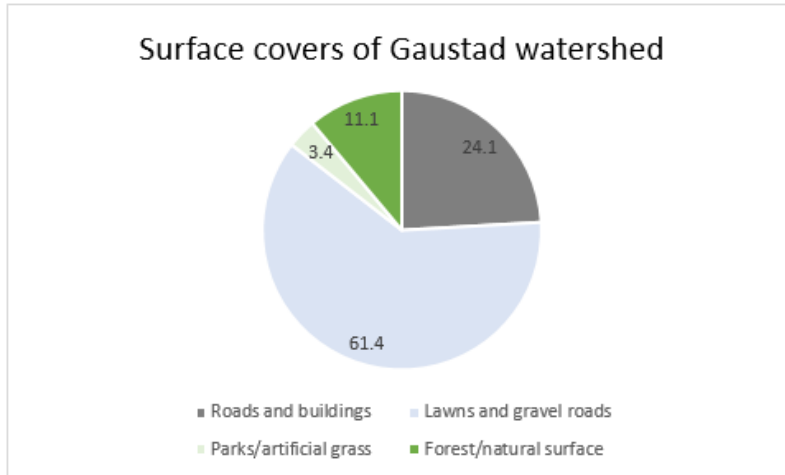


Figure 5.3: Surface covers of Gaustad watershed as found in ArcGIS Pro and illustrated in figure 5.2, presented as a table and pie-chart.

The investigations into the surface covers at Gaustad (ref. fig. 5.2, 5.3 and table 5.5) shows the dominance of lawns and gravel roads (61.4 %), consistent with villa housing in the area. These areas are considered of limited infiltration potential, with runoff coefficients of 0.1-0.6 (Mays, 2001). There is also a substantial amount of roads and buildings (24.1 %) which are considered to allow for no infiltration. There are some areas of forest in the watershed (11.1 %) as well as some parks and artificial grass fields (3.4 %).

### 5.3 Discharge of Gaustadbekken during the study period

Gaustadbekken was surveyed through the period 8.10.20 - 30.6.21 by an Ott Orpheus mini water level logger device and manually measured water levels at the weir. The discharge series (see fig. 5.4) was used when calibrating the hydrological model in Mike+, both by visual comparison of the observed vs. simulated hydrographs and by efficiency criteria such as the R2, RMSE and NSE (described in subsection 2.5).

#### Observed discharge

The observed discharge of Gaustadbekken for the surveying period is shown in figure 5.4. The discharge was found by the method described in subsection 4.1, the location of the measurement device is shown in figure 4.3.

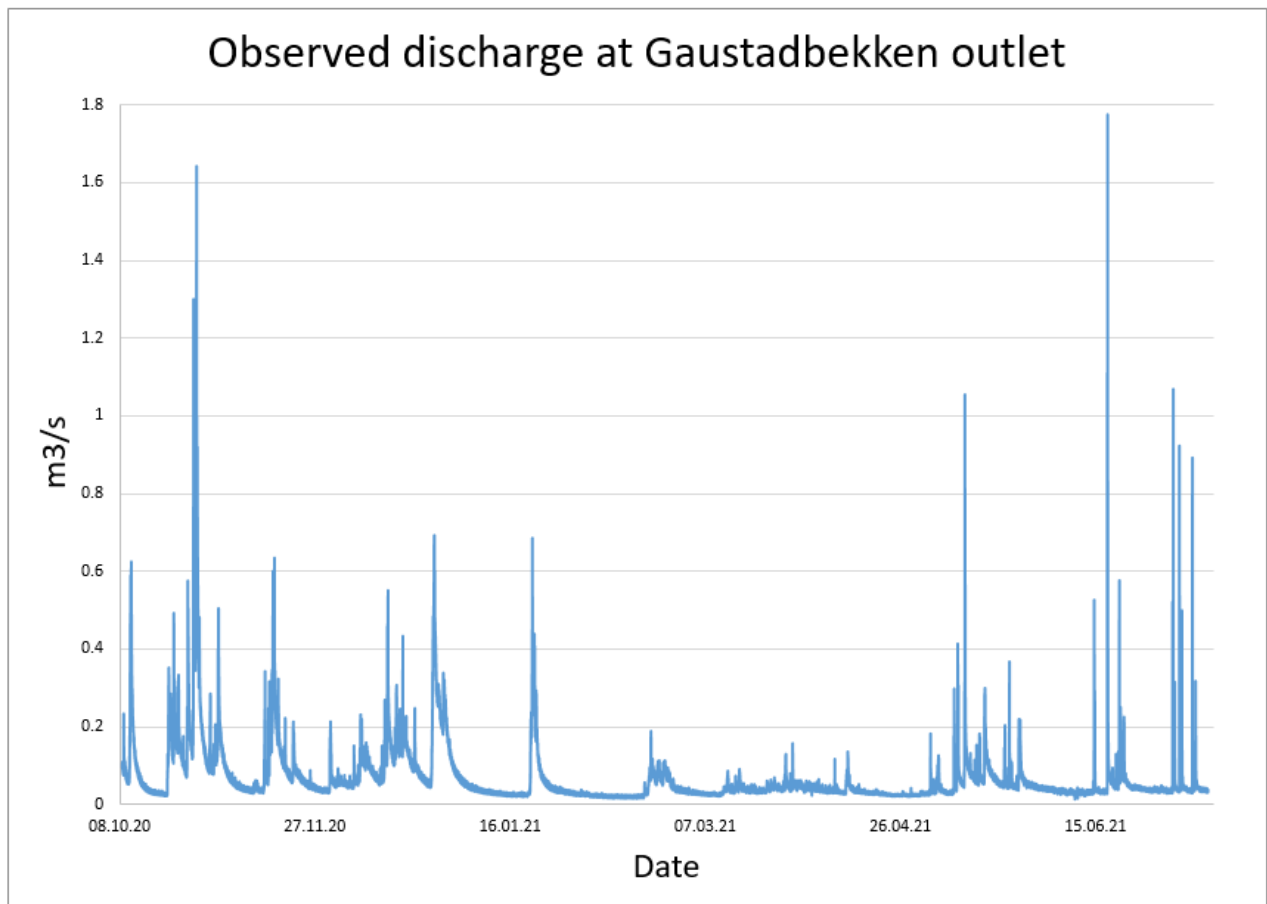


Figure 5.4: Measured discharge of Gaustadbekken through the study period, used for calibration of the hydrological model in Mike+.

The observed discharge of Gaustadbekken outlet (fig. 5.4) illustrates typical seasonal variations, with higher discharge during autumn and spring. The surveying period includes both wet and dry periods, which is necessary for calibration of a rainfall-runoff model.



### Verification of the observed discharge data

The rating curve in figure 5.5 illustrates the discharge (L/s) corresponding to water levels (m) from the bottom of the v-notch at Gaustadbekken weir.

To verify the discharge series, the tracer dilution method was applied (described in subsection 4.1) at three events during the surveying period. The results of the tracer dilution validates the calculated discharge, as illustrated in figure 5.5.

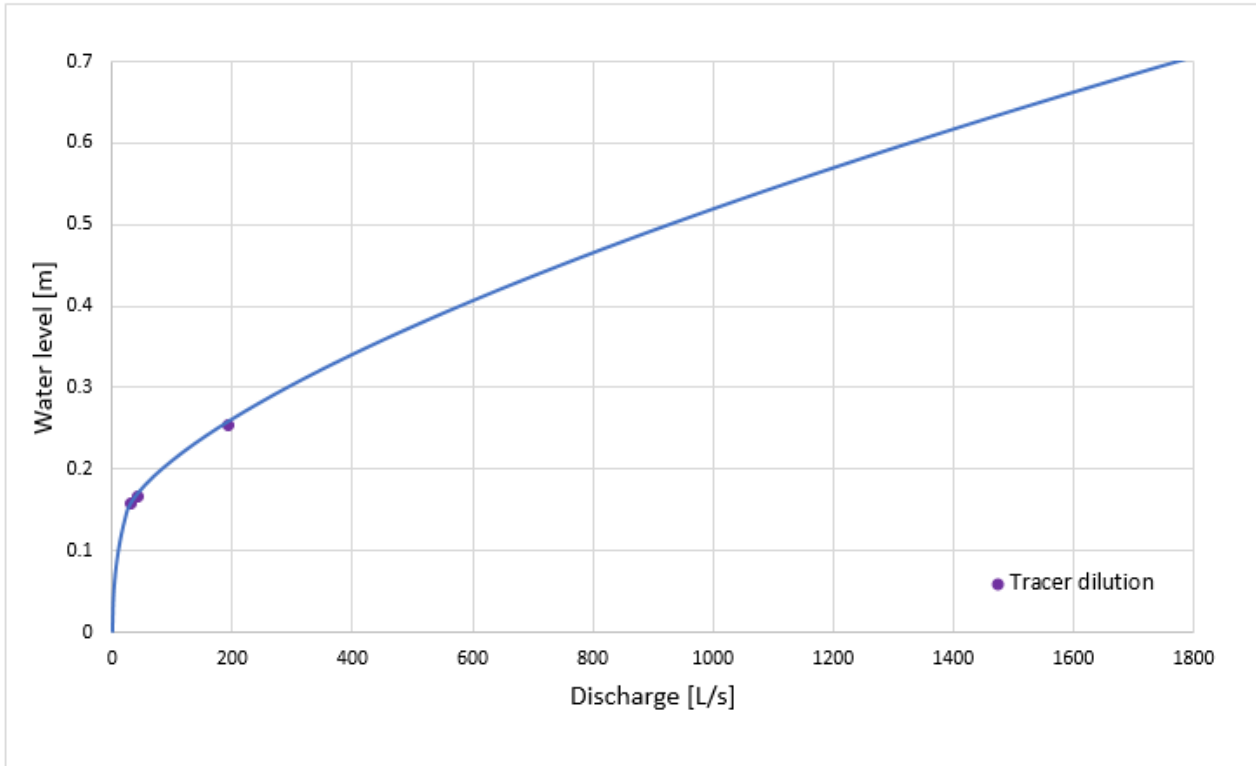


Figure 5.5: Rating curve comparing the discharge found by the method described in subsection 4.1 by the observed tracer dilution method results.

As can be seen in figure 5.5, the observed values from the tracer dilution method correlates well with the calculated discharge by the equation 4.3.

## 5.4 Chemical properties of Gaustadbekken and Sognsvannbekken

Investigations into the chemical properties of Gaustadbekken and Sognsvannbekken was conducted to shed light on any variations throughout the Gaustad watershed and Sognsvannbekken, as well as comparing the two streams in search of evident differences. Field properties like pH, electrical conductivity (EC) and temperature was measured at several locations in Gaustadbekken (25.8.20) and Sognsvannbekken (26.8.20) in collaboration with students in the course "Field Methods in Hydrogeology (GEO4360)". Locations are shown in the figure 4.7. Water samples at these locations were also collected. Field parameters were measured by Anja Sundal for some of the locations (3.4.20) and is included in the results with permission.

Field parameters was measured at the joining point of Gaustadbekken and Sognsvannbekken (see fig. 4.7) with approximately one month intervals to investigate changes through the study period and differences between the streams. Water samples were collected at the joining point in both rivers at two dates after a rainfall event (17.12.20 and 2.1.21). All water samples were analysed for heavy metals and ion concentrations. The samples from the joining point of Gaustadbekken and Sognsvannbekken was also tested for presence of *Escherichia coli* (*E. coli*).

### Measured chemical properties

#### Gaustadbekken electrical conductivity, temperature and pH

Table 5.6 shows the field parameters of Gaustadbekken throughout the watershed. The river is mostly closed in pipes (see fig. 3.2), so the points were chosen based on availability combined with the aim of a representative picture of the river water as it progresses (see map in fig. 4.7).

Table 5.6: Electrical conductivity (EC) in microsiemens/cm, pH and temperature (°C) for Gaustadbekken measured the 25.8.20.

Location	Field measurements
	25.8.20
Gaustadbekken by Blindern station (GBBS)	EC: 607 $\mu S/cm$ pH: 7.67 Temp: 11.7 °C
Konvallveien (KV)	EC: 410 $\mu S/cm$ pH: 7.80 Temp: 13.2 °C
Nils Bays vei (NBV)	EC: 266 $\mu S/cm$ pH: 7.74 Temp: 13.1 °C
Solvang Kolonihage (SK)	EC: 555 $\mu S/cm$ pH: 7.28 Temp: 12.2 °C

The field measurements of Gaustadbekken throughout Gaustad watershed shows enhanced values of EC at GBBS (607  $\mu S/cm$ ), SK (555  $\mu S/cm$ ) and KV (410  $\mu S/cm$ ). NBV exhibits a much lower EC value of (266  $\mu S/cm$ ). The pH is quite comparable for all locations, with just slightly lower value at SK (7.28). The temperature ranges from 11.7 °C at the lowest lying point of the river progression, to 13.2 °C at the highest lying point measured of the river progression.

**Sognsvannbekken electrical conductivity, temperature and pH**

Table 5.7 shows the field parameters of Sognsvannbekken measured at several locations (see map in fig. 4.7).

Table 5.7: Electrical conductivity (EC) in microsiemens/cm, pH and temperature (°C) for Sognsvannbekken measured the 26.8.20 and 31.8.20.

Location and date	Field measurements
Sognsvann 31.8.20	EC: 45 $\mu S/cm$ pH: 6.75 Temp: 16.6 °C
Risbekken (R) 26.8.20	EC: 222 $\mu S/cm$ pH: 7.71 Temp: 13.6 °C
Rikshospitalet (RH) 26.8.20	EC: 89 $\mu S/cm$ pH: - Temp: 15.3 °C
Anne Maries Vei (AMV) 26.8.20	EC: 128 $\mu S/cm$ pH: 6.69 Temp: 13.9 °C

The field measurements of Sognsvannbekken shows the highest values of EC at Rikshospitalet (222  $\mu S/cm$ ). The measured EC of Sognsvann and Rikshospitalet (RH) further downstream was respectively 45  $\mu S/cm$  and 89  $\mu S/cm$ . After mixing with Risbekken (R), the EC measures 128  $\mu S/cm$  at AMV. The pH is notably higher in R (7.71) compared to Sognsvann (6.75) and AMV (6.69). The pH of RH was not measured. The temperature of the river was highest at RH (15.3 °C), while R and AMV measured respectively 13.6 and 13.9 °C the same day (26.8.20). Sognsvann was measured a few days later (31.8.20) and the temperature was then found to be 16.6 °C.

Table 5.8: Electrical conductivity (EC) in microsiemens/cm, pH and temperature (°C) for Sognsvannbekken and Gaustadbekken measured the 3.4.20 by Anja Sundal (see map in fig. 4.7).

Location	Field measurements
Risbekken (R)	EC: 149 $\mu S/cm$ pH: 6.99 Temp: 5.3 °C
Rikshospitalet (RH)	EC: 72 $\mu S/cm$ pH: 7.24 Temp: 4.8 °C
Anne Maries Vei (AMV)	EC: 101 $\mu S/cm$ pH: 7.06 Temp: 5.1 °C
Gaustadbekken by Blindern Station (GBBS)	EC: 384 $\mu S/cm$ pH: 7.16 Temp: 6.1 °C

The EC measurements the 3.4.20 shows GBBS having a significantly higher value (384  $\mu S/cm$ ) than at any location of Sognsvannbekken. Risbekken measures the highest EC (149  $\mu S/cm$ ) of the water forming Sognsvannbekken, while RH measures 72  $\mu S/cm$  and AMV 101  $\mu S/cm$ . The pH is relatively stable throughout Sognsvannbekken with a range of 6.99 to 7.24, and GBBS measures 7.16. The

## 5. Results

temperature of Sognsvannbekken is notably lower than Gaustadbekken with a range of 4.6 °C to 5.3 °C, while GBBS measures a temperature of 6.1 °C.

### Joining point of Sognsvannbekken and Gaustadbekken electrical conductivity, temperature and pH

Electrical conductivity (EC) in micro-Siemens, pH and temperature measured at Gaustadbekken weir and Sognsvannbekken (see map in fig. 4.3) is shown in table 5.9.

Table 5.9: Electrical conductivity (EC) in microsiemens/cm, pH and temperature (°C) for Gaustadbekken and Sognsvannbekken right before the two rivers merges into Frognerbekken.

Date	Gaustadbekken	Sognsvannbekken
11.10.20	EC : 543 Temp : 11.1	
11.12.20	EC : 835 Temp : 7.9	
17.12.20	EC : 855 pH : 7.87 Temp : 7.7	EC : 129 pH : 7.37 Temp : 3.2
2.1.21	EC : 842	EC : 131
31.3.21	EC : 905 Temp : 6.7	EC : 76 Temp : 3.2
8.5.21	EC : 613 Temp : 8.2	EC : 139 Temp : 7.8
6.6.21	EC : 566 Temp : 10.1	EC : 158 Temp : 15.3

Field measurements of the pH, temperature and electrical conductivity (EC) of both Gaustadbekken and Sognsvannbekken reveal significant differences between the two surface streams. Gaustadbekken has relatively high values of EC from 543 to 905  $\mu S/cm$ . It is at its lowest in October with a value of 543  $\mu S/cm$  and at its highest in March 2021 with a value of 905  $\mu S/cm$ , while the months from December up to March is relatively stable at 835-842  $\mu S/cm$ . During spring the EC is decreasing and in may, the EC is measured to be 613  $\mu S/cm$  and 566  $\mu S/cm$  in June.

The EC in Sognsvannbekken is systematically significantly lower than in Gaustadbekken with its lowest value of 76  $\mu S/cm$  at the same time that Gaustadbekken has its highest value. December to January, the EC is 129  $\mu S/cm$  and 131  $\mu S/cm$ . After the dip in March, the EC returns to 139  $\mu S/cm$  in May before measuring 158  $\mu S/cm$  in June. The temperature is also differing between the two streams, especially in the winter months. Gaustadbekken is holding a higher temperature than Sognsvannbekken at all measurements December to may. Sognsvannbekken was also observed to be partly frozen 3.2.2020 when Gaustadbekken was seemingly unaffected by the air temperature (see fig. 5.6). During spring, however, the temperature in Gaustadbekken is measured at 10.1 °C while Sognsvannbekken holds a temperature of 15.3 °C. The pH is comparable for the one event where it was measured in the field at these locations.

The difference in temperature (table 5.9) is illustrated by figure 5.6 where Sognsvannbekken is frozen, while Gaustadbekken is flowing freely.



Figure 5.6: Gaustadbekken and Sognsvannbekken February 3rd, 2021. Sognsvannbekken is clearly frozen to a great extent, while Gaustadbekken is flowing without any ice elements.

## Chemical analysis results

### Gaustadbekken, Gaustad watershed

#### Heavy metals

The results of the heavy metal analysis of the samples collected from Gaustadbekken at several points within the Gaustad watershed the 25.8.20 (locations shown in fig. 4.7) are presented in table 5.10.

Table 5.10: Results of the heavy metals analysis of Gaustadbekken within Gaustad watershed at several points during 25.8.20.

Sample	Cr [µg/L]	Ni [µg/L]	Cu [µg/L]	Zn [µg/L]	As [µg/L]	Cd [µg/L]	Pb [µg/L]
Gaustadbekken by Blindern station (GBBS)	0.726	1.938	2.535	5.766	1.042	0.000	0.696
Konvallveien (KV)	0.173	0.713	2.964	1.439	0.572	0.000	0.200
Solvang Kolonihage (SK)	0.301	2.013	5.392	9.915	0.709	0.000	1.221
Nils Bays vei (NBV)	0.229	1.154	2.257	1.742	0.626	0.000	0.171

The heavy metal analysis of the open parts of Gaustadbekken within Gaustad watershed shows several values classifying as moderate. All samples receives the classification *moderate* for Arsenic (>0,5 µg/L) and thus the samples would all be considered as of Moderate quality (Miljødirektoratet, 2020). Solvang Kolonihage receives the classification *moderate* for Lead as well with a value of 1.22

## 5. Results

µg/L. The samples from Solvang Kolonihage and Gaustadbekken BBS is exhibiting elevated values of Zinc (Zn), but still within what would be classified as *Good* quality for freshwater. The samples of Solvang Kolonihage and Gaustadbekken BBS generally has higher concentrations of heavy metal than Konvallveien and Nils Bays vei, but they all classify within the same category of *moderate* due to the high levels of Arsenic.

### Cations

Table 5.11: Cations of water samples from Gaustadbekken within Gaustad watershed 25.8.20 (see map in fig. 4.7).

Sample	$Na^+$ [ppm]	$K^+$ [ppm]	$Mg^{2+}$ [ppm]	$Ca^{2+}$ [ppm]
Gaustadbekken by Blindern station (GBBS)	37.775	7.402	7.197	75.872
Konvallveien (KV)	25.649	2.243	4.163	50.393
Solvang Kolonihage (SK)	26.373	5.111	4.275	80.150
Nils Bays vei (NBV)	6.955	1.880	2.573	38.123

The water samples of Gaustadbekken gathered on the 25.8.20 was analysed in the chemical lab the 31.8.20 as 10 times diluted samples to fit the calibration range. The results of the cations analysis for the water samples taken the 25.8.20 in different locations of Gaustadbekken shows all samples containing high values of Calcium (Ca), with Solvang Kolonihage exhibiting the highest at 80.15 ppm. GBBS measures the second highest concentration of Ca with 75.872 ppm, while KV and NBV shows significantly lower values of respectively 50.393 and 38.123 ppm. There were higher concentrations of all cations in the samples from SK and GBBS, but especially evident for Calcium. The level of Sodium (Na) is highest at GBBS with 37.775 ppm, second highest at SK with 26.373 ppm closely followed by KV with 25.649 ppm. NBS on the other hand measures modest 6.955 ppm Sodium. For Potassium (K) and Magnesium (Mg), the measured values were more comparable for the different locations of Gaustadbekken, with ranges from respectively 1.880-7.402 ppm and 2.573-7.197 ppm.

### Anions

Table 5.12: Anions of water samples from Gaustadbekken within Gaustad watershed 25.8.20 (see map in fig. 4.7).

Sample	$F^-$ [ppm]	$Cl^-$ [ppm]	$SO_4^{2-}$ [ppm]	$Br^-$ [ppm]	$NO_3^-$ [ppm]	$PO_4^{3-}$ [ppm]
Gaustadbekken by Blindern station (GBBS)	n.a.	63.290	64.140	2.750	6.720	n.a.
Konvallveien (KV)	n.a.	25.470	31.010	2.670	5.930	n.a.
Solvang Kolonihage (SK)	n.a.	41.180	39.500	2.670	10.490	n.a.
Nils Bays vei (NBV)	0.108	10.825	11.433	0.261	4.610	0.029

The values of Chloride (Cl) and Sulphate (SO<sub>4</sub>) for the samples GBBS, SK and KV was above the range of calibration. These samples was therefore analyzed as 10 times diluted. The samples analysed from GBBS and SK notably exhibits the highest concentrations of anions of the locations within Gaustad watershed on the 25.8.20. This is especially evident for Cl and SO<sub>4</sub>. The concentration for Cl at GBBS is 63.29 ppm, SK measures 41.18 ppm, while KV and NBV has respectively 25.47 and 10.825 ppm. The levels of SO<sub>4</sub> follows the same distribution with 64.14 ppm measured at GBBS, 39.5 ppm at SK, 31.01 ppm for KV and 11.433 ppm for NBV. Bromine (Br) and Nitrate (NO<sub>3</sub>) measured relatively similar values for all locations, ranging from respectively 0.261-2.75 ppm and 4.61-10.49 ppm. Also for the anions it is GBBS and SK that holds the highest concentrations, while NBV is the lowest. The level of Fluorine (F) and Phosphate (PO<sub>4</sub>) was below the limit of detection

for the samples GBBS, KV and SK, while NBV measured a very small values of respectively 0.108 ppm and 0.029 ppm.

### Alkalinity and pH

Table 5.13: Alkalinity and pH of Gaustadbekken 25.8.20 (see map in fig. 4.7).

Sample	pH	Alkalinity [meq/L]
Gaustadbekken by Blindern station (GBBS)	8.04	2.5
Konvallveien (KV)	8.1	2.4
Solvang Kolonihage (SK)	7.6	3.2
Nils Bays vei (NBV)	8.0	1.7

The pH and alkalinity of Gaustadbekken was measured in the water samples brought in for analysis at the lab. Both the pH and alkalinity is comparable for all water samples with ranges respectively 7.6-8.1 and 2.4-3.2 meq/L. The location with the lowest pH and highest alkalinity is SK with pH 7.6 and alkalinity 3.2 meq/L. The other locations are almost identical.

### Electrical balance

Table 5.14: Electrical balance of the samples gathered in Gaustadbekken 25.8.20.

Sample	Electrical balance [%]
Gaustadbekken by Blindern station (GBBS)	4
Konvallveien (KV)	2
Solvang Kolonihage (SK)	2
Nils Bays vei (NBV)	3

The electrical balance (EB) is below 5 % for all samples gathered in Gaustadbekken at 25.8.20 (ref. table 5.14) and the samples are considered trustworthy.

### Sognsvannbekken

The results of the ion analysis for locations of Sognsvannbekken is shown in tables 5.16 and 5.17, heavy metals are presented in table 5.15.

### Heavy metals

Table 5.15: Results of Heavy metals analysis of Sognsvannbekken at several points during 26.8.20 (see map in fig. 4.7).

Sample	Cr [µg/L]	Ni [µg/L]	Cu [µg/L]	Zn [µg/L]	As [µg/L]	Cd [µg/L]	Pb [µg/L]
Risbekken (R)	0.136	0.791	3.192	2.037	0.449	0.000	0.091
Rikshospitalet (RH)	0.142	0.469	1.656	5.549	0.325	0.000	0.306
Anne Maries vei (AMV)	0.1302	0.439	0.965	2.216	0.409	0.000	0.200

There are no levels of concentration in any of the localities that is above threshold values for freshwater as set by the the Norwegian Environment Agency (NEA). By the classification of freshwater quality by

## 5. Results

(NEA), all water samples from Sognsvannbekken are therefore classified as *Good*. The concentrations are mostly comparable for all samples but it can be noted that Copper (Cu) has somewhat higher level in R (3.192 µg/L), while Zinc (Zn) measures the highest level at RH with 5.549 µg/L.

### Cations

Table 5.16: Cations of water samples from Risbekken-Sognsvannbekken 26.8.20 (see map in fig. 4.7).

Sample	$Na^+$ [ppm]	$K^+$ [ppm]	$Mg^{2+}$ [ppm]	$Ca^{2+}$ [ppm]
Risbekken (R)	4.796	1.314	1.443	34.928
Rikshospitalet (RH)	4.122	1.093	0.785	11.653
Anne Maries vei (AMV)	4.933	0.792	1.219	15.446

The samples of R and RH measured outside of the calibration range and was analysed 10 times diluted. The values are shown in table 5.16. The values of Na, K and Mg is comparable for all locations, but the concentration of Ca is notably higher in R with 34.928 ppm. RH has a value of 11.653 ppm, while after the mixing of the two rivers, AMV holds a concentration of 15.336 ppm.

### Anions

Table 5.17: Anions of water samples from Risbekken-Sognsvannbekken 26.8.20 (see map in fig. 4.7).

Sample	$F^-$ [ppm]	$Cl^-$ [ppm]	$SO_4^{2-}$ [ppm]	$Br^-$ [ppm]	$NO_3^-$ [ppm]	$PO_4^{3-}$ [ppm]
Risbekken (R)	0.024	5.837	8.754	0.257	2.512	n.a.
Rikshospitalet (RH)	0.035	4.957	6.244	0.26	1.474	n.a.
Anne Maries vei (AMV)	0.024	6.072	8.135	0.260	1.183	n.a.

The chemical concentration of anions in the different locations of Sognsvannbekken is comparable for all locations 5.17. There is a slight difference between R and RH, where R has somewhat higher values of Cl,  $SO_4$  and  $NO_3$ . There is, however, no significant diversity of the anions for the locations at Sognsvannbekken.

### Alkalinity and pH

Table 5.18: Alkalinity and pH of Risbekken-Sognsvannbekken 26.8.20 (see map in fig. 4.7).

Sample	pH	Alkalinity [meq/L]
Risbekken (R)	8.1	1.3
Rikshospitalet (RH)	7.3	0.6
Anne Maries vei (AMV)	7.6	0.7

The pH and alkalinity measured from the samples of the locations in Sognsvannbekken is presented in table 5.18. There is an evident difference between, with R having a pH value of 8.12 and an alkalinity of 1.3 meq/L, while RH has a pH of 7.3 and an alkalinity of 0.6 meq/L. After the mixing of the two river branches, AMV measures slightly higher values than RH, but much lower than R, with a pH of 7.6 and an alkalinity of 0.7 meq/L.



## 5.4. Chemical properties of Gaustadbekken and Sognsvannbekken

Table 5.19: Electrical balance of the samples gathered in Risbekken-Sognsvannbekken 26.8.20.

Sample	Electrical balance [%]
Risbekken (R)	11
Rikshospitalet (RH)	38
Anne Maries vei (AMV)	2

### Electrical balance

The electrical balance (EB) is above 5 % for the samples R and RH 5.19 and are therefore not to be trusted completely. The sample from AMV is, however, well within what is considered valid.

### Joining point of Gaustadbekken and Sognsvannbekken

Samples were gathered in both Gaustadbekken and Sognsvannbekken, right before they merge and becomes Frognerbekken (see location in fig. 4.7). The properties of Gaustadbekken and Sognsvannbekken was investigated to study potential differences between the two surface streams.

### Heavy metals

Results of the heavy metals analysis for Gaustadbekken and Sognsvannbekken is presented in table 5.20.

Table 5.20: Results of Heavy metals analysis for the samples from Gaustadbekken weir and Sognsvannbekken taken the dates of 17.12.20 and 2.1.21 (see map in fig. 4.3).

Sample	Cr [µg/L]	Mn [µg/L]	Fe [µg/L]	Ni [µg/L]	Cu [µg/L]	Zn [µg/L]	As [µg/L]	Cd [µg/L]	Hg [µg/L]	Pb [µg/L]
17.12.20										
Gaustad (GAUS17)	0.390	14.300	10.300	1.730	3.490	20.900	0.700	0.000	0.030	0.020
Sognsvann (SOGN17)	0.220	9.580	53.250	0.370	1.030	9.160	0.330	0.000	0.010	0.110
2.1.21										
Gaustad (GAUS2)	0.300	8.620	14.390	2.200	2.210	5.640	0.470	0.000	0.010	0.010
Sognsvann (SOGN2)	0.310	10.690	61.230	0.390	0.720	7.080	0.130	0.010	0.010	0.060

The samples from Gaustadbekken had concentrations outside the range of calibration for Cl and SO<sub>4</sub>, and was therefore diluted 10 times and analysed again. The table 5.20 shows the values of these concentrations from the diluted samples timed with the dilution factor of 10. The samples marked with pink colour was below the detection limit of the method. There is no threshold values for freshwater to classify the status based on Manganese (Mn) or Iron (Fe), these are therefore not coloured as any classification status.

The heavy metal analysis show high values of iron (Fe) for Sognsvannbekken both 17.12.20 and 2.1.21, respectively 53.25 µg/L and 61.23 µg/L. The concentration of Fe in Gaustadbekken for the samples collected the 17.12.20 is 10.3 µg/L and 14.39 µg/L for 2.1.21. The only sample receiving the classification of *moderate* and *bad* is Gaustad 17.12.20 with a Zinc level being classified as *bad* with a concentration of 20.9µg/L, and moderate for the Arsenic with a concentration of 0.7µg/L. All concentrations of the other samples holds a background or beneath the limit of detection. This causes the water sample of Gaustadbekken taken the 17.12.20 to classify as *bad*, while the other samples all classify as *good*. The general trend is, however, higher concentrations of heavy metals in the samples from Gaustadbekken and elevated values when heavy rainfall events (17.12.20).

## 5. Results

### Cations

Cation analysis results are presented in the table 5.21.

Table 5.21: Cations of water samples from Gaustadbekken and Sognsvannbekken collected by the location of the joining rivers (see map in fig. 4.3).

Sample	$Na^+$ [ppm]	$K^+$ [ppm]	$Mg^{2+}$ [ppm]	$Ca^{2+}$ [ppm]	$Li^+$ [ppm]	$NH_4^+$ [ppm]
17.12.20						
Gaustad (GAUS17)	66.900	3.360	4.750	60.500	0.020	n.a.
Sognsvann (SOGN17)	5.410	0.560	0.820	9.680	0.020	n.a.
2.1.21						
Gaustad (GAUS2)	43.800	3.980	6.360	70.900	0.020	n.a.
Sognsvann (SOGN2)	3.900	0.570	0.920	11.270	0.020	n.a.

10 times diluted replicas were measured to fit the calibration range of the used standards for Sodium and Calcium in both samples from Gaustadbekken (Gaustad 17.12.20 and Gaustad 2.1.21). The cation analysis (5.21) shows a general trend of Gaustadbekken having higher concentrations of cations than Sognsvannbekken. Especially elevated values are found in the sample from 17.12.20 with very high concentrations of both Sodium and Calcium with values of respectively 66.9 *ppm* and 60.5 *ppm*. The samples from Sognsvannbekken the same date had significantly lower concentrations of 5.41 *ppm* Na and 9.68 *ppm* Ca. The same bias is observed between the samples taken at 2.1.21 for Gaustadbekken and Sognsvannbekken, where Gaustadbekken measured 43.8 *ppm* Na and 70.9 *ppm* Ca, while Sognsvannbekken measures 3.90 *ppm* Na and 11.27 *ppm* Ca. The concentrations of K and Mg is comparable for the samples taken at both locations, both dates, but slightly higher levels is observed for Gaustadbekken. Li measures equal values, while  $NH_4$  is n.a. for all samples.

### Anions

Table 5.22: Anions of water samples from Gaustadbekken and Sognsvannbekken collected from the joining point of the two rivers (see map in fig. 4.3).

Sample	$F^-$ [ppm]	$Cl^-$ [ppm]	$SO_4^{2-}$ [ppm]	$Br^-$ [ppm]	$NO_3^-$ [ppm]	$PO_4^{3-}$ [ppm]
17.12.20						
Gaustad (GAUS17)	0.170	105.100	30.290	0.230	5.270	n.a.
Sognsvann (SOGN17)	0.090	6.770	4.970	n.a.	1.410	n.a.
2.1.21						
Gaustad (GAUS2)	0.220	69.570	43.460	n.a.	6.940	n.a.
Sognsvann (SOGN2)	0.100	4.660	5.870	n.a.	1.570	n.a.

10 times diluted replicas were measured to fit the calibration range of the used standards for Chloride and Sulphate in both samples from Gaustadbekken (Gaustad 17.12.20 and Gaustad 2.1.21). The anion analysis reveals significantly higher values of Cl in Gaustadbekken with values of 105.1 *ppm* for the 17.12.20 and 69.46 *ppm* for the 2.1.21 compared to Sognsvannbekken that measures 6.77 *ppm* and 4.66 *ppm* for the same dates. The level of  $SO_4$  is also notably enhanced in Gaustadbekken compared to Sognsvannbekken, as Gaustadbekken has a value of 30.29 *ppm* for the 17.12.20 and 43.46 *ppm* for the 2.1.20, while Sognsvannbekken measures 4.97 *ppm* and 5.87 *ppm* for the same dates. The  $NO_3$  concentrations is also higher for both samples from Gaustadbekken compared to Sognsvannbekken. The concentrations of F is not significant and the  $PO_4$  was not detected in any of the samples.

Table 5.23: Alkalinity and pH for Gaustadbekken and Sognsvannbekken water samples (see map in fig. 4.3).

Sample	pH	Alkalinity [meq/L]
17.12.20		
Gaustadbekken (GAUS17)	7.8	2.24
Sognsvannbekken (SOGN17)	7.8	0.48
2.1.21		
Gaustadbekken (GAUS2)	8.12	3.05
Sognsvannbekken (SOGN2)	6.7	0.54

### Alkalinity and pH

The pH is equal for the samples collected the 17.12.20 (7.8), but higher in Gaustadbekken (8.12) than Sognsvannbekken (6.7) in the samples from 2.1.21. The alkalinity is much higher for the water samples from Gaustadbekken than Sognsvannbekken for both dates, with respectively 2.24 meq/L compared to 0.48 meq/L the 17.12.20 and 3.05 meq/L to 0.54 meq/L the 2.1.21.

### Electrical balance

Table 5.24: Electrical balance of the samples gathered at the joining point of Gaustadbekken and Sognsvannbekken 17.12.20 and 2.1.21.

Sample	Electrical balance [%]
17.12.20	
Gaustadbekken (GAUS17)	4
Sognsvannbekken (SOGN17)	0
2.1.21	
Gaustadbekken (GAUS2)	0
Sognsvannbekken (SOGN2)	0

The electrical balance (EB) is below 5 % for all samples gathered at the joining points of the rivers Gaustadbekken and Sognsvannbekken, and the samples are therefore considered of good quality and can be trusted.

## 5.5 Escherichia coli

The test for presence of *E. coli* was done for the samples gathered from the joining point of Gaustadbekken and Sognsvannbekken (GAUS17, SOGN17, GAUS02 and SOGN02). There was no visible bubble inside the upside down glass after 48 hours for either Gaustadbekken or Sognsvannbekken (see section A, figure A.1) and thus no indication of sewer influence in the water samples.

## 5.6 Hydrologic Model calibration and validation

### Modification of the catchment area

The natural watershed had to be adapted to fit the situation of the collection system at Gaustad (fig. 5.7). In northeast of the watershed, a substantial area had to be added to ensure all areas leading to the outlet at Gaustadbekken weir would be included in the simulations.

The natural watershed including the watershed created from Gaustadbekken weir (see fig. 4.8) equals  $4\,024\,424\text{ m}^2$ . The watershed adjusted for the collection system, accounting for areas draining into Gaustadbekken outlet, is  $4\,785\,075\text{ m}^2$ . There is thus an expansion of the watershed by  $760\,651\text{ m}^2$ .

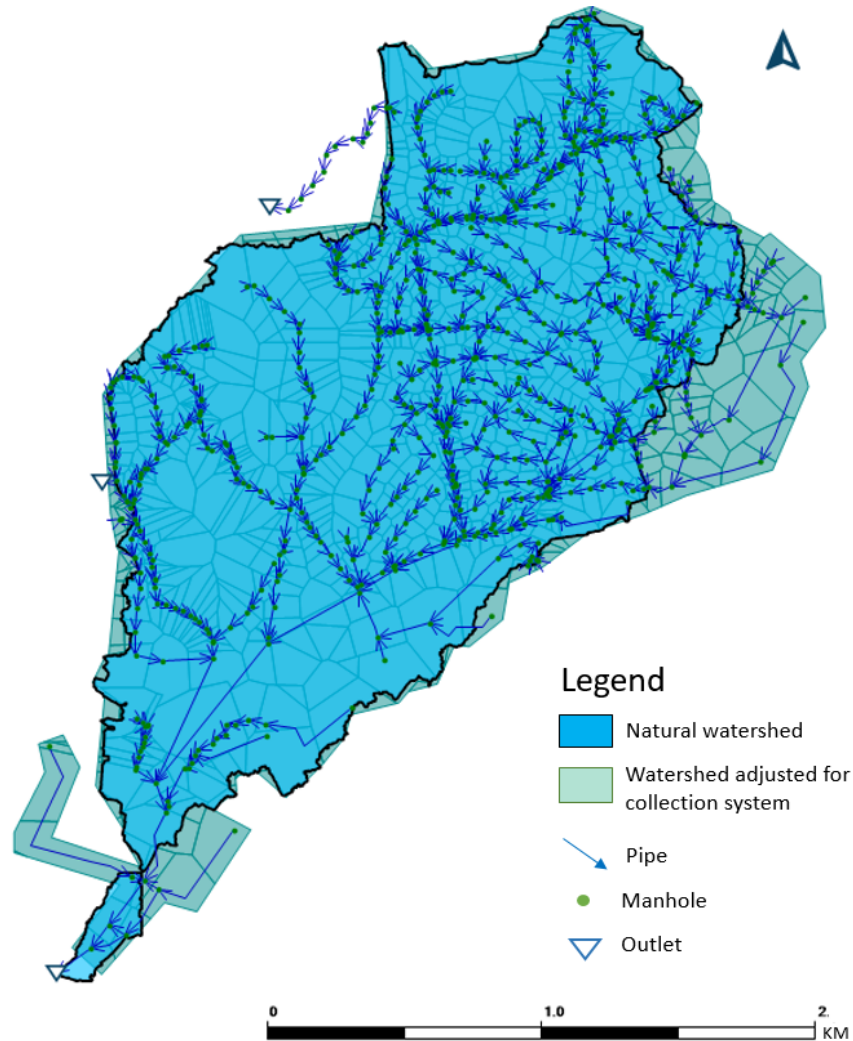


Figure 5.7: Catchment adjusted for collection system bringing water into the Gaustad catchment. Picture from the hydrologic model in Mike+, collection system data from Oslo municipality (VAV).

## Calibration

The calibration of the model achieved an  $RMSE$  of 0.0005,  $NSE$  value of 0.633 and an  $R^2$  of 0.7054 found by the methods described in subsection 2.5.

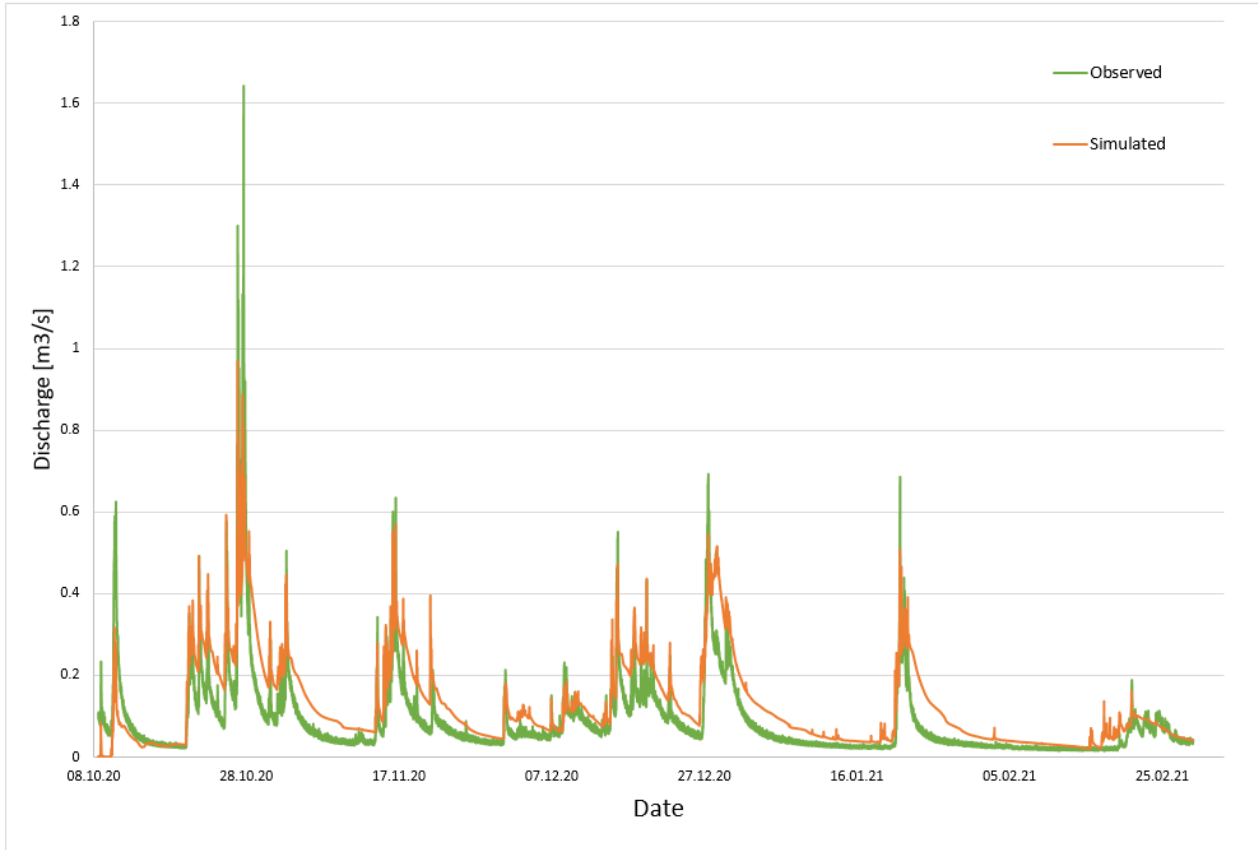


Figure 5.8: Calibration plot for visual estimation of the simulated vs observed output for the calibration period of 8.10.20-28.2.21.

The calibration plot of the simulated vs. observed discharge at Gaustadbekken outlet shows similar dynamics for the simulated discharge compared to the observed discharge (ref. fig. 5.8). This reflects the hydrodynamic parameters of the model and is evidently quite fitting for this watershed. There is, however, a systematic overestimation of the simulated discharge data at the Gaustadbekken outlet as illustrated by the figures 5.8 and 5.9. The flow peaks are consistently underestimated, while the recession flow is overestimated after every flow peak.

The simulated discharge in the calibration period was  $1\,525\,015\,m^3$ , while the observed discharge equals  $1\,103\,008\,m^3$  for the same period.

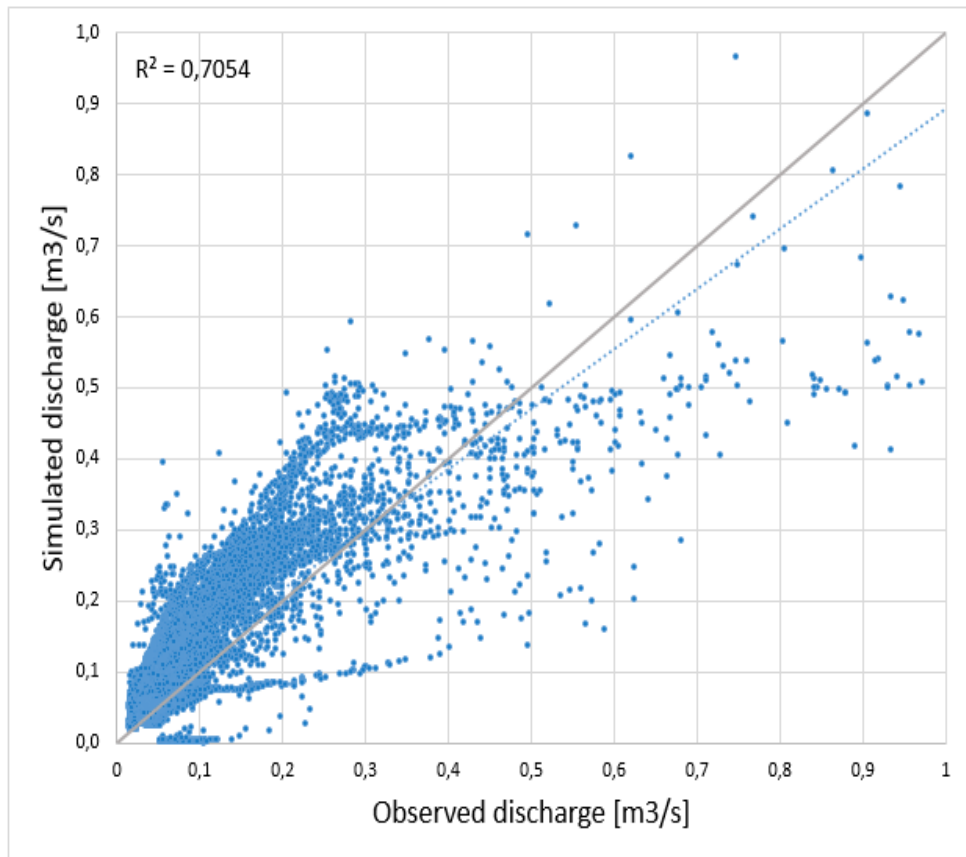


Figure 5.9: Correlation plot of the calibration period 8.10.20-28.2.21 for the discharge measurements at Gaustadbekken outlet.

The scatter plot in figure 5.9 shows there to be a systematic overestimation during low discharge, while the discharge peaks are often underestimated. The correlation still obtains an acceptable  $R^2$  value of 0.7054 for the calibration period.

## Validation

The model was validated with observed data from the time period 1.3.21 to 30.6.21. The validation period obtained an  $RMSE$  value of 0.0004, NSE of 0.332, and an  $R^2$  of 0.4273.

The validation was run together with the calibration period to ensure no storage of snow would get lost by running it as a separate model.

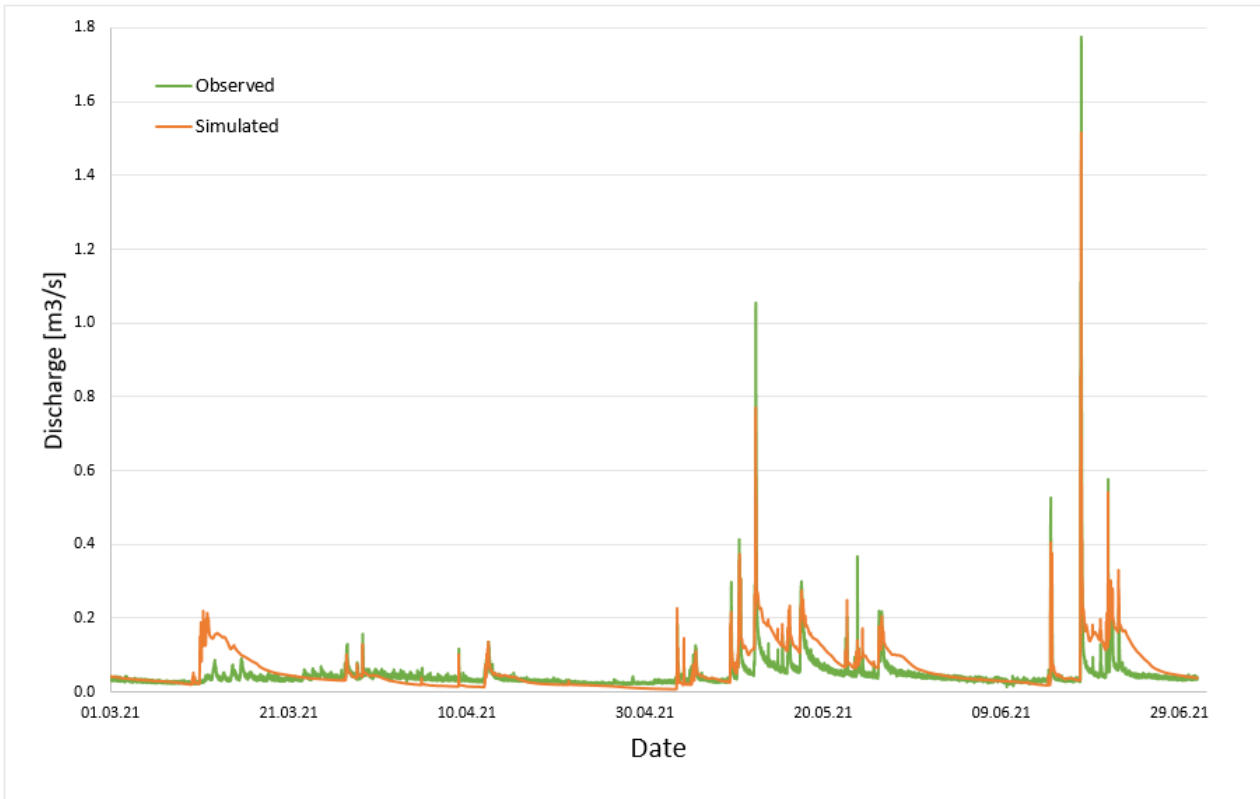


Figure 5.10: Calibration plot for visual estimation of the simulated vs observed output for the validation period of 1.3-30.6.2021.

The validation period illustrates good dynamic of the simulated data, with exception of one simulated discharge peak significantly overestimated (14.3.21) (ref. fig. 5.10).

The underestimation of the peaks flows and overestimation of the recession is comparable to the calibration period (see fig. 5.8). The efficiency criteria is lower than for the calibration period, likely due to the systematic overestimation of the recession flow (ref. fig. 5.10).

The simulated discharge in the validation period was  $641\,466\,m^3$ , while the observed discharge equals  $487\,684\,m^3$  for the same period.

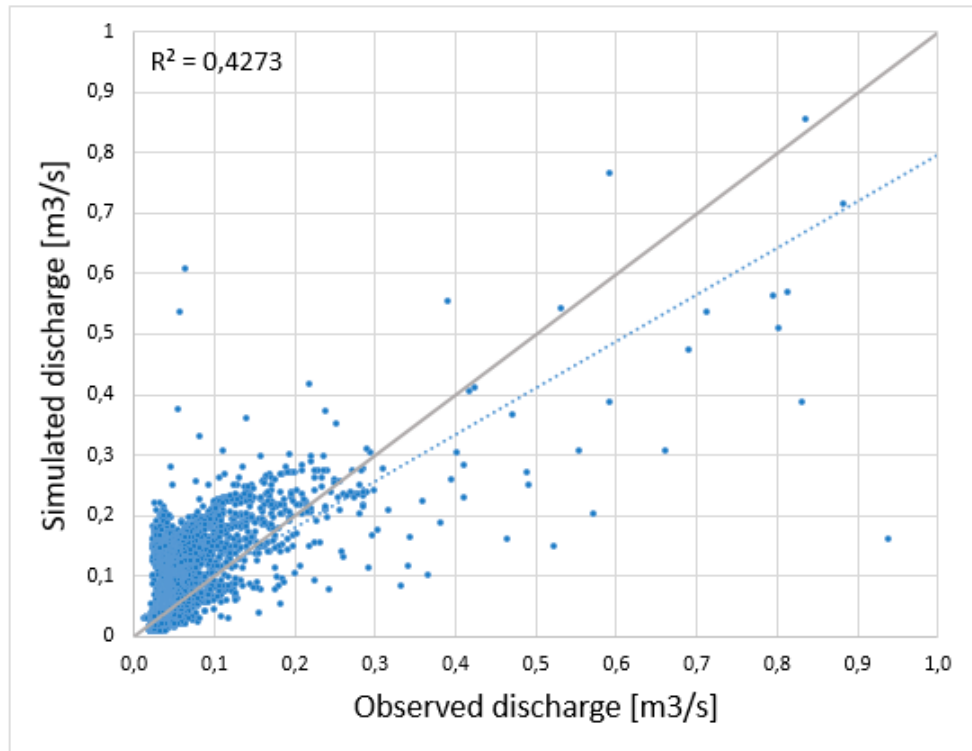


Figure 5.11: Correlation plot visualising the correlation of the simulated vs. observed discharge values for the validation period 1.3-30.6.2021.

The scatter plot in figure 5.11 further illustrates the underestimated flow peaks and overestimated recession flow seen in figure 5.10. The correlation has an  $R^2$  value of 0.4273 for the validation period.



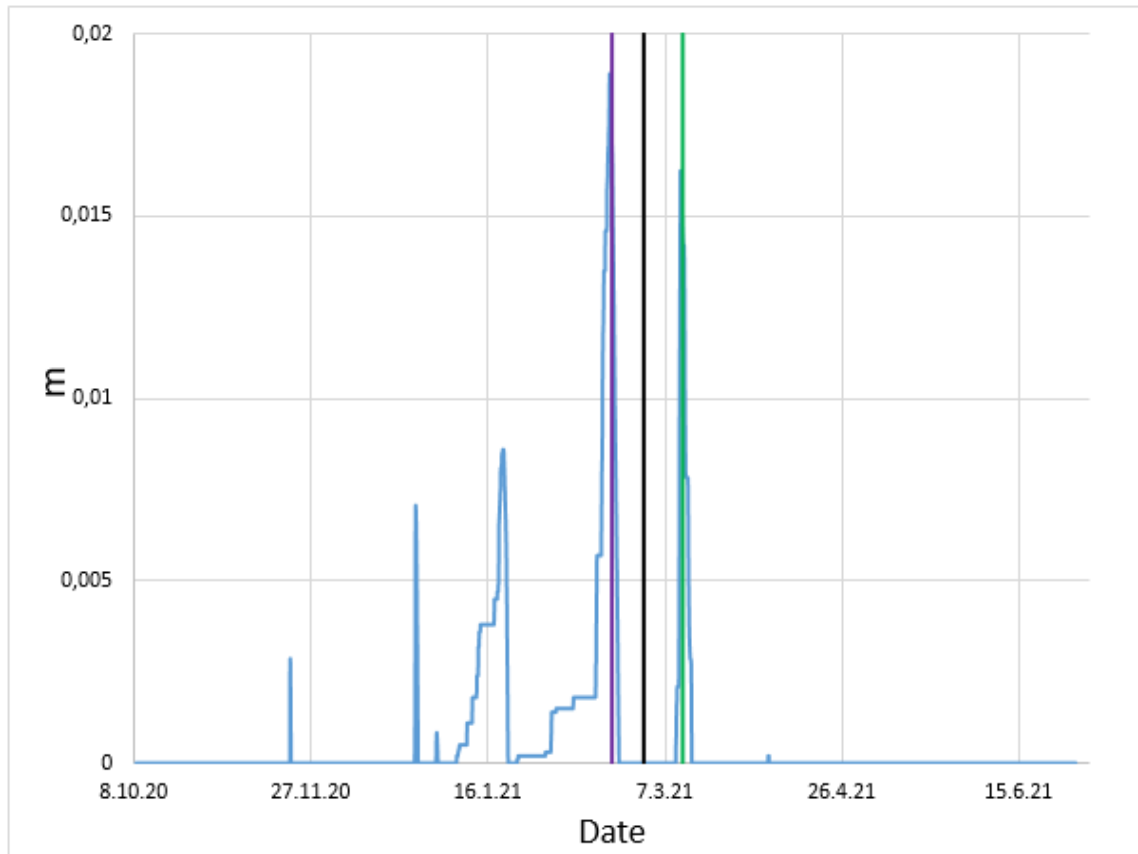


Figure 5.12: Snow storage in a representative sub-catchment during the calibration and validation period 8.10.20-30.6.21. The black line defines the divide between the calibration and validation period. The purple line marks the 20.2.20, the green line marks the 12.3.21.

Figure 5.12 shows simulated snow storage of a representative sub-catchments through the calibration and validation period. The black line marks the divide between the calibration and the validation period.

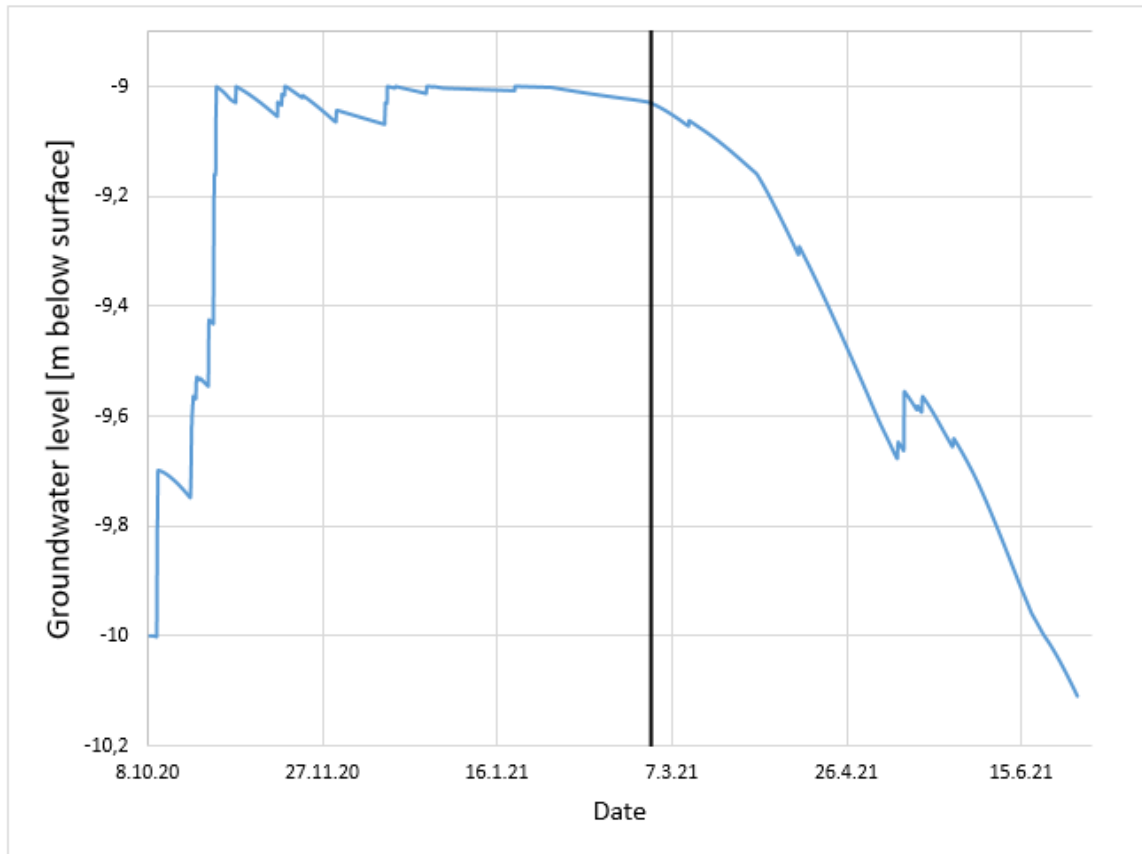


Figure 5.13: Groundwater level in a representative sub-catchment during the calibration and validation period 8.10.20-30.6.21. The black line defines the divide between the calibration and validation period.

Figure 5.13 shows simulated groundwater level of a representative sub-catchments through the calibration and validation period. The black line represents the divide between the calibration and the validation period.

### Sensitive parameters

In the Kinematic wave model, the distribution of the surface cover fractions are the most sensitive parameters. An increased fraction of impermeable surfaces causes increased surface runoff. When calibrating the model, it became clear that the RDI module had a larger impact on the dynamics of the discharge output than the kinematic wave computation. Especially the parameters overland flow time, surface storage capacity and interflow time affects the shape of the flow peaks. The overland coefficient has a large impact on the amount of surface runoff.

In efforts to improve the calibration of the model, there was an aim of increasing the peak flows and lowering the recession flow. Several parameters were changed in order to simulate more realistic values, but there was never found a combination of parameters that produced better simulation output than what is presented in this thesis.

## 5.7 Water budget, model results

The water budgets are estimated as the hydrological year in the northern hemisphere, from September 1st to August 31st the following year. Gaustad watershed as a natural setting, today's situation, the construction of the Life Science Building, as well as two future scenarios was modeled and the corresponding water budgets are presented in the results below. The parameters in the water budgets represents the sum of the Kinematic Wave model and Rainfall Dependent Infiltration model. Interflow and surface flow is not given on a catchment scale, and is therefore only available as output from each single sub-catchment of the model. As this model has over 900 sub-catchments, this was not done for the entire catchment water budgets.

The input precipitation is the hydrologic year 2018-2019, used to investigate the difference in the catchment water budget from a natural situation to a semi-urbanized area as today's situation. The local effect of the urban development was investigated by looking at the site-specific model output for the area representing the Life Science Building, presently under construction. The future scenarios was assigned additional precipitation, temperature increase and urban development relative to the year 2018-2019 as described in subsection 4.4.

### From natural to today's situation

The natural water budget was modeled by considering the entire Gaustad catchment as natural landscape, with all sub-catchments considered natural as described in subsection *Model Scenarios* (4.4) and modeled without urban drainage system. Today's situation was made to represent the current situation of Gaustad, Oslo, the distribution of *urban* and *rural* sub-catchments can be seen in figure 4.9.

Table 5.25: Water budget of the entire Gaustad catchment as a natural situation before urban development vs. today's situation as a semi-urbanized area.

Parameter	Natural situation		Today's situation	
	[mm]	[%]	[mm]	[%]
Precipitation	893.6	100.0	893.6	100.0
Runoff	424.8	47.5	651.8	72.9
Evaporation	477.2	53.4	259.9	29.1
$\Delta Storage$	-8.5	-1	-18.16	-2
Initial conditions [mm]	42.4		25.9	
End volume [mm]	33.9		7.8	

Precipitation is the rainfall input provided by the modeler (as a dfs0 time series file) into the hydrologic model, gathered from seklima.met.no. Runoff is considered the overland flow due to saturated soil, surface runoff, infiltrated water causing interflow and groundwater discharge. Evaporation is estimated by the hydrologic model in Mike+ on the basis of the potential evaporation calculated by the Thornthwaite method.

The water budget in table 5.25 shows that the catchment as a natural situation has 53.4 % evaporation and 47.5 % runoff, with a  $\Delta storage$  of -1 %. The current situation of the watershed has a significant alterations of the parameter as the simulations estimate 29.1 % evaporation and 72.9 % runoff. The  $\Delta storage$  of today's situation is -2 %.

### The impact of the Life Science Building on the catchment scale

The impact of the Life Science building (LSB) was studied at a catchment scale ( $4.785 \text{ km}^2$ ) by transforming  $0.074 \text{ km}^2$  rural area to *developed* in the hydrological model in Mike+. The sub-catchment representing the Life Science Building is shown in figure 5.14.

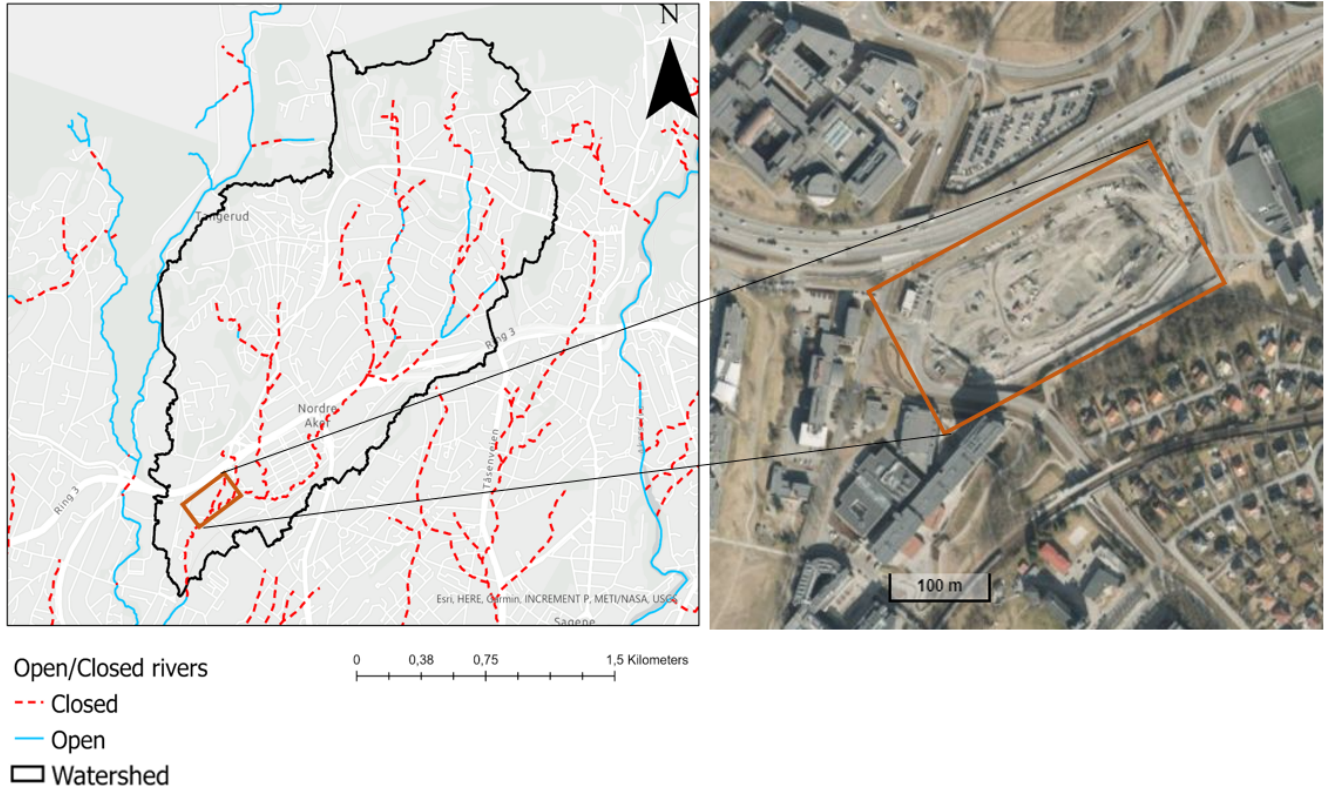


Figure 5.14: The location of the Life Science building presently under construction at Gaustad. Picture on the right from *Norgeskart.no*.

Table 5.26: Water budget of the total Gaustad catchment for the semi-urbanized scenario (2018-2019) before and after the construction of the Life Science Building (LSB) has been completed.

Parameter	Today's situation (before LSB)		LSB completed	
	[mm]	[%]	[mm]	[%]
Precipitation	893.6	100.0	893.6	100.0
Runoff	651.8	72.9	656.2	73.4
Evaporation	259.9	29.1	255.2	28.6
$\Delta$ Storage	-18.2	-2.0	-18.6	-2.1
Initial conditions [mm]	25.9		25.9	
End volume [mm]	7.8		7.4	

On the catchment scale of the hydrological model ( $4.785 \text{ km}^2$ ), the construction of a large building complex such as the Life Science Building does not present significant changes to the water budget.

Table 5.26 shows a slight change of the parameters, evaporation decreasing from 29.1 % of the water balance to 28.6 % while runoff correspondingly increase from 72.9 % to 73.4 %. The  $\Delta$  *storage* stays almost identical.

### Site specific changes to the water budget by the construction of the Life Science Building

To further investigate the changes linked with urban construction, the site specific results were studied. These are the results generated by the model for the site of  $74\,538\text{ m}^2$  that was changed from *rural* to *urban* (see subsec. 4.4) to investigate the effects these changes might pose for the water environment. The figures 5.15 and 5.16 illustrate the difference in reaction to an equal precipitation event for the area of the LSB before and after construction.

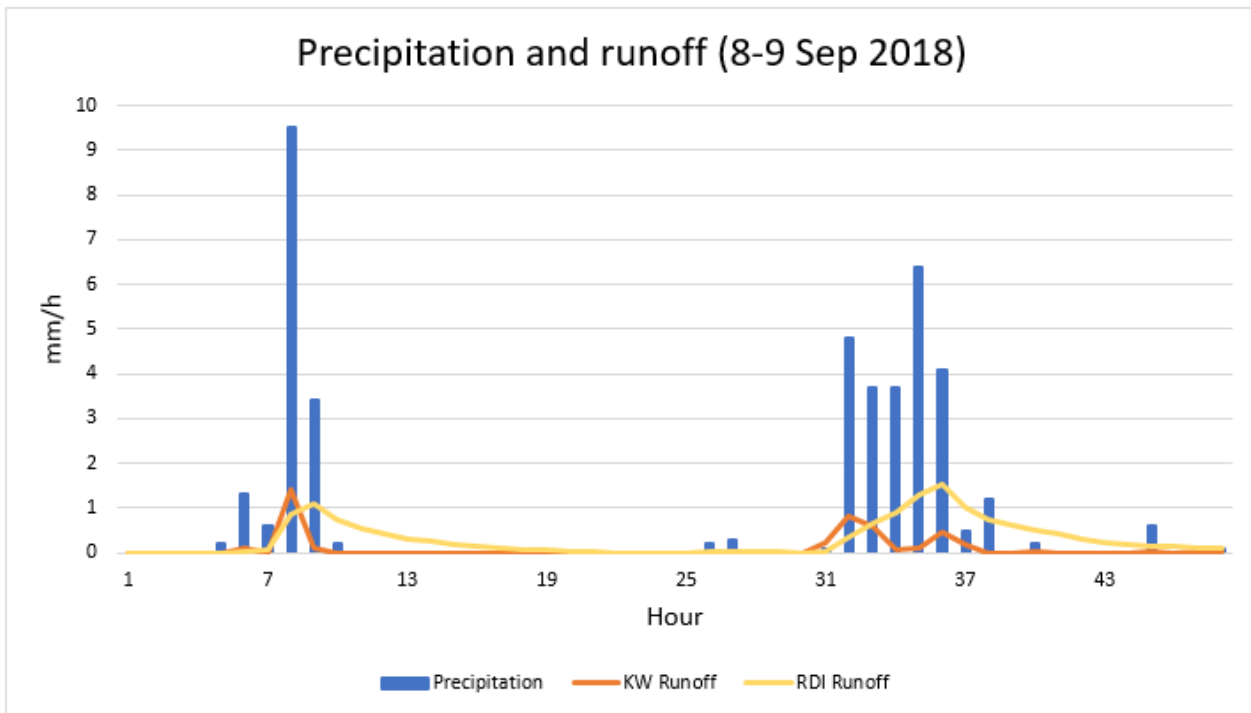


Figure 5.15: Precipitation together with runoff generated by the Kinematic Wave (KW) model and Rainfall Dependent Infiltration (RDI) model illustrating the different reactions to a rainfall event. The values are from the model with the Life Science Building as *rural*.

The runoff generated by the Kinematic Wave (KW) model clearly reacts quickly to a rainfall event, indicating that this represents surface runoff. The RDI runoff on the other hand reacts slower to the rainfall event, and has a much slower recession. This indicated the RDI runoff representing interflow and baseflow, and thus stems from the infiltrated water.

There is a significant increase of runoff computed by KW after the LSB is considered as urban, while the RDI runoff decrease slightly. The interpretation of the Kinematic wave model estimating surface runoff, while the Rainfall Dependent Infiltration model runoff output represent the infiltrated water through interflow and baseflow can be made. The overland flow generated by the RDI model is considered surface runoff. On the basis of this, the local water budget in table 5.27 could be made.

The results in table 5.27 shows the water budgets for the sub-catchment representing the Life Science Building *before* and *after* the completion of the construction. The numbers were rounded to the closest integer.

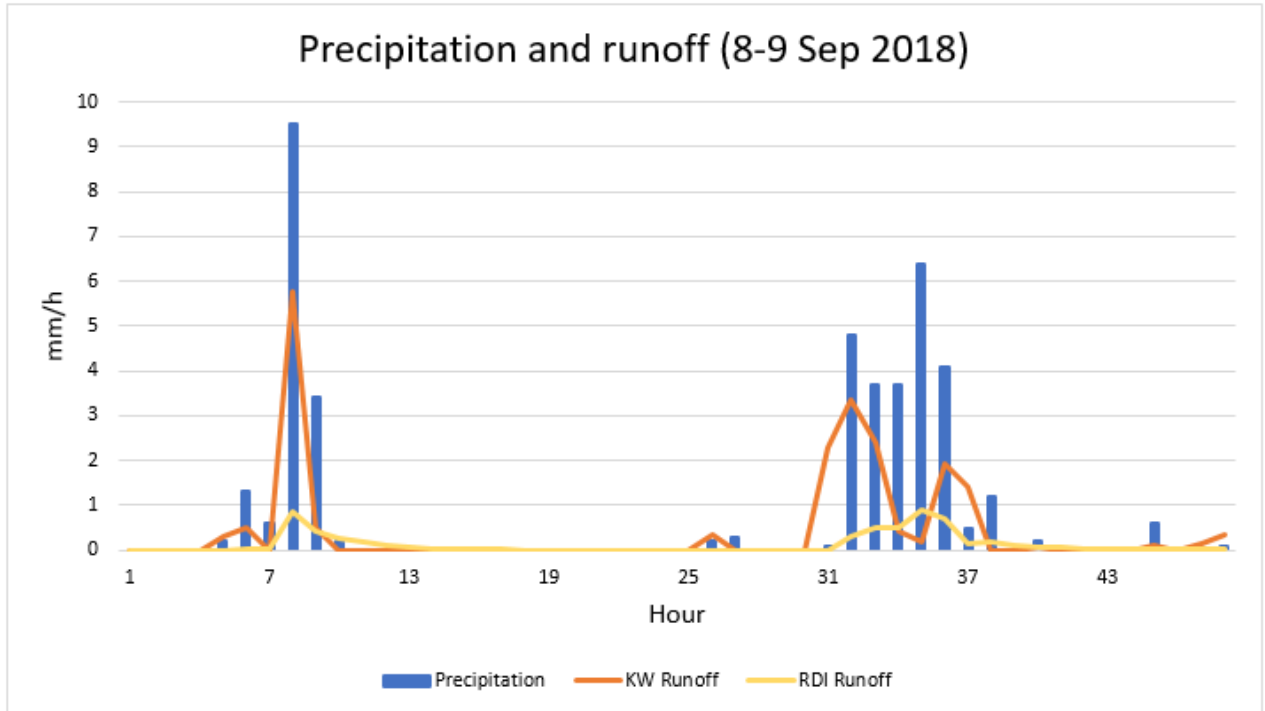


Figure 5.16: Precipitation together with runoff generated by the Kinematic Wave (KW) model and Rainfall Dependent Infiltration (RDI) model illustrating the different reactions to a rainfall event. The values are from the model with the Life Science Building as *urban*.

Table 5.27: Water budget for the Life Science Building site before and after completion of the construction as a total of both KW and RDI.

Parameter	Before construction	After construction
Precipitation [mm]	894	894
Surface runoff [mm]	186	719
Interflow [mm]	307	61
Evaporation [mm]	386	133
$\Delta$ Storage [mm]	15	-18

The surface runoff is considered as the runoff generated by the Kinematic wave model and overland flow generated by the Rainfall dependent infiltration model. This is supported by the calculations of the interflow (total runoff minus overland flow from RDI and runoff from KW) coinciding with the generated interflow by the RDI model. This interpretation is therefore considered sufficiently validated and was used for analysis of the model results. The interflow is the infiltrated water contributing to flow in the unsaturated zone.

### Future scenario

To simulate possible future scenarios, the urban fraction of the model was increased from 66 % (representing the current situation) to 76 %, combined with projected climatic changes.

Table 5.28: Water budget of the entire Gaustad catchment representing today's situation and climate scenarios RCP4.5 and RCP8.5 simulated together with a 15 % increase of *urban* sub-catchments.

Parameter	Today's situation (before LSB)		Future scenario RCP4.5		Future scenario RCP8.5	
	[mm]	[%]	[mm]	[%]	[mm]	[%]
Precipitation	893.6	100.0	934.7	100.0	975.8	100.0
Runoff	651.8	72.9	703.0	75.2	734.1	75.2
Evaporation	259.9	29.1	242.2	25.9	252.1	25.9
$\Delta Storage$	-18.16	-2	-10.5	-1.1	-10.5	-1.1
Initial conditions [mm]	25.9		18.1		18.1	
End volume [mm]	7.8		7.6		7.6	

The scenarios RCP4.5 and RCP8.5 for the years 2071-2100 shows the water budget changing from today's situation as illustrated in table 5.28. The amount of precipitation is increased by 3.3 % in model scenario RCP4.5, and 9.2 % in the model scenario RCP8.5. The runoff increase in the future scenarios compared to today's situation, from 72.9 % of the water budget to 75.2 %. The evaporation consequently decrease in the future scenarios, from 29.1 % of the water budget in today's situation to 25.9 %. The  $\Delta storage$  changes approximately the same, but the initial conditions are lower for the future scenarios than in today's situation.





## CHAPTER 6

---

# Discussion

---

For a holistic approach to the urban effects on the water environment, the infiltration capacity and water chemistry was studied together with alterations to the water budget. To get an understanding of how the water budget at Gaustad might be affected by urbanization in a changing climate, a hydrological model was created to simulate the water budgets for different scenarios.

### 6.1 Infiltration capacity of Gaustad watershed

The infiltration capacity of a watershed is important when creating a water budget, and it was therefore of interest in this study. The infiltration capacity of Oslo is, however, difficult to assess. The heterogeneity of the soil makes for significant variations within small areas, as illustrated by the fieldwork results obtained by the Mariotte device in Gaustad watershed (ref. table 5.1). There are few reports documenting the infiltration capacity of Oslo, and the map indicating the infiltration potential from NGU (ref. fig. 3.3c) has clear weaknesses. The boundaries of the polygons indicating the different degrees of infiltration potential follows the soil maps from NGU and are clearly derived from the geological mapping. The boundaries are very definite, and are likely not representative for the actual situation in Oslo. The map does not provide any actual infiltration capacity, only an indication of the infiltration potential relative to each other. This is not very practical when assessing the need for LID solutions, and using this map as input when planning stormwater management might end up producing misleading results. The infiltration capacity map (ref. fig. 5.1) was made in an effort to create a more concretized overview of the infiltration capacity of the Gaustad watershed. The infiltration map created in this study is based on the quaternary deposits map by NGU, presumably the same way NGU made their infiltration potential map. The improvement lies in the parameterized infiltration capacity, which is derived from Freeze and Cherry (1979), a report from GrunnTeknikk AS (2020) and results from fieldwork. The map is, however, not better than the geological mapping of the area and is certainly not sufficient to make local estimations of infiltrated water. The infiltration capacity is also dependent on several other factors, such as the initial conditions of the soil in advance of a rain event, and groundwater level, which makes it very difficult to create a general map over large areas.

The fieldwork results validates the empirical hydraulic conductivities by Freeze and Cherry (1979). The measured infiltration capacity at the locations Mariotte 1-5 (table 5.1), verified by the MPD measurements (table 5.2), all corresponds with the grain size distributions classification (table 5.3) range of hydraulic conductivity from table 2.2 in Freeze and Cherry.

The stratigraphy made in this study (see fig. A.2) might be useful when a general estimation of the thickness of the clay layer is sufficient. In combination with the surface covers of the watershed (ref. fig. 5.2, 5.3 and 5.5) and infiltration capacity map (5.1), suitable areas for LID solutions might be found. For local and precise estimations of the infiltration capacity, there should be conducted tests on the area in question, while keeping in mind the stratigraphy in the area as well as the depth to bedrock, providing advantageous information for investigations into the area.

### Uncertainties in the hydraulic properties

As Oslo is largely covered by fine grained marine deposits (see fig. 3.3b), the infiltration capacity is generally relatively low. Due to anthropogenic activity, there are several areas of filling material, and sites where the soil has either been loosened or compacted even further. This is difficult to assess, and might cause misleading infiltration potential measurements in an area. This is illustrated by the observed change of soil characteristics in the holes dug at the locations Mariotte 4 and 5 (ref. fig. 4.1 and table 5.3). If the locations were to be investigated by a Modified Philippe Dunne falling head infiltrometer, this would not be accounted for as it only measures the top soil (see method, 4.1). This illustrates the need for knowledge about the stratigraphy when assessing the infiltration potential of an area. In Oslo there is for example several areas of filling material on top of the marine clay, possibly producing high infiltration rates if only testing the top soil. Solheim et al. (2017) found that the infiltration capacity decrease with depth, and discussed the influence of biological processes, such as cracks in the soil as a result of worms or old roots from trees.

There was not done any adjustments for soil moisture at the infiltration measurement sites, which could affect the results of the measurements. This is exemplified in Solheim et al. (2017) by large variations of the saturated hydraulic conductivity, depending on the premise of the soil being saturated for an hour before the experiment or if soil moisture measurements was used for correction later.

The differences between the two measurement locations in this study, and also within the sites itself, are of interest as they are marked as the same soil in the quaternary deposits by NGU. This further illustrates how inaccurate the general maps of the soil and consequently the infiltration capacity can be. The infiltration capacity map from NGU (ref. fig. 3.3c) indicates a soil "poorly suited for infiltration" at the sites of the fieldwork by the Mariotte. This is a relative term and does not provide very useful information when trying to assess how much water would infiltrate the soil and not end up as surface runoff. The range of infiltration capacity found by fieldwork in this study (ref. table 5.1) for areas considered the same infiltration potential by NGU illustrates the need for upgrading the infiltration potential map in Oslo. The infiltration capacity map made in this study (ref. fig. 5.1) is an effort to increase the information about infiltration capacity of Gaustad, but is still very inaccurate. It presumably follows the same strategy as NGU's map, but with actual values of hydraulic conductivity (K) indicating how much water might infiltrate. It is made on the base of the quaternary map by NGU and therefore is still very uncertain as the boundaries are not realistic. There are also igneous intrusions in the area which are not accounted for either in NGU's map or the map produced in this study. The choice of fieldwork sites does not give a properly representative picture of the watershed as it is only conducted within one layer by NGU and should preferably be performed at several locations both within the already investigated layer, as well as others, to study their properties. The Mariotte cylinder device should be applied at several more locations in different seasons to investigate the properties of the watershed.

As the cross section in figure A.2 illustrates, there might be a layer of filling material or anthropogenic masses the first few centimeters of the soil. This might lead to misleading indications of good infiltration capacity, when the reality is an extensive layer of marine clay underneath. This could cause inaccurate estimations of the infiltration capacity of the soil at Gaustad (Oslo), also illustrated in the modifications that had to be done in the model setup to calibrate the Kinematic Wave and Rainfall Dependent Infiltration model in relation to the amount of water able to infiltrate the soil.

The grain size analysis was conducted by hand, and might therefore not be as well sieved as it could be if it was done by a shaking machine. This creates an uncertainty in both that it can not be quantified by time and shaking intensity, as well as the possibility of not sieving well enough.

### 6.2 Subsurface of Gaustad watershed

The geology of Oslo is mapped by the Geological Survey of Norway (NGU) and is available as official records at their website. However, the quaternary deposits map indicates the thickness of the layer in terms of "up to 10-20 m thickness" for large areas, not specifying any further. The boundaries

between the different deposits are also quite imprecise with definite contours of a layer not realistic in nature (see fig. 3.3b). There is also several igneous intrusions in the area that is not shown in the maps produced by NGU as mentioned in section 3.

This makes it difficult to assess the stratigraphy of Gaustad watershed, which could be an obstacle for stormwater management planning as the thickness of the layers is of relevance for the infiltration capacity in an area. For this reason, the subsurface of Gaustad watershed was estimated by the data from "the subsurface archive" (Oslo municipality) in ArcGIS Pro by point interpolation. The results was visualised in MODFLOW (ref. fig. A.2) to get an overview of how the subsurface might look like and to illustrate how a stratigraphy of Oslo could be represented.

#### **Uncertainties of the subsurface at Gaustad**

As a simplification during this process all clay was considered as one layer, and when no ground surface level was provided the depth to bedrock and clay was set as minus values with reference to a terrain level found at a later stage by interpolation. This might cause uncertainties in the method, as well as human error when interpreting the data of the reports.

### **6.3 Groundwater - surface water interaction**

As the results of the field measurements in Gaustadbekken and Sognsvannbekken (table 5.9) shows, Gaustadbekken has a much more steady temperature than Sognsvannbekken throughout the year. The water temperature of Gaustadbekken is constantly higher than Sognsvannbekken for the winter months, while when spring is approaching the temperature seems to correlate better. This might be due to Gaustadbekken being led in pipes in several areas and thus being shielded from the cold air temperature, or could be an indication of groundwater interaction. Sognsvannbekken is flowing openly all the way and will therefore be much more affected by the temperature in the air. The water of Sognsvannbekken was observed frozen February 3rd (2021) when the water of Gaustadbekken was seemingly unaffected by the cold air temperatures (ref. fig. 5.6). The stable temperature in Gaustadbekken argue for groundwater influence as it does not seem to be affected by the air temperature. The electrical conductivity is also significantly higher in Gaustadbekken than Sognsvannbekken at all measurements (ref. table 5.9). This might also indicate groundwater influence, as it is typical for groundwater to conduct electricity better than surface water due to the aquifer matrix dissolving.

The assumption of groundwater influence of Gaustadbekken further complicates the modeling of the hydrologic situation as it creates the need for including a groundwater aspect. This means enabling another module in the hydrologic model (RDI), consequently bringing several parameters that has to be calibrated to fit the situation. The model becomes more complicated and complex with both infiltration and baseflow included in the simulations through the RDI module in Mike+. It does, however, make the model more intricate in the positive way of having additional parameters to adjust for the best possible correlation between the observed and simulated discharge at the Gaustadbekken weir.

Modeling the groundwater of Oslo is a complicated task due to heterogeneity of the soil and steep surface topography. The geological setting with the fractured bedrock aquifer covered by marine sediments causes parts of the aquifer to be confined, while areas of exposed bedrock acts as unconfined aquifer. Mike+ accounts for the groundwater through letting the modeler assign a specific yield as well as initial conditions of the groundwater level (ref. subsection 4.4). As the depth to the fractured bedrock aquifer in Oslo varies greatly, along with anisotropy of the aquifer, assigning one groundwater level and specific yield for the entire model is a source of error and uncertainty.

### 6.4 Filling material

Filling material is frequently used for a various of purposes in urban areas. It is fairly common to use the material from excavations from for example tunnels or other infrastructure as stabilization other places or for multi-functional reasons. The material might be used as a layer for infiltration on top of for example clay with low infiltration capacity, to increase the areas storage potential and detaining abilities. It also serves the objective of less pollution from traffic as the material can be used in nearby areas instead of being transported long distances. Filling material is, however, not always a positive feature in construction as the masses might inherit properties not suitable for the new area, and is often not well documented. Filling material can be everything from natural clay or whichever grain size fraction, crushed bedrock, or even be the source of contaminants. During the time where Oslo experienced a significant urban development (1937-1971, see fig 2.3) there was no restrictions on how these masses should be managed, as the law on how to dispose of excavation masses entered into effect in October 1983 (Lov om vern mot forurensninger og om avfall, "forurensningsloven", Norges lover, 1983). There are several areas of filling material recorded in Oslo (fig. 3.4) and as discussed in section 6.6, the filling material appears to contribute to the enhanced values of EC, heavy metals and ions (ref. tables 5.18, 5.15, 5.16 and 5.17) in Risbekken of Sognsvannbekken running next to an area of documented filling material.

This heterogeneity of the areas covered by filling masses are not well documented, and could be a source of both enhanced infiltration capacity in areas where the original soil might not be able to infiltrate much water or it could serve as a source of contaminants which is not even recognised.

### 6.5 Discharge measurements

The weir pond did not have optimal conditions for continuous measurements of the discharge, as there are still rocks and sediments that might disturb the water flow. The calculations of the discharge from the water level logged by the Ott Orpheus mini water level logger (Ott) device might have inaccuracies as two of the parameters ( $k_h$  and  $C_{td}$ ) were developed as empirical relations by the authors of the article Jan et al. (2006). There might also be uncertainties related to the manually measured water levels at the weir, which were used to correct the water level measured by the Ott.

The tracer dilution validates the discharge found by the calculations based on the Ott at three events. There are, however, only measurements for relatively low discharge, and the accuracy during high discharge is therefore still uncertain. The rating curve is only valid until the water level is 0.68 meters, as the weir would experience overflow above this level. This is not considered an issue during this study, as the water level only exceeds this value at one point for 15 minutes during the entire gauging period.

## 6.6 Urban impact on water quality

Urbanization being the cause of lowered water quality has been discussed as a serious problem in watersheds experiencing urbanization (e.g. Paul and J. L. Meyer, 2001; Qin et al., 2014). It has been referred to as *the urban stream syndrome* by Walsh et al. (2005) describing the observed deterioration of water draining from urban landscapes. The water samples analysis and field measurements of Gaustadbekken and Sognsvannbekken was therefore put in context with known and suspected polluted areas, as well as degree of urbanization, to examine any correlation (see fig. 6.1 and table 6.1). Gaustadbekken and Sognsvannbekken are two surface streams running in relative close proximity (ref. fig. 3.2), and it was therefore of interest to compare the degree of urbanization in relation to the water quality. The precipitation is assumed to fall with identical chemical composition across the entire watershed.

Table 6.1: Locations of the rivers Gaustadbekken (KV, SK, NBV, GBBS) and Sognsvannbekken (R, RH, AMV) related to urban degree, environmental classification status and electrical conductivity.

Location of sample	Draining area [ $km^2$ ]	Urban degree [%]	Status	EC [ $\mu S/cm$ ]
Konvallveien (KV)	0.4	94.4	Moderate	410
Solvang Kolonihage (SK)	0.06	78.2	Moderate	555
Nils Bays vei (NBV)	1	69.1	Moderate	266
Gaustadbekken Blindern station (GBBS)	4.1	87.7	Moderate	607
Risbekken (R)	1.1	32.2	Good	222
Rikshospitalet (RH)	11.3	5.3	Good	89
Anne Maries vei (AMV)	12.9	10.5	Good	128

The draining area and urban percentage of each location was gathered from NEVINA (nevina.nve.no). The urban degree (table 6.1) assumes that unclassified area in Nevina is a form of urban development.

From the results of this study, there is a clear correlation between the degree of urbanization and quality of the surface water. The correlation is illustrated in table 6.1, showing the urban degree, environmental classification status and electrical conductivity of the locations sampled 25.8.20 and 26.8.20. All samples with an urban degree of above 69.1 % are classified as of *moderate* quality in relation to the freshwater standards by the NEA, while the samples with less than 32.2 % all classify as *good*. The concentration of ions, reflected in the electrical conductivity, is also systematically higher for the locations of higher urban degree. The urban degree is linked with the presence of anthropogenic filling material (known or suspected) (see table 6.1 and fig. 6.1). The filling material can consist of various pollutants and other elements, creating a source of contamination.

The lowered quality of the water in areas with higher urban degree is expected, as urban development is linked with several sources of contamination. Surface runoff from impermeable surfaces collect pollutants from urban activity such as heavy metals from traffic and salt used for deicing roads. Sodium (Na) could also originate from weathering of the marine deposits in the area, and Chloride (Cl) from fossil seawater within the marine deposits. There is, however, clearly a systematic correlation between the locations of high urban degree and high levels of Na and Cl. The three locations of highest urban degree (GBBS, SK and KV) has significantly higher levels of both Na and Cl than the other locations (see results, tables 5.12, 5.11, 5.17 and 5.16). Sodium and Chloride concentrations of rainwater often increase with decreasing distance to the ocean (Appelo and Postma, 2005) and this

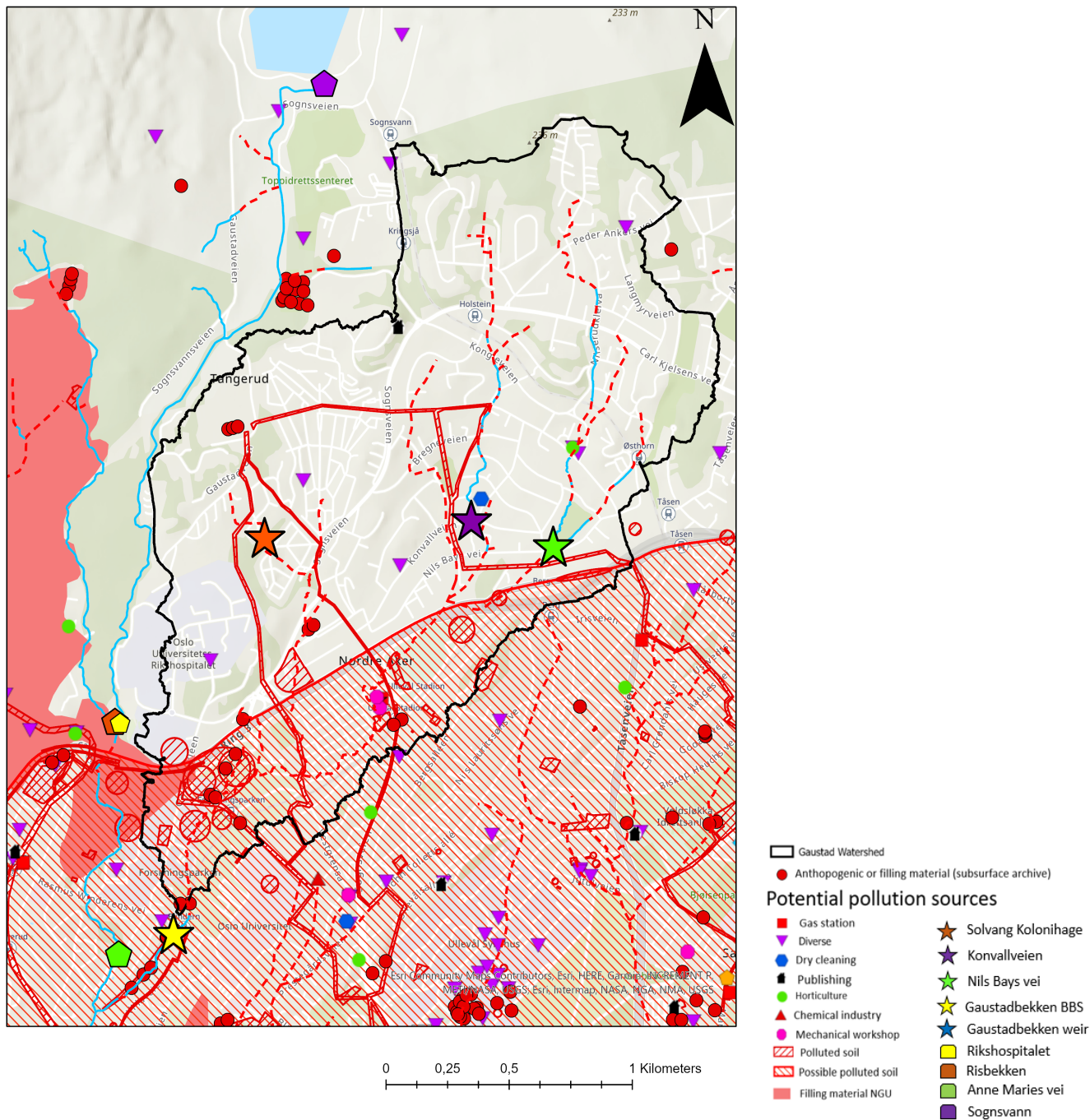


Figure 6.1: Recorded anthropogenic material in Gaustad watershed together with sampling sites in the river. Map created in ArcGIS Pro, data from NGU, subsurface archive and the municipality of Oslo.

could be a contributing factor as Gaustadbekken progresses towards the outlet in the Oslo fjord. It does, however, not explain the enhanced values of heavy metals, and should not exhibit such large variations as the Gaustad watershed is approximately  $4 \text{ km}^2$  of size.

The source of Calcium (Ca) might be the Cambro-Silurian bedrock. Anthropogenic filling material might consist of crushed bedrock from excavations, as there is a history of using material removed from one site as filling at another to avoid transportation. This can cause good conditions for rainwater to come in contact with Ca rich material, and could be the reason for the significant concentration of Ca in Risbekken (34.9 ppm, see table 5.16). The Calcium concentration of Risbekken (R) is approximately equal to that of Nils Bays vei (NBV). NBV has an urban degree of 69.1 %, while R has an urban degree of 32.3 %. This indicate there being a source of Ca in the area of Risbekken, most likely the filling material as Risbekken is flowing by a large area of recorded anthropogenic filling material (see fig. 6.1).

As this study assumes the precipitation falls evenly with equal chemical properties across the watershed, the results indicate there being influence from urban development on the water quality. The correlation of urban development and lowered water quality found in this study should, however, be investigated further. The samples represent one point in time, and might not be representative.

### **Gaustadbekken and Sognsvannbekken joining point throughout the surveying period**

The field parameters of Gaustadbekken and Sognsvannbekken (presented in table 5.9) measured right before the two streams merges into Frognerbekken (see map in fig. 4.7) indicate there being groundwater influence in Gaustadbekken as previously discussed in subsection 6.3. This is assumed to be the reason for the stable water temperatures throughout the year, unlike Sognsvannbekken which evidently is more dependent on the air temperature (e.g. fig. 5.6). Through the months of surveying the two rivers, the EC of Gaustadbekken was systematically significantly higher than the water of Sognsvannbekken. The pH, however, is quite similar between the two surface streams, but is only measured at one event and is therefore not very reliable.

The ion analysis shows elevated values of Sodium and Chloride for Gaustadbekken at both sample dates (ref. tables 5.21 and 5.22). Sodium-Chloride is a common substance to use for deicing, and Kelly et al., 2008 found that NaCl from traffic accounted for 91 % of the Sodium and Chloride input in the watershed studied. Gaustadbekken flows through an area of high degrees of urbanization (69.1-94.4 % for the locations studied, ref. table 6.1), which is closely linked with traffic. Deicing of roads is therefore a plausible explanation for the heightened concentrations in Gaustadbekken. By looking at the water properties as the water flows downward in Gaustad watershed it also becomes reasonable to assume that the water is affected by the polluted sites of the watershed (6.1) which adds to the concentrations of heavy metals and ions in the water.

The heavy metals of Gaustadbekken is in general higher than the water of Sognsvannbekken with exception of Iron (Fe) (ref. 5.20). The samples collected in Gaustadbekken after a relatively heavy rainfall event (17.12.20) is the only sample receiving the classification of *bad* with high levels of Arsenic (As) and Zinc (Zn), while the other samples all classify as *good* by the freshwater standards of the NEA. This might be an example of the "first flush" as discussed by Li-qing et al. (2007) describing enhanced chemical concentrations in the beginning of a runoff volume in precipitation events. The results indicate that the water at Gaustadbekken weir is of lower quality after a precipitation event of 5.3 mm during the last 10 hours. This might differ related to the amount of dry days previous to the rainfall, but suggests that the aquatic biota is negatively affected by surface runoff carrying pollutants into the river.

Sognsvannbekken is flowing through less urbanized areas (<32.2 % ref. table 6.1) and consistently measures lower EC than Gaustadbekken, and in general has lower concentrations of ions and heavy metals. The exception is Iron (Fe) which is significantly higher in Sognsvannbekken compared to Gaustadbekken for both sampling dates (ref. table 5.20). This might indicate other sources of pollution along Sognsvannbekken such as the filling material, or it could be a result of weathering from the natural geological setting. A large and heavily trafficked road runs over both Sognsvannbekken and Gaustadbekken, which could be a source of the elevated Iron levels as traffic is major source of heavy metals in the environment (Tsihrintzis and Hamid, 1997). Sognsvannbekken flows in the open

very close to this road, while Gaustadbekken might be shielded from Iron pollution due to it flowing in pipes in this area. The Iron concentration is not known for the locations further upstream for either Gaustadbekken or Sognsvannbekken, and the source should be investigated.

There was no indication of *E. coli* in any of the water samples from Gaustadbekken or Sognsvannbekken (see fig. A.1). The samples were taken after rainfall events, the samples from 17.12.20 when the discharge level was still high, while the ones from 2.1.21 was collected after the discharge level had returned to normal. This suggest there was no combined sewer overflow (CSO) into Gaustadbekken or Sognsvannbekken during these rainfall events, indicating the collection system not overflowing (see discharge points in figure 2.4) by precipitation of 5.3 mm during the last 10 hours. This also points towards there being no water from combined sewer systems leading to the point of Gaustadbekken weir. The test is, however, not exclusive and can not refute there being sewer influence in the water. It should also be mentioned that 5.3 mm in 10 hours is not considered as a heavy rainfall event.

### Uncertainties in the chemical properties of the water

The water samples from Sognsvannbekken and Gaustadbekken used for investigating the changes of chemical concentrations as the water progresses was taken one day apart. This could potentially cause divergence that would be avoided if the sampling was conducted on the same day. The samples represent one point in time, and might not be representative for the water chemistry of the rivers. The samples comparing the chemical properties of Sognsvannbekken and Gaustadbekken where they join and form Frognerbekken was taken at the same day with only minutes apart. The sampling was done two times with approximately one month time interval and should be representative for the two streams in their differences and is more trustworthy in their representation of the water properties.

As the lab was closed due to Christmas vacation, the samples collected in December had to be stored in the fridge from 17.12.20 to 04.01.21, which could potentially lower the quality of the samples and consequently the analysis. The samples collected in January were stored for two days as they were gathered on the 2.1.21. The samples from Sognsvannbekken 2.1.21 were collected as one unfiltered sample because of the lab being closed and thus a lack of proper sampling containers. The water was filtered, placed in fitting containers and acidified in the lab on the 4 of January prior to the analysis.

The water sample analysis was not done for one of the major anions, bicarbonate  $HCO_3^-$ . This makes the electrical balance ineffective and the validity of the sample analysis hard to determine. For that reason, the alkalinity was assumed equal to the concentration of  $HCO_3^-$  as suggested in Appelo and Postma (2005). The electrical balance for the samples Risbekken and Rikshospitalet was above 5 % and should be investigated further at the lab. These sample analysis are therefore not to be trusted completely.

As the water is mainly running in a closed system, it would be relevant to investigate the condition of the pipes. As the closing of the river system in Oslo was done previous to the change of strategy in 1990 (where approximately 72 % of rivers in Oslo was closed (Sandaas and Halvorsen, 2000)), the pipes might experience deterioration over time. This could potentially be a contributing factor to the ion concentrations of the water increasing downstream. This is, however, not further examined in this study as the water of Konvallveien and Nils Bays vei both flow for a considerable length in a closed system before the measurement point, still exhibiting very different values. It was therefore not considered as a major impact in this study.



## 6.7 Hydrologic model in Mike+

Modeling an urban water environment is complicated due to the complexity of urban infrastructure. The model made in Mike+ is an effort to recreate the situation in Gaustad, Oslo to the best of the modeler and the software's ability. The natural watershed had to be adjusted to include all inlets of surface water contributing to the outlet at Gaustadbekken weir as shown in figure 5.7, illustrating the need of *sewersheds* as discussed by Welty (2009).

The calibration is an important step in adapting the model to the actual situation, but a model will always be somewhat inaccurate. It is like George E. P. Box said in 1976, "*all models are wrong – but some are useful*".

### Model performance

In the calibration of the hydrologic model, the RDI module should ideally be calibrated with more than 3 years of observed data to obtain high accuracy. For the calibration of the rainfall-surface runoff model, only months (preferably with high resolution) is needed (DHI, 2021c p.117). When calibrating the hydrologic model used for this study, the time-span of the observed data was months, with intervals of 15 minutes. This is sufficient for a properly calibrated surface runoff model, but might be less optimal for the rainfall dependent infiltration model. As it covers periods of both wet and dry weather (see fig. 5.4), the model calibration was considered sufficient, even if some parameters might not be of optimal value.

The calibration period of the model obtained an *RMSE* value of 0.0005,  $R^2$  of 0.7054 and *NSE* of 0.633, reflecting the good dynamics correlation of the simulated and observed discharge data. The underestimation of the flow peaks and overestimation of the recession likely affects the model evaluation criteria negatively, but the model still produces adequate values.

The validation period got an *RMSE* value of 0.0004,  $R^2$  of 0.4273 and *NSE* of 0.332, which is a poorer fit than was observed for the calibration period. This is common in hydrological modeling, and for the purpose of this study was deemed acceptable. The main aim of this model was to estimate the water budget of the area, as well as investigate the urban impact the Life Science Building would pose for the local area. For this, the flow peaks was considered of most importance when calibrating the model, and the overestimated recession was considered less significant for the purpose of the model. It does, however, indicate there being errors in the model setup, and should be corrected if further use of the model is to be accurate depending on the aim of the simulations output.

The validation period severely overestimates the flow peak around 14Th of March (ref. fig. 5.10). One reason for this could be inaccurate computation of the snow storage and consequently melting. The snow storage in a representative catchment shows there to be approximately 1.3 meter snow stored the 13.3.21 (see green line in fig. 5.12), presumably melting and adding to the peak flow in the validation period in the same time interval to be overestimated. This might also be the reason for the inaccurate dynamics at the flow of 20.2.20. The snow storage of a representative sub-catchment shows the snow pack accumulated up until this date disappearing (see purple line in fig. 5.12), possibly causing the peak in the simulated discharge. In an urban environment, some of the snow might be removed, causing less melting during the spring. This might contribute to the enhanced simulated flow peak in the validation period. This indicates the snow melt coefficient being too high, causing melting of snow to happen too early compared to reality.

### Systematic errors of the model

The timing of the peak flows are nearly perfect, and the dynamic of the simulated discharge is considered very fitting. The model does, however, overestimate the recession after flow peaks, especially in the validation period. There is also underestimation of the flow peaks in both the calibration and validation period. This could be due to errors in the distribution of the water in the model, and less than optimal parameter settings. The model setup might incorporate too much

water to infiltrate, causing there to be less water running off during intense rainfall events leading to underestimated discharge peaks. The infiltrated water could then be the cause of higher interflow and groundwater discharge during dry periods.

Both the calibration period and validation period reveals the simulated discharge to be higher than the observed discharge. This is likely due to an error in the parameters or setup of the model, or caused by the additional areas included in the model to fit the collection network. As illustrated in figure 5.7, the natural watershed was expanded to include all areas that is connected to the collection system network leading to the Gaustadbekken weir. These areas only contribute with surface runoff to the outlet of Gaustadbekken through the pipes collecting surface water. In the hydrological model used for this study, it is included as a part of the watershed and thus also contributes with interflow and baseflow. This might be the reason for the systematic overestimation of the recession after flow peaks found in both the calibration and validation period (ref. fig. 5.8 and 5.10). The added area is largely covered by combined collection system (see fig. 2.4). The analysis for E. coli in the water samples from Gaustadbekken weir indicates no sewer influence of the water. This argues that there is no combined sewer system leading to the Gaustadbekken weir, even though the data from the municipality of Oslo points towards it. The collection system leading surface water to the Gaustadbekken weir in the hydrological model in Mike+ might thus overestimate the amount of contributing areas and consequently the runoff.

All water budgets for the entire watershed in the hydrological model has negative  $\Delta$  storage, indicating the initial conditions of the model setup might be too high.

### Identified errors in the Mike+ software

The model results revealed an error in the distribution of precipitation. The Kinematic Wave model and RDI model should be provided rainfall at the same interval and frequency, but this is not the case when examining the result files as illustrated in figure 6.2. The figure shows the RDI model input precipitation to be exactly how the precipitation input file was set up. The KW model on the other hand differs from the input precipitation file, indicating a computational error. The inaccuracy in precipitation input for the KW model creates uncertainty and difficulty in calibrating the model. Precipitation is an extremely important input of a hydrological model, and while the model receives the correct amount of rainfall during the simulation, it seems to be inaccurately distributed.

The groundwater flow computations of the model is very insensitive to changes in important parameters. In the calibration efforts, there was observed little to no result when changing vital parameters such as the Carea and the groundwater level (see subsec. 2.6). Changes in these parameters should cause alterations to the output of the model, and the low response indicate there being some inaccuracies in the model computations of the groundwater aspect.

A source of confusion in Mike+ is the date label on output features. The date format might change within a single plot from American to European style. This makes the interpretation of the data unnecessary complicated and all plots from Mike+ has a modified x-axis to ensure correlating date formats on the results.

### Uncertainties of the hydrological model

The hydrological model created in Mike+ did not account for rivers as a part of the collection system network, even though Gaustadbekken river has some parts running as an open stream. This was solved by creating large pipes connected to each points of the open stream, making sure there would be no hindrance for the water to flow. The open streams are relatively short (up to 400 m) and the potential inflow of water to the river at these stages are accounted for through large manholes allowing for inflow of water in the area. If there is any surface water not able to find its way to the river at the exact point it would in the actual situation, this will be collected by a nearby manhole. Influence of interflow and baseflow in these areas on the other hand, might be lost by the closure of the river.

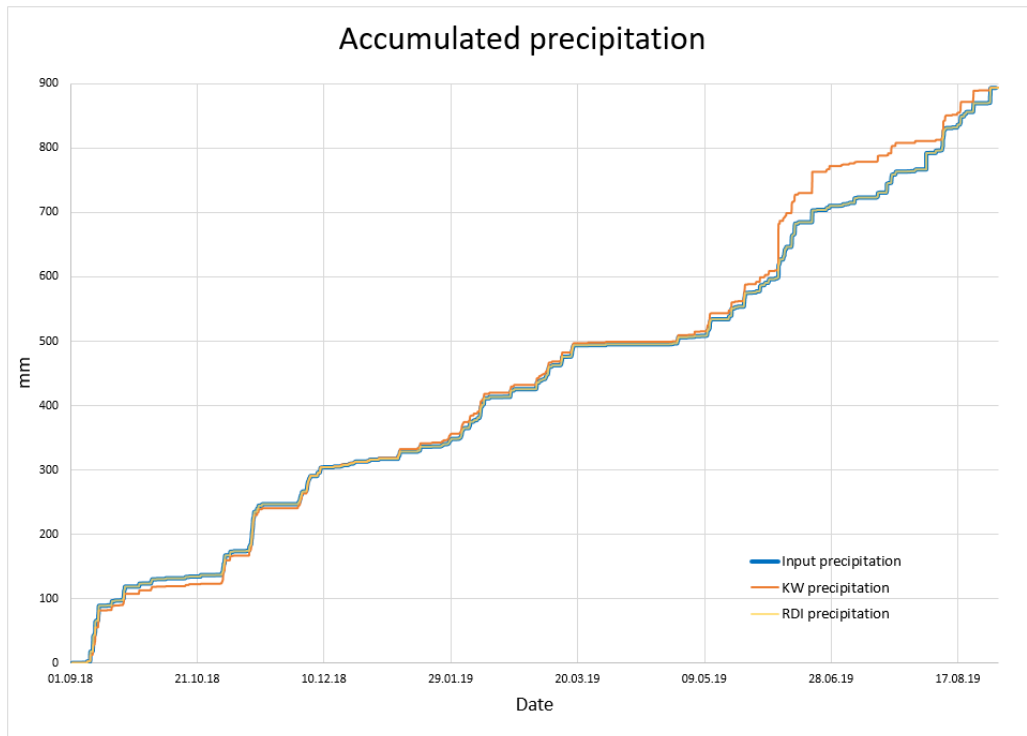


Figure 6.2: Accumulated precipitation [mm] for the input, the Kinematic Wave (KW) and RDI model, illustrating the deviation in the KW model.

At *seklima.met.no*, there was observed a difference in sum of the precipitation when selecting hourly values instead of 10 minute values (e.g. 20 mm difference in the calibration period of 8.10-28.2). This might be due to different sources of data, different methods of processing, or how the data is presented. The choice of using 10 minute values was mainly due to wanting a higher resolution of the output simulation, but this is an uncertainty as the precipitation input is very important in hydrological modeling.

As the original data from Oslo municipality had to be modified, there exist uncertainties in the accuracy of the collection system network. The collection system as provided by the municipality of Oslo (VAV) was lacking necessary information for it to be used in a Mike+ model. This was filled in by using the feature manipulator engine (FME) to extract the bottom level of the manholes corresponding to the up and down level of the connecting pipes. The data-set contained only a few of the manholes diameter, the rest was set to default 1.5 m. A suggestion for future use of the collection system network in Oslo would be to update the digital archive of the manholes and connecting pipe-system. There was obvious missing information such as the diameter of the manholes, the bottom elevation of the manholes corresponding to the upper or lower level of the pipes. There was also several orphan nodes not connected to any pipes, and numerous pipes not leading anywhere. This should be corrected for proper and appropriate use and modeling using the data. As it stands now, there are considerable sources of errors as the collection system had to be adapted by assumptions of the modeler, giving room for human errors and wrongful interpretations. This might consequently lead to inaccurate estimations of surface runoff and water level in the pipe-network, causing unreliable model results and imprecise estimations of water budget parameters. An update and upgrade of the digital archive of the collection system would make modeling for stormwater management more accurate and efficient.

When running any rainfall-runoff model in combination with the RDI model, fractions of contributing areas has to be predefined in the model setup. This means that the fractions of the sub-catchments

has to be divided on the Kinematic Wave model and the RDI model, indicating the percentages of the area active in each of the models. The sum of the fractions equals 1 to cover the sub-catchment. By determining the fractions of the two models that are active on each sub-catchment, the amount of rainfall into each model is correspondingly distributed. This necessarily affects the output of the model, as the two models use different sets of mathematical equations to deal with the different hydrological processes.

In the calibration of the hydrological model, the site of the Life Science building was considered as a rural area. During the time the observation data was obtained, the construction work had begun. This makes the hydrological properties of the area hard to determine, and could be an uncertainty of the model calibration.

The Thornthwaite method for calculating the potential evaporation is based on an empirical correlation between monthly air temperature and the potential evaporation. This method has its disadvantages, and Rijtema (1959) mention the method only being in agreement with observations of potential evaporation after having been corrected for a time lag and the wind velocity (on the basis of a study by Makkink (1957)). Xu and Chen (2005) performed a comparison of different methods to estimate potential evaporation. The study found that the radiation-based methods performed better than the temperature-based methods (including the Thornthwaite method). The evaporation estimations of the model in this study is based on the potential evaporation calculated by the Thornthwaite method and is therefore linked with the uncertainties associated with this method.

A more thorough investigation into the properties of the watershed would increase the accuracy of the models reflection of the actual situation of the study site.

## 6.8 Urban water budget

Creating an urban water budget is a complicated task and will therefore be linked with uncertainties. Modeling the hydrologic situation might, however, give an insight into what might be representative for an area. The water budgets in this study are based on modeling results from an up to date urban hydrological software (Mike+). The water budgets presented in the results (section 5.7) might therefore be a contribution into the work on mapping the urbanization's effect on local urban water budgets. To understand the effects of urbanization on the water budget there is a need for cooperation between different disciplines such as hydrology, hydro-geology, ecology, geography and even social science (DeFries and Eshleman, 2004). It is thus a huge undertaking and will require extensive research, reliable observations and suitable modelling software.

### From natural to developed area

As illustrated by the model results in table 5.25, the water budget is changed dramatically by urbanization of a natural area. The water budget for the natural situation simulates 53.4 % evaporation and 47.5 % runoff. After the area was changed to represent today's situation as a semi-developed watershed, the evaporation is decreased to 29.1 % of the water budget, while the runoff has increased to 72.9 %. This corresponds the evaporation decreasing 45.5 %, together with runoff increasing 53.4 % by the transformation of Gaustad from a natural setting to today's situation. This is consistent with knowledge of hydrological responses to introduction of impermeable surfaces, reducing evaporation and increasing the surface runoff (e.g. Baker, 2009; Dupont et al., 2006; Feng et al., 2016; Fletcher, Andrieu et al., 2013; Göbel et al., 2004; Healy et al., 2007; Herricks, 1995; Schirmer et al., 2013; Trinh and Chui, 2013).

The initial conditions of the model is notably lower in the semi-urbanized scenario, than in the natural scenario. This represents less areas of vegetation and soil with initial moisture at the beginning of the simulation, as natural areas were replaced by surfaces related to urban development.

The water running off on the saturated soil in the pre-developed model is assumed to be feeding the river branches of Gaustadbekken, which in a natural situation flows freely (illustrated in figure 2.5). In the semi-urbanized model representing today's situation, the river water is mainly closed in pipes, and the surface runoff has to be dealt with by urban water collection system. The collection network of the semi-urbanized model shows all surface runoff being collected by the drainage network at some point. Despite this, there are areas of Gaustad watershed experiencing excess surface water in streets or accumulated in small ponds (e.g. Sogn Kolonihage, discussed in section 6.9). This is most evident in the south of the catchment, where the slope is lower and water more easily accumulate.

### Life Science Building site before and after construction

By looking at the graph in figures 5.15 and 5.16, the interpretation of Kinematic Wave runoff representing the surface runoff could be made. The RDI model runoff clearly has a slower reaction time, and comprise the slow response component, the interflow. The interflow is water movement in the unsaturated zone, and thus stems from infiltrated water. The Mike+ summary output file states that the total loss of the model is both infiltration and evaporation, but interpretation of the model results contradicts this. The total loss of the model is therefore considered as only evaporation in this study, while the infiltration is treated as a part of the runoff volume presented in the water budgets. In the site specific results, looking in detail into the sub-catchment of the Life Science Building (LSB), the surface runoff and subsurface runoff were separated and are presented as individual water budget parameters.

When the LSB was included in the model as a completed building complex, the water budget was changed only slightly (ref. table 5.26) on the catchment scale. The total catchment modeled in Mike+ covers  $4785075\text{ m}^2$ , and a change like the LSB exhibits is not significant as it only accounts for 1.6 % of the total catchment. The difference on the catchment scale is a 1.8 % reduction of evaporation, consequently causing 0.7 % more runoff. To investigate the local effects of the construction work, the

## 6. Discussion

model results of the Life Science Building sub-catchment (see fig. 5.14) was studied before and after the construction of the building.

The results in table 5.27 illustrates the changes the Life Science Building (LSB) area exhibits before and after the completion of the building complex. When comparing the sub-catchment's local water budget before and after the completion of the LSB, it is clear that the evaporation decrease significantly, while the surface runoff increase quite dramatically, consistent with known response to the establishment of impermeable surfaces. The evaporation decrease 65.5 %, the interflow decrease by 80.0 %, while the surface runoff increase by 286.5 %. These changes are dramatic for the water environment at the site of the Life Science Building. The decreased evaporation means less water lost out of the system, which contribute to increased surface runoff when water does not infiltrate due to impermeable surfaces. The removal of permeable area also means less soil able to store water, and overland flow might occur more frequently also adding to the increased runoff.

The increased surface runoff and decreased infiltration is also visible in the simulated groundwater level at the site of the LSB (fig. 6.3). The groundwater level decrease by 0.65 m when the LSB sub-catchment is considered rural, while the simulated root zone storage is reduced by 25 % (see fig. A.3). After the sub-catchment of the LSB is considered as a building complex with little opportunity for infiltration, the simulated groundwater level decrease by 1.3 m (see fig. 6.3) and the simulated root zone storage is reduced with 40 % (see fig. A.4). This represents the loss of infiltrated water due to more surface runoff on impermeable surfaces, and thus a decrease of water recharging the groundwater.

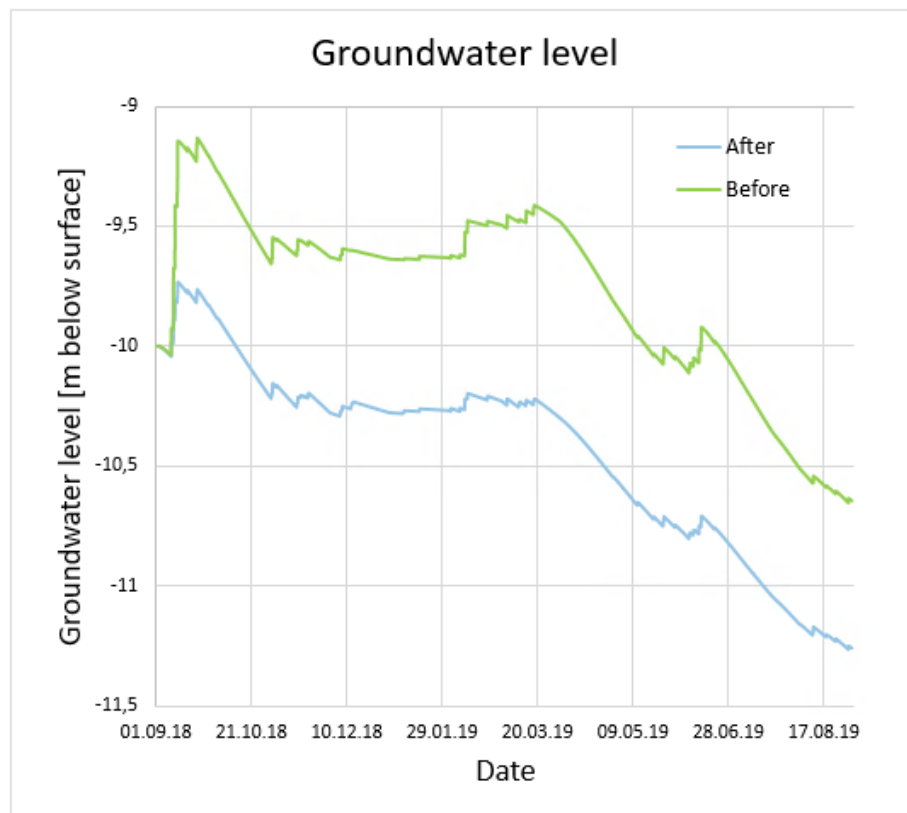


Figure 6.3: Groundwater level through the hydrological year 2018-2019 for the sub-catchment representing the Life Science Building, before and after the construction of the building. The y-axis is groundwater level from surface elevation [m]. The start water level is -10m for both scenarios. The groundwater level is a result of the simulations by the hydrological model in Mike+.

The simulated decrease of the groundwater table at the Life Science building area might be inaccurate

in reality, as there could be leakage from pressurized water supply pipes contributing to recharge of the groundwater. Leakage from water supply pipes in Oslo might be up to 30 % according to data gathered from SSB by Solvang (2015).

### Increased urbanization in a changing climate

The future scenarios of Gaustad watershed shows the water budget being altered by the increase of precipitation and future urbanization. The fraction of *urban* sub-catchments of the model was changed from 66 % to 76 %, together with climate changes representing the RCP4.5 and RCP8.5. The future scenarios thus aims to exemplify possible situations of the Gaustad watershed in the years 2071-2100.

Compared to the water budget of today's situation, the future scenario of RCP4.5 brings an evaporation reduction of 6.8 %, while the runoff increases by 7.8 %. The scenario RCP8.5 amplifies the changes, with the evaporation being reduced 3.0 % and runoff increased 12.6 % compared to today.

Scenario RCP4.5 is assuming stable or slightly increasing emissions until 2040 before green house emissions are reduced. This is considered a medium scenario in relation to global warming, and is achievable in an energy efficient world with an ambitious climate politic environment. The climate scenario RCP8.5 on the other hand, represents increasing emissions until the end of this century (Hanssen-Bauer et al., 2015). The simulated changes related to the scenario RCP4.5 is therefore relatively likely to occur, while the scenario RCP8.5 is less likely.

The future scenarios are built on predictions for future climate changes, and is therefore influenced by uncertainties. The degree of urbanization is also unknown and will depend on population increase of Oslo city, as well as how the development of more housing is conducted. The aim of Oslo municipality is to build in already developed areas to minimize the need for more urban infrastructure such as transportation, but any increase of inhabitants will necessarily cause urban development to some degree. It was therefore reasonable to assume there might be at least 15 % increase of urban areas at Gaustad watershed by the years 2071-2100.

To deal with changes of the water budget being brought on by the climate changes together with increased urbanization, implementation of LID solutions might become very important. Detaining and delaying water could be essential for urban infrastructure in events of extreme rainfall to avoid damages related to surface runoff.

## 6.9 Reflections on the drainage system network at Gaustad

In urban areas water is commonly drained by a collection system, through either a separate or a combined system, and Oslo is no exception. The drainage system is not always sufficient for collecting all surface water generated by precipitation on impermeable surfaces and undesirable surface water can occur. This is a source of damage to infrastructure (NOU15:16, 2015) and should be addressed to avoid further harm. Surface runoff not collected by the system network might also deteriorate surface streams as well as receiving water bodies at Gaustad as the drainage lines clearly follows the historic river path (see figure 2.5) which is partly open (see fig. 3.2), allowing for inlet of surface runoff and groundwater inflow. The combined sewer system has several outlet points in Gaustadbekken (see fig. 2.4), which might further pollute the stream with water of bad quality in cases of CSO. The pollution of the surface water is usually highest in the beginning of a rainfall as the precipitation catch atmospheric particles, as well as wash off pollution from urban sources such as traffic. Li-qing et al. (2007) suggested that the first period of a heavy rainfall event causing overland flow is the most important to contain with respect to reducing urban surface runoff pollution.

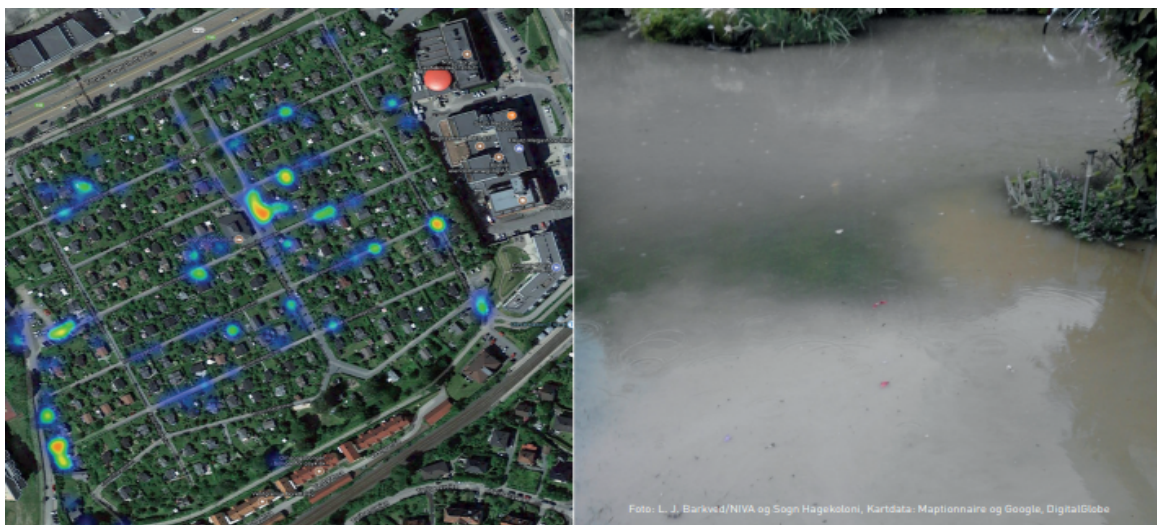
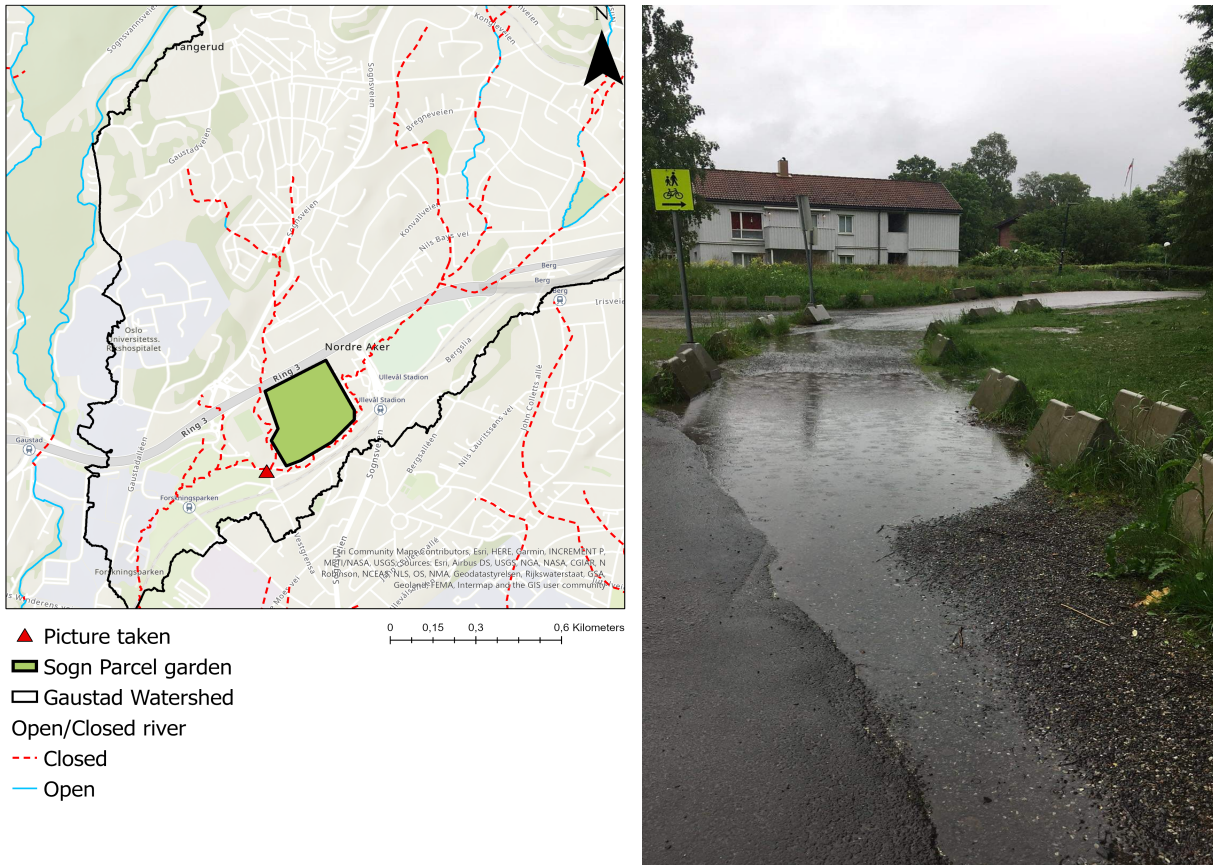


Figure 6.4: Surface water problematic areas as registered by the owners and users of the parcel garden. Picture by L. J. Barkved/NIVA and Sogn Hagekoloni from Barkved et al. (2018). The map on the left illustrates the problem areas of the parcel garden, and the picture on the right exemplifies a situation of unwanted surface water.

Areas without a proper drainage system, however, might experience unwanted surface runoff also in moderate rain events as the concentration time on the surface increase by the impermeable cover percentage if not steered to a collection network (Shuster et al., 2005, illustrated in fig. 2.2). This becomes visible in the south east of the watershed at "Sogn parcel garden" (fig. 6.4) where there is no surface runoff collection system and no drainage system implemented. The parcel garden is an area with substantial vegetation due to one of the prerequisites for owning a parcel garden is to maintain the flora. This might increase the root zone storage as well as uptake by the plants and consequently evapotranspiration. On the other hand, the infiltration capacity of the area is low as the soil is fine grained marine clay (Geological Survey of Norway B, 2020). The area is quite flat (slope of  $<1.7\%$ ) and water might accumulate instead of running towards a drainage system close by, as seen in figure 6.5. As discussed in Barkved et al. (2018) there are areas of unwanted surface water at several locations within the parcel garden. These follow the gravel roads to a large extent as shown in picture 6.4.

Sogn parcel garden is also vulnerable in events of extreme rain, as the drainage lines of Gaustad flow both on the north and south side of the area (ref. fig. 2.5). If the velocity and amount becomes too large, the area might suffer from erosion of the surrounding stabilizing material as marine clay can





(a) Location of Sogn Parcel garden together with the point of (b) Picture taken 6.6.20 of surface water accumulation close nearby Sogn Parcel garden within Gaustad watershed.

Figure 6.5: Surface water accumulation at the bottom of Sogn Parcel garden after rainfall. Picture taken the 6.6.2020.

be quick and might be sensitive to changes in the land masses. To implement LID solutions at Sogn parcel garden would therefore serve many purposes as it would reduce the runoff from the garden itself, and if placed nearby the drainage lines - might help lower the peak flows in events of extreme rainfall. LID solutions such as rain gardens also provide appealing blue elements and is favoured by the users of the garden (Barkved et al., 2018).

### Potential consequences of an altered water budget

In a changing climate combined with increased urbanization of Gaustad watershed, the incidents of combined sewer overflow is likely to occur more frequent. After heavy rainfall in Oslo, there are often several warnings about insufficient water quality, after wastewater discharged at favoured bathing locations in Oslo (e.g. Gullud Omar Jibril, 2019; Eggen, 2019; Solberg, 2019; Helgheim, 2020). In general, the municipality of Oslo advises against bathing at locations close to river outlets due to surface runoff collecting pollutants and animal excrement, as well as CSO events contaminating the water and consequently the receiving waters (Nordal, 2021). The official website of the municipality of Oslo presenting different sites for bathing during summer, advises to avoid the water for 24 hours after heavy rainfall at all locations (Oslo kommune, 2021).

The increased precipitation combined with urbanization is causing more runoff (ref. results 5.28) and

increased water levels in rivers after heavy rainfall. This can cause erosion of the river-bed and sides, consequently increasing the sediment load of the river water (Hu et al., 2009). Sediments might lead to even heavier strain on the pipes, it could be disposed in the closed pipe-system leading to smaller diameters of the pipes, and in worst case scenario end up clogging the pipes entirely.

The wastewater increases as a function of the population increase, consequently contributing to a higher wastewater load of the combined collection system. As large areas of Gaustad watershed carries stormwater together with wastewater (combined system, see fig. 2.4), the load on the pipes will be even heavier than what the increase in surface runoff created by the urbanization might indicate. The collection system is also deteriorating with time, and sedimentation might decrease the dimensions of the pipes. This can lead to the events of contamination increasing, as leakage from the pipes might occur, and events of CSO might happen more frequent. As discussed in section 6.6, the properties of Gaustadbekken indicate influence of urban pollution. This trend is assumed to be enhanced in events of CSO and increased load of surface runoff, but was not studied further in this thesis.

To avoid CSO incidents, a separate system might be preferable. There is, however, more considerations to take into account when deciding which type of collection system to place in an area. There has been discussions of what might be the best sewer system to ensure restricted amounts of pollution into receiving water bodies. Brombach et al. (2005) found that the separate system might not necessarily be the best solution, although it did prevent most nutrients to enter water bodies in surrounding areas. When looking at heavy metals on the other hand, the combined system caused less loads to the receiving waters. It is therefore recommended to choose a type of collection system based on the individual prerequisites of the location.

More intense and frequent precipitation in the future might make the municipal wastewater treatment facilities clean to an unsatisfactory degree due to short retention time, and increase the amount of CSO incidents if the water treatment facilities and collection system is not upgraded. This causes a risk of degrading the receiving water bodies, possibly ruining bathing sites and other recreational areas (Mæhlum and Hensel, 2009–2011). Mæhlum and Hensel (2009–2011) advises that neither treated or untreated wastewater should be led to receiving water bodies if infiltration in soil is possible.

The top-soil in Oslo is to a large extent marine deposits of both fine and more coarse grained clay (Geological Survey of Norway B, 2020). This is of importance when deciding infiltration measures, as the infiltration capacity increase by the coarseness of the soil, while the cleaning capacity of the soil increase by reduced grain size (Mæhlum and Hensel). One of the biggest concerns with this method, however, is pollution of the recipient water. For infiltration strategies, the concern is mainly for the groundwater quality. Collaboration with hydro-geology is therefore important to ensure the quality of the groundwater. Groundwater is not used as drinking water in Norway and the possibilities of the infiltration filtering strategy for cleaning the surface runoff might therefore be considered as a good prospect.

To adapt for the climate changes in an urban environment, proper stormwater management is essential. To estimate the necessary LID solutions, modeling of the water ways and water budget is an important and helpful tool. For efficient modeling of the drainage system of Oslo, the data should be updated with relevant information for use in hydrological softwares. Mike+ is a suitable program for simulating the urban drainage network, and might be a great resource in planning for future challenges related to surface runoff.

## CHAPTER 7

---

# Conclusions

---

### **Infiltration capacity of the Gaustad watershed**

The infiltration capacity of Gaustad watershed is difficult to parameterize due to heterogeneous soil and urban impacts. Gaustad is largely covered by marine clay with relatively low infiltration capacity, with some areas of sand or filling material possessing a much higher infiltration potential. The infiltration capacity is therefore very variable and differs within small areas. There are areas of filling material or anthropogenic masses that might pose a risk of contamination as well as have extremely various properties in relation to infiltration potential. An infiltration capacity map was created, as well as a simplified stratigraphy of the watershed.

### **Correlation between urbanization and water quality**

The results of the water quality investigation finds a correlation between urbanization and lowered quality of the surface water. Presence of anthropogenic filling material might be an additional source of contaminants. The water quality of Gaustadbekken classifies as *bad* when compared to the freshwater standard (by NEA) after relatively heavy rainfall (5.3 mm in 10 hours). In relation to standards for bathing water quality in Norway, only thermotolerant coliform bacteria (mainly *E. coli*) is addressed. This study did not find any *E. coli* in the water samples and therefore concludes there to be little to no sewer discharge into the river Gaustadbekken or Sognsvannbekken for the examined precipitation events.

The observed discharge series and field measurements shows that Gaustadbekken is influenced by groundwater flow, even though it is closed in large parts.

### **Hydrological model of the Gaustad watershed**

The hydrological model in Mike+ was run with a combination of the rainfall-surface runoff model Kinematic Wave (KW) and rainfall-runoff model Rainfall Dependent Infiltration (RDI). Groundwater influence adds several parameters to the modeling task by including the RDI model. This further complicates the calibration task, but provides important aspects to the simulation. The calibration of the hydrological model was done manually, obtaining the efficiency criteria  $R^2$  of 0.7054,  $NSE$  of 0.633 and  $RMSE$  of 0.0005 for the calibration period and respectively 0.4273, 0.332 and 0.0004 for the validation period.

Mike+ is a promising software for use when modeling urban watercourses, and has a more user-friendly interface compared to its predecessor Mike Urban.

### **Water budgets alterations due to urbanization and climate changes**

The urbanization of Gaustad watershed has caused closing of the natural surface streams, as well as a 53.4 % increase of runoff and a 45.5 % decrease of evaporation compared to the natural situation.

## 7. Conclusions

---

The construction of the Life science building has a relatively small impact on the total water budget for the simulated Gaustad watershed. The runoff increase 0.7 % relative to today's situation, while the evaporation decrease 1.8 %. However, the local water budget of the area representing the LSB shows dramatic changes. The evaporation decrease 65.5 %, interflow decrease 80.0 %, while the surface runoff increase 286.5 %. The model simulation estimates the groundwater level at the site of the LSB to decrease 0.65m after the construction of the building complex is finished, relative to the site as a *rural* setting. This reflects the reduced infiltration due to establishing impermeable surfaces.

If urban development continue increasing in a changing climate, the water budget changes might be even further amplified. In the climate scenario RCP4.5 combined with a 15 % increase of *urban* sub-catchments, the precipitation increase 4.6 %, the runoff 7.8 % while the evaporation decrease 6.8 % relative to today's situation. The climate scenario RCP8.5 in combination with 15 % more *urban* sub-catchments, results in the precipitation increasing 9.2 %, the runoff 12.6 % while the evaporation decrease 3.0 % relative to today's situation. There will likely be more frequent incidents of combined sewer overflows in the future due to increased precipitation and more surface runoff.

### 7.1 Further work

- Infiltration capacity should be mapped by extensive fieldwork and modeling tools. Suggestions for this task is to apply the Mariotte device in different locations through all seasons, as well as apply other methods for estimating the infiltration capacity of a soil. A soil infiltration capacity map that is updated and backed up by fieldwork and other investigation is necessary for the planning of LID solutions as well as for modeling the water cycle of an area.
- The source of the high ion concentrations in some of the locations in Gaustadbekken should be investigated further. It would be interesting to do continuous measurements of the ion concentration, heavy metal concentration and consequently the water quality over a longer time interval to follow seasonal variations and to identify effects of heavy rainfall. It would also be interesting to model the water chemistry of Gaustadbekken to investigate the concentration change through the watershed. The high concentrations of Iron (Fe) in Sognsvannbekken should be investigated further to identify the source. Presence of E. coli should be tested after several rainfall events. The results of this study is not representative as it was only conducted at two occasions.
- A suggestion for improving the model calibration process in Mike+ is to add an automatic calibration option that could be applied in combination with the manual calibration. As discussed in Boyle et al. (2000), this would ease the work of the modeler as well as take advantage of statistical methods and sensitivity of the model parameters. The parameter values found in the optimization could provide a helpful starting point for adjusting the parameters further to obtain the most suitable set of parameters. After experiencing the time consuming and challenging process of calibrating a hydrological model, this is a modest encouragement of adding this feature to the Mike+ model potential.
- Mike+ could be improved by an option of summarizing the results for all sub-catchments of the model. It could also be favourable to add an option of including areas outside the natural watershed only as active for the surface runoff and collection system computation.
- It would be interesting to apply 30 years long simulations on the hydrological model to be able to create statistics of the simulated changes. This was not done for this thesis due to time limitations, as simulations for one year used approximately 12 hours and produced sizable output files.

---

## Bibliography

---

- Antrop, M. (2004). 'Landscape change and the urbanization process in Europe'. In: *Landscape and urban planning* vol. 67, no. 1-4, pp. 9–26.
- Appelo, C. and Postma, D. (2005). *Geochemistry, Ground water and Pollution*. Vol. 536. AA Balkema Publishers New York, USA.
- Baker, L. A. (2009). 'Introduction'. In: *The Water Environment of Cities*. Ed. by Baker, L. A. Boston, MA: Springer US, pp. 1–16.
- Barkved, L. J., Seifert-Dahnn, I. and Langaas, S. (2018). *Overvannshåndtering i Sogn Hagekoloni - kartbaserte spørreundersøkelse om overvann og blågrønne løsninger*. 7236-2018, p. 42.
- Bjørlykke, K. (2001). *Sedimentologi og petroleumsgeologi*. Gyldendal Norsk Forlag AS 2001.
- Bogena, H., Herbst, M., Kunkel, R., Vereecken, H. and Wendland, F. (2004). 'Skalenabhängige Modellierung des Wasserhaushalts im Flusseinzugsgebiet der Rur'. In: *7. Workshop zur großskaligen Modellierung in der Hydrologie—Neue methodische Ansätze zur Modellierung der Wasser- und Stoffumsätze in großen Einzugsgebieten*. Kassel University Press, Kassel, Germany, pp. 87–97.
- Booth, D. B., Hartley, D. and Jackson, R. (2002). 'Forest cover, impervious-surface area, and the mitigation of stormwater impacts 1'. In: *JAWRA Journal of the American Water Resources Association* vol. 38, no. 3, pp. 835–845.
- Borba, B. D. and Rohrer, J. (2003). 'Determination of Inorganic Anions in Environmental Waters Using a Hydroxide-Selective Column. Application note 154.' In: *Thermo Fisher Scientific, Sunnyvale, CA, USA*.
- Box, G. E. (1976). 'Science and statistics'. In: *Journal of the American Statistical Association* vol. 71, no. 356, pp. 791–799.
- Boyle, D. P., Gupta, H. V. and Sorooshian, S. (2000). 'Toward improved calibration of hydrologic models: Combining the strengths of manual and automatic methods'. In: *Water Resources Research* vol. 36, no. 12, pp. 3663–3674.
- Brombach, H., Weiss, G. and Fuchs, S. (2005). 'A new database on urban runoff pollution: comparison of separate and combined sewer systems'. In: *Water science and technology* vol. 51, no. 2, pp. 119–128.
- Chaolin, G. (2020). 'Urbanization'. In: *International Encyclopedia of Human Geography (Second Edition)*. Ed. by Kobayashi, A. Second Edition. Oxford: Elsevier, pp. 141–153.
- DeFries, R. and Eshleman, K. N. (2004). 'Land-use change and hydrologic processes: a major focus for the future'. In: *Hydrological processes* vol. 18, no. 11, pp. 2183–2186.
- Department of Biology (2021). 'Microbiology and Mycology, 2021'. In:
- DHI (2021a). *Cities - Facing the urban water challenges of tomorrow*. URL: <https://www.mikepoweredbydhi.com/areas-of-application/cities> (visited on 04/09/2021).
- (2021b). 'MIKE 1D. DHI Simulation Engine for 1D river and urban modelling. Reference Manual'. In: p. 344.
- (2021c). *Mike+ Collection System*.
- (2021d). *MIKE+ Urban-River-Flooding*. URL: [%7Bhttps://www.mikepoweredbydhi.com/products/mikeplus%7D](https://www.mikepoweredbydhi.com/products/mikeplus%7D) (visited on 04/09/2021).
- (2021e). 'MIKE+. User Guide. Model Manager'. In: p. 410.

- DHI (2021f). *Urban water: Urbanization - the challenge of the century*. URL: [https://www.dhigroup.com/areas-of-expertise/urban-water?\\_ga=2.117782409.187875954.1617702056-1833329875.1613463816](https://www.dhigroup.com/areas-of-expertise/urban-water?_ga=2.117782409.187875954.1617702056-1833329875.1613463816) (visited on 04/09/2021).
- Dingman, L. (2015). *Physical Hydrology*. Illinois: Waveland Pr Inc. 643 pp. ISBN: 9781478611189.
- Dupont, S., Mestayer, P. G., Guilloteau, E., Berthier, E. and Andrieu, H. (2006). 'Parameterization of the urban water budget with the submesoscale soil model'. In: *Journal of applied meteorology and climatology* vol. 45, no. 4, pp. 624–648.
- Eggen, S. (2019). *Fraråder bading i indre Oslofjord*. URL: <https://www.vg.no/nyheter/innenriks/i/2Gbb8x/fraraader-bading-i-indre-oslofjord> (visited on 18/06/2021).
- Endresen, S. (1998). 'Lokal og total overvannsdiskontering (LOD/TOD) - Beskrivelse av anlegg, erfaringer mm.' In: *HYDRA*, no. T03.
- Erichsen Horgen AS (2016). 'Ny kulvert og åpen bekk ved Livsvitenskapsbygget'. In: vol. NO-RIVA-70-04-, p. 18.
- Feng, Y., Burian, S. and Pomeroy, C. (2016). 'Potential of green infrastructure to restore predevelopment water budget of a semi-arid urban catchment'. In: *Journal of Hydrology* vol. 542, pp. 744–755.
- Finn.no (n.d.). *Historiske kart*. URL: <https://kart.finn.no/>. (accessed: 17.07.2021).
- Fletcher, T. D., Andrieu, H. and Hamel, P. (2013). 'Understanding, management and modelling of urban hydrology and its consequences for receiving waters: A state of the art'. In: *Advances in water resources* vol. 51, pp. 261–279.
- Fletcher, T. D., Shuster, W., Hunt, W. F., Ashley, R., Butler, D., Arthur, S., Trowsdale, S., Barraud, S., Semadeni-Davies, A., Bertrand-Krajewski, J.-L. et al. (2015). 'SUDS, LID, BMPs, WSUD and more—The evolution and application of terminology surrounding urban drainage'. In: *Urban water journal* vol. 12, no. 7, pp. 525–542.
- Freeze, R. A. (1974). 'Streamflow generation'. In: *Reviews of Geophysics* vol. 12, no. 4, pp. 627–647.
- Freeze, R. A. and Cherry, J. (1979). *Groundwater*. Prentice-Hall Inc., New Jersey.
- Geological Survey of Norway B (2020). *Nasjonal løsmassedatabase*. URL: <http://geo.ngu.no/kart/losmasse/> (visited on 18/07/2020).
- Geological Survey of Norway C (2020). *Nasjonal berggrunnsdatabase*. URL: [http://geo.ngu.no/kart/berggrunn\\_mobil/](http://geo.ngu.no/kart/berggrunn_mobil/) (visited on 18/07/2020).
- Gilman, K. (1994). 'Gauging of the Rivers Dulas and Vyrnwy using the chemical tracer dilution method'. In:
- GrunnTeknikk AS (2019). '1004501 UiO Livsvitenskapsbygget Grunnforhold. Geoteknisk datarapport.' In: vol. RA-RIG-20-001, p. 18.
- (2020). '1004501 UiO Livsvitenskapsbygget. Hydrologisk prosjektering. Hydrologisk modellering av ulike scenarioer at tetttiltak for byggegrenen mot grunnvannsløkkasjer.' In: vol. NO-RIG-20-39, p. 24.
- Gulled Omar Jibril Kristine Eid, H. M. (2019). *Fraråder bading i indre Oslofjord*. URL: <https://www.nrk.no/osloogviken/frarader-bading-i-indre-oslo-fjord-1.14606152> (visited on 18/06/2021).
- Göbel, P., Stubbe, H., Weinert, M., Zimmermann, J., Fach, S., Dierkes, C., Kories, H., Messer, J., Mertsch, V., Geiger, W. F. et al. (2004). 'Near-natural stormwater management and its effects on the water budget and groundwater surface in urban areas taking account of the hydrogeological conditions'. In: *Journal of Hydrology* vol. 299, no. 3-4, pp. 267–283.
- Hafezparast, M., Araghinejad, S., Fatemi, S. E. and Bressers, H. (2013). 'A conceptual rainfall-runoff model using the auto calibrated NAM models in the Sarisoo River'. In: *Hydrology Current Research* vol. 4, no. 1, pp. 1–6.
- Hanssen-Bauer, I., Førland, E.J., Haddeland, I., Hisdal, H., Mayer, S., Nesje, A., Nilsen, J.E.Ø., Sandven, S., Sandø, A.B., Sorteberg, A., Ådlandsvik, B (2015). 'Klima i Norge 2100 : kunnskapsgrunnlag for klimatilpasning oppdatert 2015'. In: vol. M-406, no. 2, p. 204.
- Healy, R. W., Winter, T. C., LaBaugh, J. W. and Franke, O. L. (2007). *Water budgets: foundations for effective water-resources and environmental management*. Vol. 1308. US Geological Survey Reston, Virginia.

- Helgheim, E. P. B. (2020). *Bymiljøetaten: - Styr unna badevannet de neste timene*. URL: <https://vartoslo.no/bymiljoetaten-oslo-sommer/bymiljoetaten---styr-unna-badevannet-de-neste-timene/254537> (visited on 18/06/2021).
- Herricks, E. (1995). *Stormwater runoff and receiving systems: Impact, monitoring, and assessment*. CRC Press.
- Hersch, R. W. (1995). *Streamflow measurement*. Elsevier Applied Science Publishers Ltd, 1995.
- Hirabayashi, Y., Mahendran, R., Koirala, S., Konoshima, L., Yamazaki, D., Watanabe, S., Kim, H. and Kanae, S. (2013). 'Global flood risk under climate change'. In: *Nature Climate Change* vol. 3, no. 9, pp. 816–821.
- Hiscock, K. M. (2009). *Hydrogeology: principles and practice*. John Wiley & Sons.
- Hood Clausen, B. o. W. (2006). 'Forsinket avrenning fra urbane felt. Et eksempel på lokal overvannshåndtering'. In: *Vann*, no. 1.
- Hu, G., Guo, J., Luo, X., Chen, S., Xu, M., Mai, B., Li, F. et al. (2009). 'Distribution, sources, and risk assessment of polycyclic aromatic hydrocarbons (PAHs) in surface sediments from Baiyangdian Lake.' In: *Research of Environmental Sciences* vol. 22, no. 3, pp. 321–326.
- Haase, D. (2009). 'Effects of urbanisation on the water balance—A long-term trajectory'. In: *Environmental Impact Assessment Review* vol. 29, no. 4, pp. 211–219.
- Jan, C.-D., Chang, C.-J. and Lee, M.-H. (2006). 'Discussion of "Design and calibration of a compound sharp-crested weir" by J. Martinez, J. Reza, MT Morillas, and JG Lopez'. In: *Journal of Hydraulic Engineering* vol. 132, no. 8, pp. 868–871.
- Kelly, V. R., Lovett, G. M., Weathers, K. C., Findlay, S. E., Strayer, D. L., Burns, D. J. and Likens, G. E. (2008). 'Long-term sodium chloride retention in a rural watershed: legacy effects of road salt on streamwater concentration'. In: *Environmental science & technology* vol. 42, no. 2, pp. 410–415.
- Kirkby, M. (1988). 'Hillslope runoff processes and models'. In: *Journal of Hydrology* vol. 100, no. 1-3, pp. 315–339.
- Klemeš, V. (1986). 'Operational testing of hydrological simulation models'. In: *Hydrological sciences journal* vol. 31, no. 1, pp. 13–24.
- Klæboe, H. (1957). 'Grunttrekk av hydrologien, saerlig Norges Hydrologi'. In:
- Krause, P., Boyle, D. and Bäse, F. (2005). 'Comparison of different efficiency criteria for hydrological model assessment'. In: *Advances in geosciences* vol. 5, pp. 89–97.
- Lindholm, O., Endresen, S., Thorolfsson, S., Særgrov, S., Jakobsen, G. and Aaby, L. (2008). 'Veiledning i klimatilpasset overvannshåndtering'. In: *Norsk Vann* vol. 162, no. 162, p. 79.
- Lohani, A. K. (2018). 'Rainfall-Runoff Analysis and Modelling'. In: *National Institute of Hydrology: Roorkee, India*.
- Madsen, H. (2000). 'Automatic calibration of a conceptual rainfall-runoff model using multiple objectives'. In: *Journal of Hydrology* vol. 235, no. 3, pp. 276–288.
- Makkink, G. F. (1957). 'Testing the Penman formula by means of lysimeters'. In: *Journal of the Institution of Water Engineers* vol. 11, pp. 277–288.
- Martinez, J., Reza, J., Morillas, M. and Lopez, J. (2005). 'Design and calibration of a compound sharp-crested weir'. In: *Journal of hydraulic Engineering* vol. 131, no. 2, pp. 112–116.
- Mattilsynet. Statens tilsyn for planter fisker, d. o. n. (2014). *Norges mål for vann og helse. Vedtatt av Regjeringen 22 Mai 2014*. P. 38.
- Mays, L. W. (2001). *Stormwater collection systems design handbook*. McGraw-Hill Education.
- Mejia, A. I. and Moglen, G. E. (2010). 'Impact of the spatial distribution of imperviousness on the hydrologic response of an urbanizing basin'. In: *Hydrological Processes* vol. 24, no. 23, pp. 3359–3373.
- Miljødirektoratet (2020). 'Veileder M608|2016. Grenseverdier for klassifisering av vann, sediment og biota - revidert 30.10.2020'. In:
- Moriasi, D. N., Arnold, J. G., Van Liew, M. W., Bingner, R. L., Harmel, R. D. and Veith, T. L. (2007). 'Model evaluation guidelines for systematic quantification of accuracy in watershed simulations'. In: *Transactions of the ASABE* vol. 50, no. 3, pp. 885–900.
- Myhre, J. E. (2015). *Byene vokser*. URL: <https://www.norgeshistorie.no/industrialisering-og-demokrati/1524-byene-vokser.html> (visited on 05/06/2021).

- Müller, A., Österlund, H., Marsalek, J. and Viklander, M. (2020). 'The pollution conveyed by urban runoff: a review of sources'. In: *Science of the Total Environment* vol. 709, p. 136125.
- Mæhlum, T. and Hensel, G. R. (2009–2011). 'Infiltrasjon av avløpsvann. (Momenter fra innlegg på flere fagtreff i Norsk vannforening i perioden 2009-2011).' In: *Norsk Vann* vol. 4, no. 4, pp. 499–506.
- Mæhlum T Kohler J.C., J. P. and G.R., H. (2010). 'Grunnundersøkelser for infiltrasjon - mindre avløpsanlegg.' In: *Norsk Vann* vol. 178, no. 178, p. 79.
- Nachabe, M., Shah, N., Ross, M. and Vomacka, J. (2005). 'Evapotranspiration of two vegetation covers in a shallow water table environment'. In: *Soil Science Society of America Journal* vol. 69, no. 2, pp. 492–499.
- Nash, J. E. and Sutcliffe, J. V. (1970). 'River flow forecasting through conceptual models part I—A discussion of principles'. In: *Journal of hydrology* vol. 10, no. 3, pp. 282–290.
- Nestingen, R. S. (2007). 'The Comparison of Infiltration Devices and Modification of the Philip-Dunne Permeameter for the Assessment of Rain Gardens (Master thesis).' In: p. 58.
- Nie, L., Lindholm, O., Lindholm, G. and Syversen, E. (2009). 'Impacts of climate change on urban drainage systems—a case study in Fredrikstad, Norway'. In: *Urban Water Journal* vol. 6, no. 4, pp. 323–332.
- Nix, S. J. (1994). *Urban stormwater modeling and simulation*. CRC Press.
- Nordal, A. G. (2021). *Han vokter badevannet i Oslo*. URL: <https://www.tekna.no/magasinet/han-vokter-badevannet-i-oslo/> (visited on 18/06/2021).
- Norges lover, K. o. M. (1983). *Lov om vern mot forurensninger og om avfall (forurensningsloven)*. URL: <https://lovdata.no/dokument/NL/lov/1981-03-13-6> (visited on 21/06/2021).
- Norsk KlimaServiceSenter (2021). *Klimaprofil Oslo og Akershus*. URL: <https://klimaservicesenter.no/kss/klimaprofiler/oslo-og-akershus> (visited on 19/05/2021).
- NOU15:16 (2015). *OVERVANN I STORBY*. URL: <https://www.regjeringen.no/no/dokumenter/nou-2015-16/id2465332/> (visited on 20/10/2020).
- Ogden, F. L. (2021). 'Geohydrology: Hydrological Modeling'. In: *Encyclopedia of Geology (Second Edition)*. Ed. by Alderton, D. and Elias, S. A. Second Edition. Oxford: Academic Press, pp. 457–476.
- Oslo kommune (2013). 'Strategi for overvannshåndtering i Oslo'. In:  
— (2018). *Wastewater management*. URL: [https://ec.europa.eu/environment/europeangreencapital/wp-content/uploads/2017/06/Indicator\\_9\\_Wastewater\\_Management.pdf](https://ec.europa.eu/environment/europeangreencapital/wp-content/uploads/2017/06/Indicator_9_Wastewater_Management.pdf) (visited on 23/08/2020).  
— (2021). *Badeplasser og temperaturer*. URL: <https://www.oslo.kommune.no/natur-kultur-og-fritid/tur-og-friluftsliv/badeplasser-og-temperaturer/> (visited on 18/06/2021).
- Ott (2020). *Ott Orpheus Mini Water Level Logger*. URL: <https://www.ott.com/products/water-level-1/ott-orpheus-mini-water-level-logger-3/> (visited on 23/01/2021).
- Pachauri, R. and Meyer, L. (2014). 'Climate Change 2014: Synthesis Report. Contribution of Working Groups I, II and III to the Fifth Assessment Report of the Intergovernmental Panel on Climate Change'. In: *IPCC, Geneva, Switzerland, 151 pp.*
- Paul, M. J. and Meyer, J. L. (2001). 'Streams in the urban landscape'. In: *Annual review of Ecology and Systematics* vol. 32, no. 1, pp. 333–365.
- Paus, K. H. (2018). 'Forslag til dimensjonerende verdier for trinn 1 i Norsk Vann sin tre-trinns strategi for håndtering av overvann'. In: *Vann* vol. 1, pp. 66–77.
- Peel, M. C., Finlayson, B. L. and McMahon, T. A. (2007). 'Updated world map of the Köppen-Geiger climate classification'. In: *Hydrology and earth system sciences* vol. 11, no. 5, pp. 1633–1644.
- Qin, H.-p., Su, Q., Khu, S.-T. and Tang, N. (2014). 'Water quality changes during rapid urbanization in the Shenzhen River Catchment: An integrated view of socio-economic and infrastructure development'. In: *Sustainability* vol. 6, no. 10, pp. 7433–7451.
- Li-qing, L., Cheng-qing, Y., Qing-ci, H. and Ling-li, K. (2007). 'First flush of storm runoff pollution from an urban catchment in China'. In: *Journal of Environmental Sciences* vol. 19, no. 3, pp. 295–299.
- Reynolds, W. D. and Elrick, D. E. (1986). 'A method for simultaneous in situ measurement in the vadose zone of field-saturated hydraulic conductivity, sorptivity and the conductivity-pressure head relationship'. In: *Groundwater Monitoring & Remediation* vol. 6, no. 1, pp. 84–95.
- Rijtema, P. (1959). *Calculation methods of potential evapotranspiration*. Tech. rep. ICW.



- Sandaas, K. and Halvorsen, K. (2000). 'Oslo - Byen og Vassdragene.' In: *Vann* vol. 2, pp. 113–119.
- Schirmer, M., Leschik, S. and Musolff, A. (2013). 'Current research in urban hydrogeology—A review'. In: *Advances in Water Resources* vol. 51, pp. 280–291.
- Semadeni-Davies, A., Hernebring, C., Svensson, G. and Gustafsson, L.-G. (2008). 'The impacts of climate change and urbanisation on drainage in Helsingborg, Sweden: Combined sewer system'. In: *Journal of Hydrology* vol. 350, no. 1-2, pp. 100–113.
- Shuster, W. D., Bonta, J., Thurston, H., Warnemuende, E. and Smith, D. (2005). 'Impacts of impervious surface on watershed hydrology: A review'. In: *Urban Water Journal* vol. 2, no. 4, pp. 263–275.
- Solberg, T. (2019). *Oslo kommune fraråder bading i Oslofjorden etter regnværet onsdag*. URL: <https://www.nettavisen.no/nyheter/oslo-kommune-frarader-bading-i-fjorden-frykter-e-coli/s/12-95-3423806546> (visited on 18/06/2021).
- Solheim, E. B., French, H. K. and Braskerud, B. C. (2017). 'Måling av infiltrasjon fra overflaten for bruk av åpen LOD i praksis.' In: *Vann*, no. 3.
- Solvang, R. (2015). *Norges Vannforsyning*. URL: <https://www.tu.no/artikler/i-denne-kommunen-forsvinner-73-prosent-av-vannet-ut-i-ingenting/193802> (visited on 01/08/2021).
- Standardization (ISO), I. O. for (1992). '9555-3—Measurement of liquid flow in open channels—Tracer dilution methods for the measurement of steady flow—Part 3: Chemical tracers'. In: *Geneva (Switzerland): ISO—International Organization for Standardization*.
- (1994). '9555-1—Measurement of liquid flow in open channels—Tracer dilution methods for the measurement of steady flow—Part 1: General'. In: *Geneva (Switzerland): ISO—International Organization for Standardization*.
- Stephenson, G. R. and Freeze, R. A. (1974). 'Mathematical simulation of subsurface flow contributions to snowmelt runoff, Reynolds Creek Watershed, Idaho'. In: *Water Resources Research* vol. 10, no. 2, pp. 284–294.
- Syse, A. (2018). *Lower population growth in future*. URL: <https://www.ssb.no/en/befolkning/artikler-og-publikasjoner/lower-population-growth-in-future> (visited on 19/08/2020).
- The Federal Interagency Stream Restoration Working Group US (2001). *Stream Corridor Restoration Principles, processes and Practices*. Vol. 653. USDA-Natural Resources Conservation Service, p. 637.
- Thomas, D. and Rohrer, J. (2013). 'Determination of Inorganic Cations and Ammonium in Environmental Waters by Ion Chromatography Using the Dionex IonPac CS16 Column. Application note 141.' In: *Thermo Fisher Scientific, Sunnyvale, CA, USA*.
- Thornthwaite, C. W. (1948). 'An approach toward a rational classification of climate'. In: *Geographical review* vol. 38, no. 1, pp. 55–94.
- Time and date Oslo (2020). *Oslo, Norge - Soloppgang, solnedgang og dagens lengde*. URL: <https://www.timeanddate.no/astronomi/sol/norge/oslo?month=1&year=2020> (visited on 19/07/2021).
- Trinh, D. and Chui, T. (2013). 'Assessing the hydrologic restoration of an urbanized area via an integrated distributed hydrological model'. In: *Hydrology and Earth System Sciences* vol. 17, no. 12, pp. 4789–4801.
- Tsihrintzis, V. A. and Hamid, R. (1997). 'Modeling and management of urban stormwater runoff quality: a review'. In: *Water resources management* vol. 11, no. 2, pp. 136–164.
- University of Oslo (2019). *The ICPMS*. URL: <https://www.mn.uio.no/geo/english/research/about/infrastructure/facilities/analysis/geochemical-analysis/the-icpms-laboratory/> (visited on 19/02/2021).
- (2021). *Livsvitenskapsbygget*. URL: <https://www.uio.no/tjenester/eiendom/vare-byggeprosjekter/livsvitenskapsbygget/> (visited on 01/07/2021).
- Vázquez-Suñé, E., Sánchez-Vila, X. and Carrera, J. (2005). 'Introductory review of specific factors influencing urban groundwater, an emerging branch of hydrogeology, with reference to Barcelona, Spain'. In: *Hydrogeology Journal* vol. 13, no. 3, pp. 522–533.
- Velpuri, N. M., Senay, G. B., Singh, R. K., Bohms, S. and Verdin, J. P. (2013). 'A comprehensive evaluation of two MODIS evapotranspiration products over the conterminous United States: Using point and gridded FLUXNET and water balance ET'. In: *Remote Sensing of Environment* vol. 139, pp. 35–49.

- Walsh, C. J., Roy, A. H., Feminella, J. W., Cottingham, P. D., Groffman, P. M. and Morgan, R. P. (2005). 'The urban stream syndrome: current knowledge and the search for a cure'. In: *Journal of the North American Benthological Society* vol. 24, no. 3, pp. 706–723.
- Welty, C. (2009). 'The Urban Water Budget'. In: *The Water Environment of Cities*. Ed. by Baker, L. A. Boston, MA: Springer US, pp. 17–28.
- Xu, C.-Y. and Chen, D. (2005). 'Comparison of seven models for estimation of evapotranspiration and groundwater recharge using lysimeter measurement data in Germany'. In: *Hydrological Processes: An International Journal* vol. 19, no. 18, pp. 3717–3734.
- Younger, P. L. (2009). *Groundwater in the environment: an introduction*. John Wiley & Sons.
- Ødegaard, Heistad, Lindblom, Mosevoll, Thorolfsson, S. and Østerhus (2014). *Vann- og avløpsteknikk*. Ed. 2. Hamar: Norsk Vann.

PART II

---

**Part two**

---

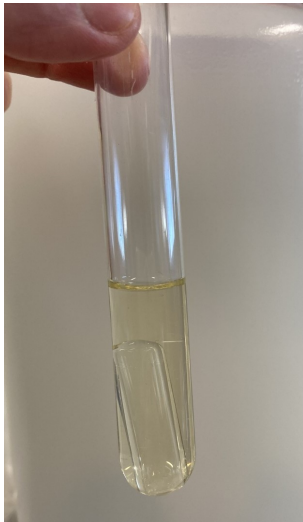


# APPENDIX A

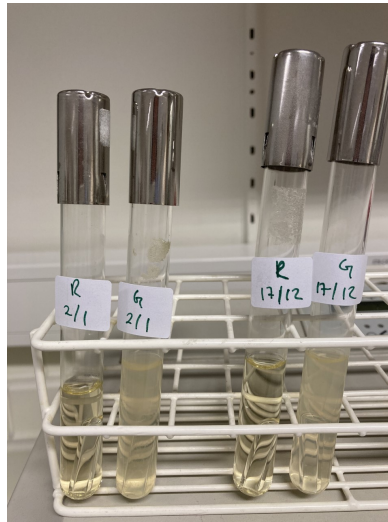
## Appendix

All raw data used for this study is included as attachments in the format of excel files. This includes the measurements by the Ott Orpheus mini water level logger, the calculated discharge, field work results of the infiltration measurements and tracer dilution. The summaries for the model simulations and a selection of the parameters are also included as attachments in the format of an excel file. All data is stored by the University of Oslo and can be provided upon request.

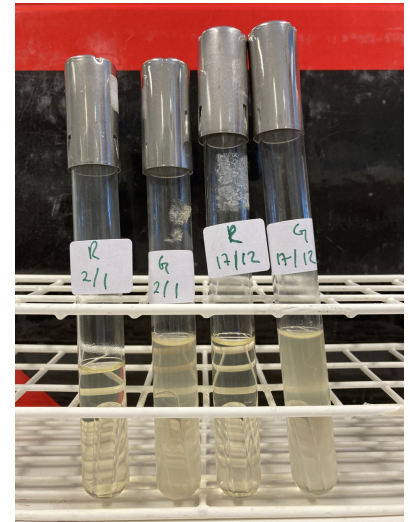
### A.1 Figures



(a) Initial solution at time 0.

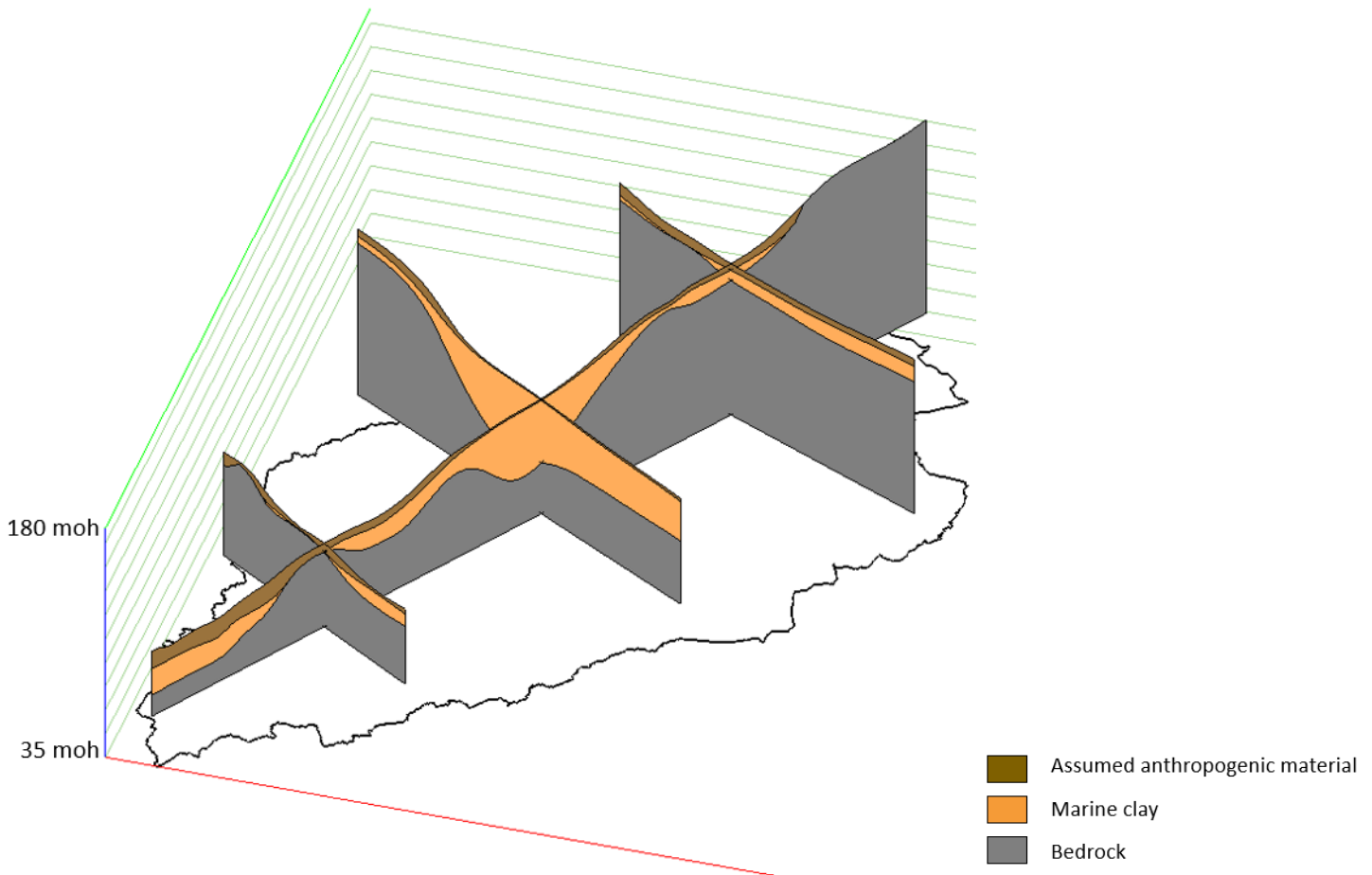


(b) The samples after 24 hours incubation at 37°C.



(c) The samples after 48 hours incubation at 37°C.

Figure A.1: Laboratory experiment to check for *E. coli* as an indication of sewer influence on the river water in Gaustadbekken and Sognsvannbekken.



(a) Simplified stratigraphy of Gaustad watershed.

(b) Legend.

Figure A.2: Simplified stratigraphy of Gaustad watershed illustrating presence of anthropogenic material at several areas of the catchment. Made as an illustration of the findings by ArcGIS Pro based on data by NGU and the subsurface archive as described in methods. Figure created in MODFLOW.

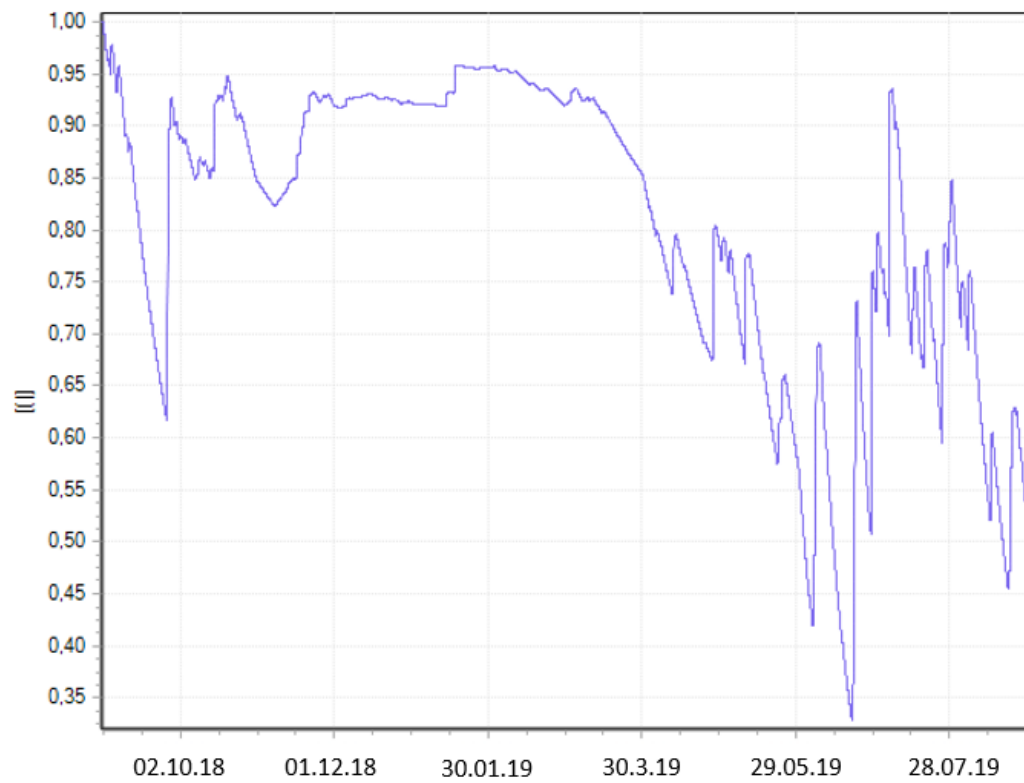


Figure A.3: Root zone storage through the hydrological year 2018-2019 for the sub-catchment representing the Life Science Building, before the construction of the building. The y-axis is percentage [%]. Figure from Mike+.

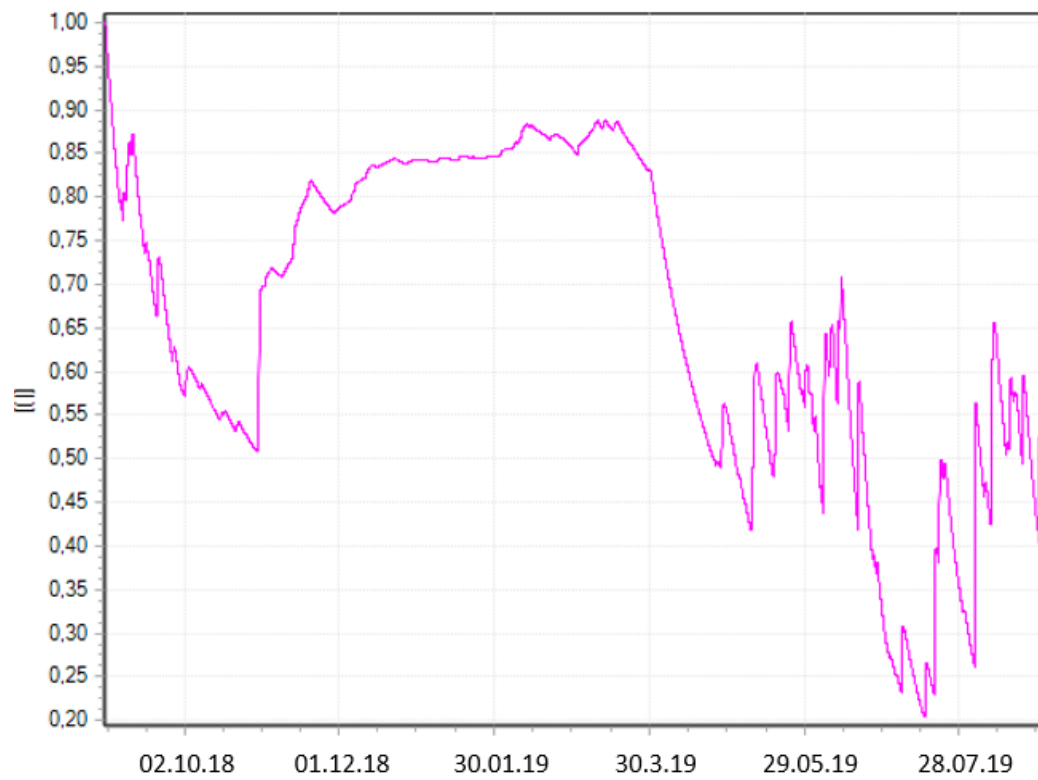


Figure A.4: Root zone storage through the hydrological year 2018-2019 for the sub-catchment representing the Life Science Building, after completion of the construction. The y-axis is percentage [%]. Figure from Mike+.



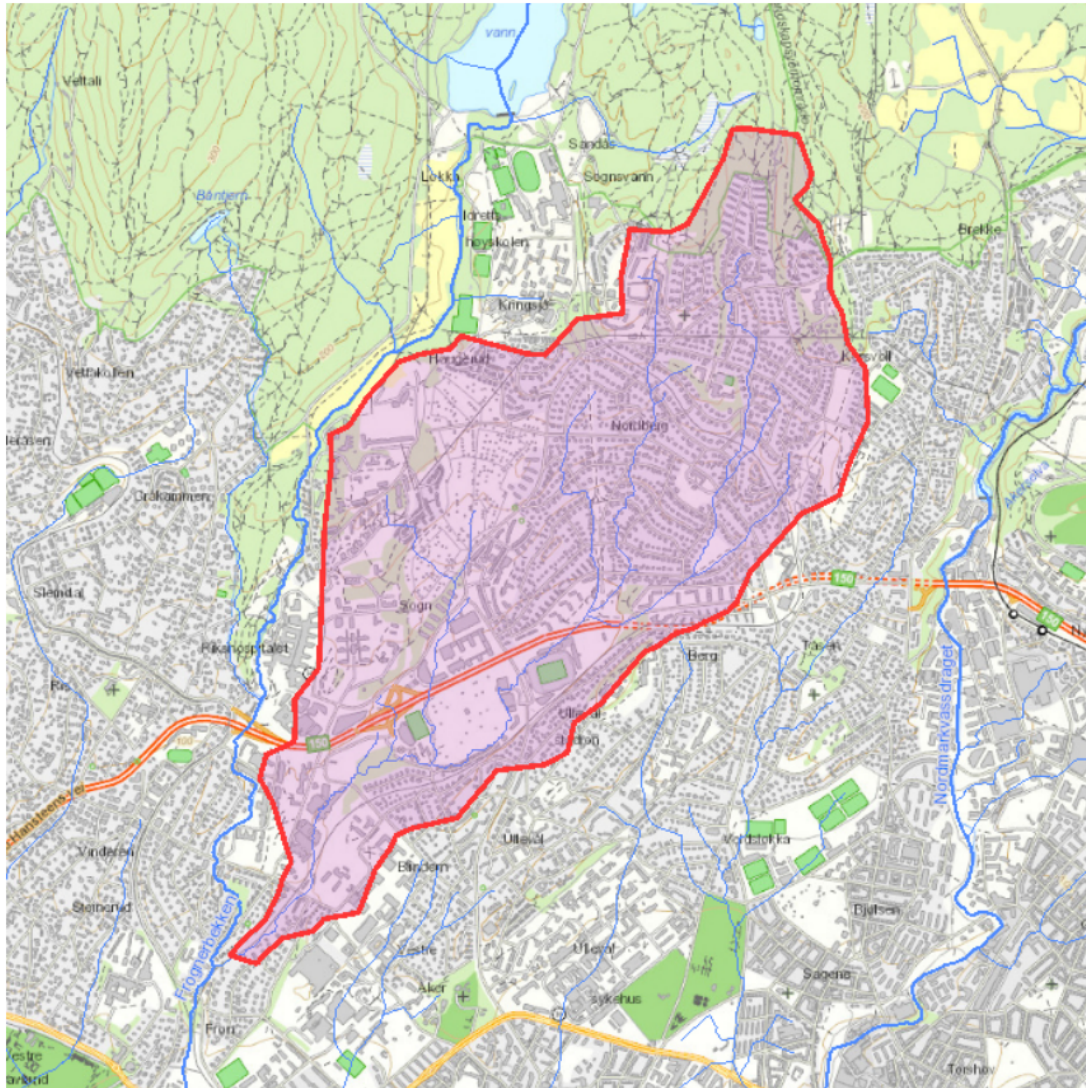


Figure A.5: Gaustad watershed by NEVINA.

## A.2 Fieldwork

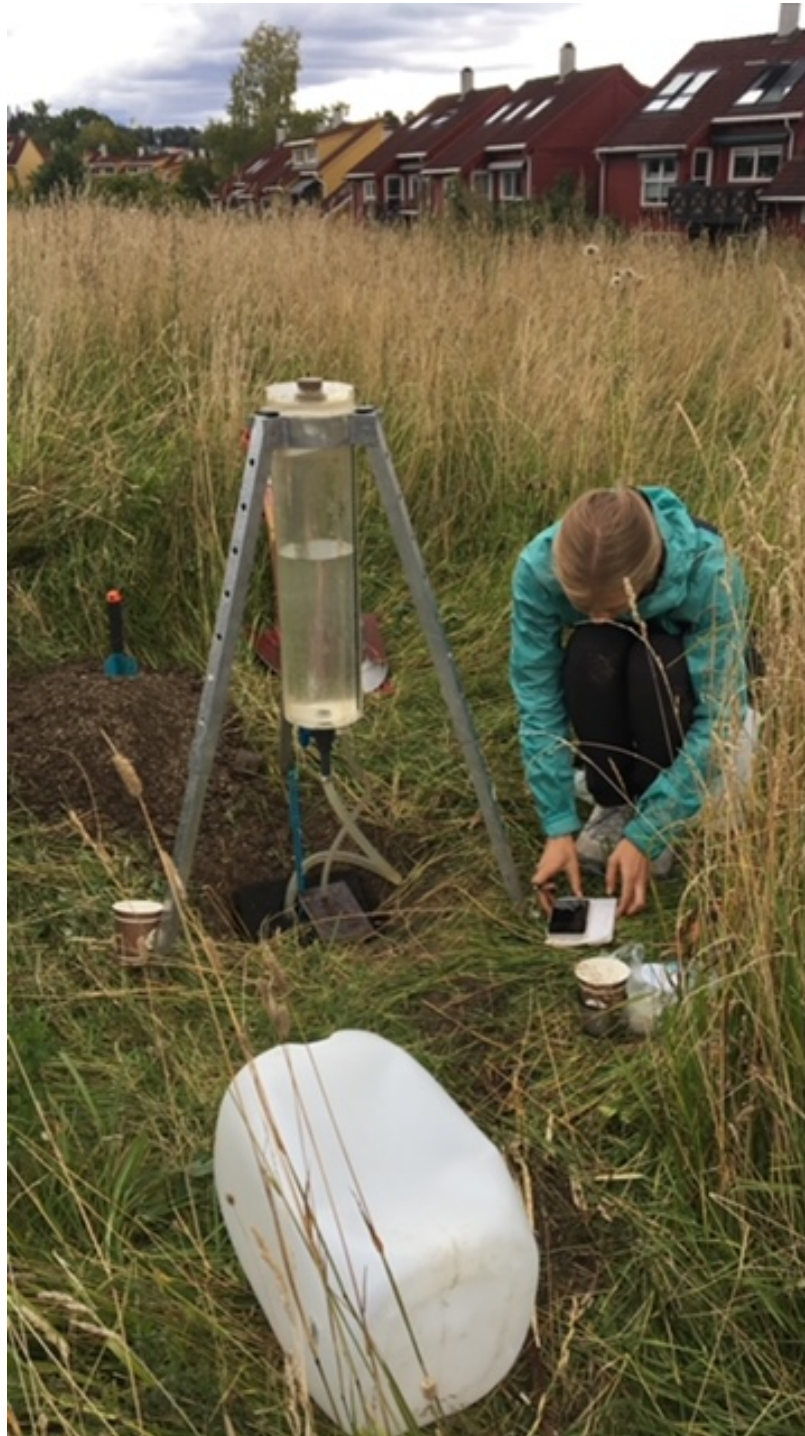


Figure A.6: Field work with Mariotte cylinder together with fellow student Rannveig Brørvik Sæten. Location of Sognsvannveien.



Figure A.7: Clearing the Gaustadbekken weir pond together with supervisors Nils Roar Sælthun and Hong Li.



Figure A.8: Water sampling in front and measurement of pH in the background. Photo by Jorge Torres.



Figure A.9: Filtering of the water samples. Photo by Jorge Torres.



Figure A.10: Forskningsparken artificial stream as an open part Gaustadbekken.

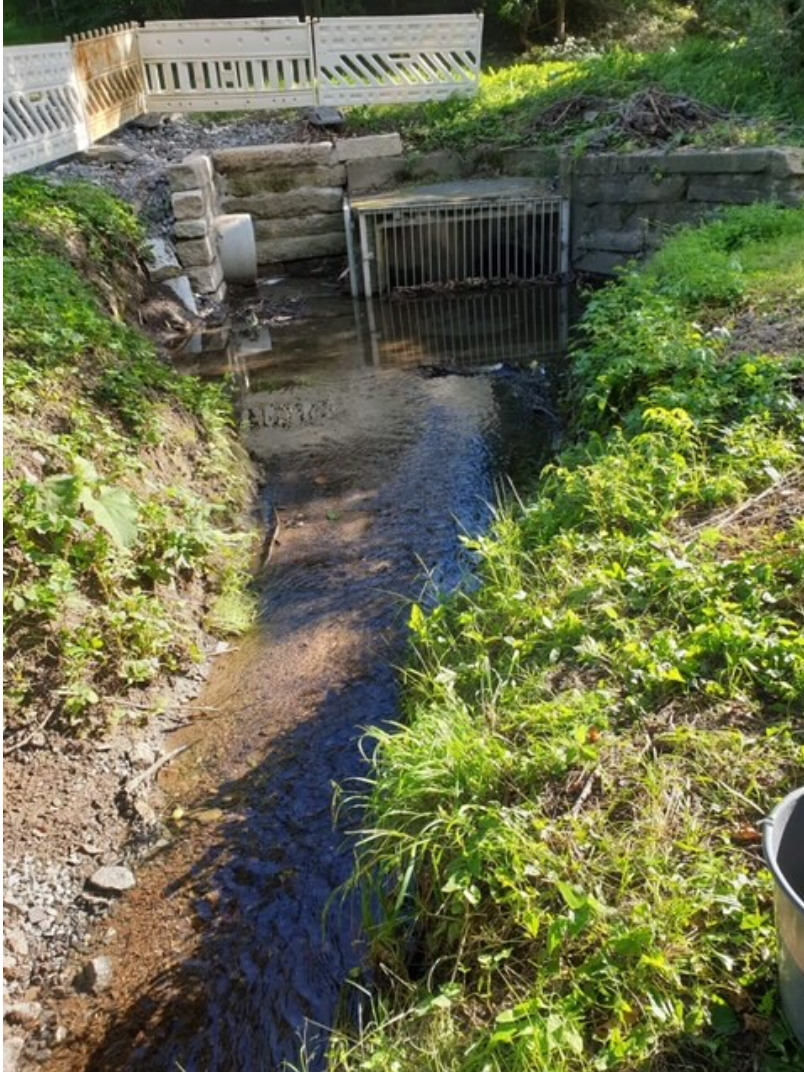


Figure A.11: Location Nils Bays vei (NBV), see map in figure 4.7.



Figure A.12: Location Konvallveien (KV), see map in figure 4.7.





Figure A.13: Location Gaustadbekken by Blindern station (GBBS), see map in figure 4.7.



Figure A.14: Location Solvang Kolonihage (SK), see map in figure 4.7.